ABSTRACT

Childs Jr., Peter P. Numerical Simulations of Mesoscale Boundary Layer Structure over New York City. (Under the direction of Dr. Sethu Raman)

Roughness length variations and the urban heat island effect are the dominating influences of highly urbanized terrain on boundary layer structure and evolution. Variations in roughness length can alter the surface wind flow by slowing it down, turning it, or a combination of both. The urban heat island effect keeps surface temperatures warmer than surrounding rural areas, leading to a more turbulent nocturnal boundary layer over the urbanized terrain than the surrounding regions. With a pronounced heat flux gradient, surface wind speeds are often enhanced as they flow across the urban regions.

This thesis explores the influences of New York City on the structure and evolution of the boundary layer through a combination of numerical model simulations and observational analysis following the destruction of the World Trade Center buildings on 11 September 2001. Mesoscale processes, such as sea breeze circulations, urban heat island, and terrain modified flows are addressed in this research through the use of observations and several numerical simulations. Surface based observations from the National Weather Services' ASOS network are examined. Additionally, observations from an independent 10 m micrometeorological tower and two Sound Detection and Ranging (SODARS) are used. These observations are also used for model validation.

An observational analysis of 10 m tower data and SODAR data is conducted for an extended study period between 10 September 2001 and 10 December 2001. Tower measurements of wind speed and direction (10 m) and temperature (2 m) are presented. SODAR data of wind speed and direction is also examined. Several different synoptic flow regimes were analyzed during this study period. Aerodynamic roughness length calculations were also made for two independent flow direction sectors. Results from this analysis showed that roughness lengths less than 1 m, if the predominant flow was between 180 to 359 degrees. Twenty-four hour averaged surface temperatures were observed to be warmer over the city center than the surrounding rural areas. Near surface wind speeds were also observed to be lower over the highly urbanized terrain associated with New York City.

Simulations using 1 km grid spacing output from the Advanced Regional Prediction System (ARPS) and PSU/NCAR Mesoscale Model 5 (MM5) are examined during a high ground level pollutant concentration episode in lower Manhattan. The ARPS simulation showed a more defined sea breeze frontal formation and propagation than the MM5 simulation did over lower Manhattan. The ARPS simulation also showed a better defined slowing and turning of the 10 m wind speed over the highly urbanized terrain of lower Manhattan and Brooklyn relative to the MM5 simulation. Since both simulations used the same landuse data and roughness length parameterization, the planetary boundary layer scheme in both models is likely contributing to the observed differences.

The urban heat island effect, urban blocking effect and sea breeze front are analyzed using the ARPS mesoscale model. The sea breeze frontal development and inland propagation agrees well with previous research by Michael (1998) and Bornstein (1994),

who showed similar results using WSR-88D imagery and numerical simulations, respectively. Additionally, the turning of the surface (10 m) wind flow agrees well with previous research by Bornstein and Johnson (1977) that showed nighttime conditions during stronger flow regimes (>4 m/s) to be associated with distinctive roughness induced cyclonic turning in the winds over the main core of Manhattan and Brooklyn.

REFERENCES

Bornstein et. al., 1994, Observation and simulation of urban-topography barrier effects on boundary layer structure using the three-dimensional TVM/URBMET model. "Air Pollution and its Application X", Plenum Press, New York, 1994.

Bornstein, R. D. and D. S. Johnson, 1977: 'Urban-rural wind velocity differences', *Atmos. Environ.*, **11**, 597-604.

Micheal P., M. Miller, J.S. Tongue, 1998: Sea breeze regimes in New York City region-Modeling and Radar Observations. Transactions of Second Conference on Coastal Atmospheric and Oceanic Prediction and Processes, 78th AMS Annual Meeting. 11-16 January 1998. Phoenix, Arizona.

NUMERICAL SIMULATIONS OF MESOSCALE BOUNDARY LAYER STRUCTURE OVER NEW YORK CITY

By

Peter P. Childs Jr

A Masters thesis submitted to the Graduate Faculty of

North Carolina State University

In partial fulfillment of the

Requirements for the Degree of

Masters of Science

MARINE, EARTH AND ATMOSPHERIC SCIENCES

Raleigh

2003

Approved by:

_____	_____
Dr. S. Pal Arya	Dr. Gary Lackmann
_____	
Dr. Sethu Raman, Chair	

BIOGRAPHY

Peter P. Childs Jr was born in Vorhees, New Jersey on April 16, 1978 to Mr. and Mrs. Peter P. Childs Sr. Growing up Peter enjoyed playing baseball, basketball and tennis. Peter loved to travel to the Jersey Shore during the summer months, where he spent much time fishing and swimming. Ever since he can remember, Peter has been fascinated with the weather, from watching thunderstorms roll in off the Atlantic Ocean while at the Jersey Shore, or watching the first flakes fall during a major east coast snowstorm. His decision to pursue a career in meteorology came after the so-called "Blizzard of 1996" dropped nearly 3 ft of snow in his backyard. Peter graduated from Haddonfield Memorial High School in 1997 and enrolled at North Carolina State University in August 1997. In the spring of 2001, Peter graduated with a B.S. degree in Meteorology from North Carolina State University. Peter's thirst for more knowledge led him to enroll in the graduate program at North Carolina State University to pursue an M.S. degree in Meteorology. His interests have grown to include advanced numerically modeling of various weather phenomena, as well as short and long-range weather forecasting. With the help of the State Climate Office of North Carolina, he finished his Masters degree in the Summer of 2003.

ACKNOWLEDGEMENTS

I would like to thank and recognize three main contributors for the completion of my Masters of Science Degree in Meteorology. First I would like to thank Dr. Sethu Raman for providing me with the financial needs, computer resources and professional expertise to complete my degree. Secondly, I would like to thank Dr. Gary Lackmann for his support and expertise throughout my research and for teaching me how to become a good weather forecaster. Additionally, I would like to thank Dr. S. Pal Arya for his assistance in my research and for agreeing to serve on my thesis committee. On the same line, I would like to thank Robert Gilliam who taught me so much about scripting and modeling and who has been such a great friend throughout my thesis research. Moreover, Dr. Alan Huber and the Environmental Protection Agency deserve a thank you for their support and willingness to share resources. Ryan Boyles, and the entire State Climate Office of North Carolina, have provided me with emotional support as well as technological support and I am very thankful for their help.

I would also like to thank the North Carolina Supercomputing Center, which has provided me with countless computing resources over the last few years. I also need to recognize National Center for Atmospheric Research (NCAR) and the Pennsylvania State University for their assistance with the Mesoscale Model 5 (MM5). Thanks go out to the Center for Analysis and Prediction of Storms (CAPS) for their years of work on the Advanced Regional Prediction System (ARPS).

On a more personal level, I would like to express my sincere thanks and gratitude to my parents for supporting my obsession with weather growing up. Finally, I would like to

thank my wife, Jessica Childs, for her support, as without it I would not have completed my thesis.

TABLE OF CONTENTS

LIST OF TABLES

LIST OF FIGURES

LIST OF SYMBOLS

A	Advection
c_p	Specific heat of dry air at constant pressure
D_u	Diffusion of u-component of velocity (including subgrid-scale fluxes)
D_v	Diffusion of v-component of velocity (including subgrid-scale fluxes)
D_w	Diffusion of w-component of velocity (including subgrid-scale fluxes)
D_θ	Diffusion of potential temperature (including subgrid-scale fluxes)
e	Coriolis effect ($f = 2\Omega\cos\lambda$)
$\bar{e}$	Turbulence Kinetic Energy (TKE)
$\in$	Viscous dissipation of TKE
f	Coriolis effect ($f = 2\Omega\sin\lambda$)
f_y	Dimensionless time function in the horizontal
f_z	Dimensionless time function in the vertical
g	Gravitational force constant (9.82 m/s)
H	Sensible heat flux
h_u	Relative humidity at the ground surface
k	von Karman Constant
L	Monin-Obukhov length
LE	Latent heat flux

m	Map factor
p	Pressure
p'	dp/dt
p_o	Reference state pressure
ρ_a	Air density
p_s	Surface pressure
p_t	Pressure at the top of the atmosphere
p^*	$p_s - p_t$
ρ_w	Density of water
q	Specific humidity
$\dot{Q}$	dQ/dt
Q_H	Surface sensible heat flux
Q_E	Surface latent heat flux
Q^*_s	Net Radiation
Q_G	Total Ground fluxes
R_a	Aerodynamic resistance
R_g	Short wave radiation at the surface
Ri_b	Bulk Richardson number
R_d	Dry air gas constant
r_{earth}	Radius of the earth, 6371 km

T	Air temperature
T_o	Background temperature
T′	dT/dt
t	Time
t_{ty}	Time scale in the horizontal
t_{tz}	Time scale in the vertical
u	Wind speed relative to earth in the x-direction
u_*	Friction Velocity
$\overline{u'^2}$	Mean gustiness of the u-component
V	Three dimensional wind vector
v	Wind speed relative to earth in the y-direction
$\overline{v'^2}$	Mean gustiness of the v-component
w	Wind speed relative to earth in the z-direction
w_*	Convective velocity scale
$\overline{w'^2}$	Mean gustiness of the w-component
x	Cartesian coordinate representing east-west direction
y	Cartesian coordinate representing north-south direction
z	Vertical Cartesian coordinate
z_0	Aerodynamic Roughness Length
α	Albedo

γ	Parameter in the equation of motion resulting from Lambert conformal map projection
θ	Potential temperature
θ_o	Background initial temperature
ρ_o	Initial value of density
σ	Terrain following vertical coordinate
$\dot{\sigma}$	$d\sigma/dt$
χ	Similarity function
χ_0	Similarity function scaled by the surface roughness
z	Height above the surface
z_i	Boundary layer height

CHAPTER 1

INTRODUCTION

1.1 URBAN HEAT ISLAND AND THE ATMOSPHERIC BOUNDARY LAYER

Meteorological effects of urbanization are well documented throughout atmospheric literature. Most studies have focused on the urban heat island and its interactions with larger-scale atmospheric phenomena. The urban area has been documented as causing a heat-island circulation (HIC), which can significantly alter lower tropospheric winds and low-level pollutant diffusion. Scientists have often concentrated on the urban heat island, which is most notable during the night. However, more recent studies have examined both the urban heat island and the HIC. Shreffler (1978, 1979) conducted observational studies of St. Louis, while Asai (1990) analyzed observed data from Tokyo. Additional observational studies by Kimura (1975, 1976), Bornstein (1975) and Sawai (1978) and physical modeling studies by SethuRaman and Cermak (1974) and Yamada and Mellor (1975), have focused on the urban heat island and its effects on local circulations and flow alterations. Few numerical studies have attempted to simulate the very complex micro and mesoscale meteorology associated with urban areas such as New York City, the focus region of this study.

Atmospheric boundary layer (ABL) inhomogeneity is most apparent over a dense urban center like NYC that lies adjacent to an ocean or a large lake, especially when compared to the ABL over rural, inland areas. NYC's landuse is characterized as a highly developed urban core on Manhattan Island and a sprawling dense suburban area that covers northeastern New Jersey and western Long Island. Adding to this complex urban

surface is a highly variable coastline consisting of many small bays, rivers and sounds (Jamaica Bay, New York Harbor, Hudson River, East River and Long Island Sound). All of these features and their influence on the lower atmosphere make attempts at modeling the region difficult (Michael et al., 1998).

Historical studies have focused both directly and indirectly on the unique small-scale variations of the ABL in and around NYC. The NYC urban blocking effect and urban heat island phenomena have been examined in detail (Bornstein and Johnson, 1977; Bornstein, 1994). The blocking effect can be described as the modification of the flow by an abnormally rough surface presented by Manhattan Island. The urban heat island develops because of both anthropogenic heating and heat-holding structures. This local heating further modifies the wind flow patterns over the city. Past research shows that wind speed along a streamline are found to be decreased below (increased above) those at sites outside of the city when synoptic scale winds speeds are above (below) 4 m/s. Above this critical value the wind over the city is less than in rural areas and turns cyclonically as the air passes over the city because of the increased frictional effect. Conversely, when the wind speed is below this criterion, the urban heat island is allowed to develop and the wind over the city is slightly stronger during both the daytime and nighttime. This urban enhancement of the wind speed is a result of the increase in mesoscale baroclinicity and decrease in stability, which allows for efficient downward flux of momentum. This wind enhancement during lower wind speed regimes, especially at night, results in a more anticyclonic curvature of the wind trajectory as it passes over the city. Many studies have been performed on this topic (Angell et. al., 1971; Wong and

Dirks, 1978; Lee 1979; Draxler, 1986) and most agree with this behavior of wind flow over a rough urban surface.

Another complicating factor in the NYC region is the land-water contrast. A thermal internal boundary layer (TIBL) often develops along the coast, influencing the boundary layer structure over land. Its variation downwind depends on the surface roughness, upwind atmospheric stability and land-sea temperature contrast (Raynor et al., 1979). A TIBL exists to some extent during all conditions, but is most pronounced during light to moderate synoptic flow cases where the local temperature and wind variation can dominate the meteorology of the region. Frizzola and Fisher (1963), Bornstein (1994), Reiss et al. (1996) and Michael et al. (1998) examine the sea breeze over NYC in detail using numerical models, surface and upper-air observations, and radar imagery. From these numerical and observational studies, it appears that the geography of the region has a major impact on the inland penetration, depth, vertical wind distribution and timing of the sea breeze. Complicating things even further, the sea breeze structure is distorted by the urban roughness, coastline configuration and topography relative to the large-scale flow direction (Frizzola and Fisher, 1963; Simpson et al., 1977; Arritt, 1993; Bornstein, 1994; Michael et al., 1998, Gilliam et al. 2003). With all these factors to consider, it is extremely difficult to accurately replicate the boundary layer over New York City and the surrounding region.

As a result of the urban heat island and the resulting HIC, and their effect on surface-layer wind flow, numerical modeling over highly urbanized areas is complex. As the realization of potential bio-terrorism hazards in urbanized area continues to grow, reliable numerical modeling of urban areas is rapidly becoming an important research and

operational issue. Studies involving high-resolution mesoscale models, and pollutant dispersion models, are currently underway (Arya, 1999). Historically, air pollution has been regarded as a serious problem only for large cities and commercial centers. As a result of the industrial revolution and the advent of the automobile, air quality in most of the large urban and industrialized areas has been suffering greatly. Various urban air quality models have been developed to help implement new strategies and techniques to help regulate pollutants being released from automobiles and industry.

There are five main components of an air quality model. They are sources and emissions inventory, transport winds, diffusion parameterizations, chemical transformations and removal processes (Arya, 1999). While individual models have different representations of each of these components, all of these components are included in the latest urban diffusion models. There are a variety of urban diffusion models used to predict pollutants resulting from urban emissions. The Gaussian diffusion models are widely used currently in regulatory applications, as are the simple Box Model and more complex three-dimensional grid models, the latter being the most comprehensive and sophisticated of the urban air quality models. Three-dimensional grid models, such as the U.S. EPA's latest version of the Urban Airshed Model, require all five of the above-mentioned components of air quality models. Because of the complexity of these models, high-resolution meteorological input conditions are required. In many cases, a mesoscale model is used to simulate the ABL and surrounding environment to obtain fine resolution boundary conditions to input into the urban airshed models. However, as mentioned above, numerical simulations over a highly urbanized area are challenging and complex.

1.2 RESEARCH OVERVIEW AND OBJECTIVES

The main objective of this investigation is to analyze observations and numerically simulate the mesoscale and microscale boundary layer structure over New York City. Observations from two SOund Detection And Ranging (SODAR) units, a 10 m micrometeorological tower and five Automated Surface Observing Stations (ASOS) are examined during several synoptic scale flow regimes. Then, numerical simulations are conducted to explore the complex mesoscale boundary layer structure over New York City. The first numerical investigation examines the ability of two high-resolution mesoscale prediction models, the Advanced Regional Prediction System (ARPS) and the Mesoscale Model 5 (MM5) to simulate the complex low-level (10 m) flow over the New York City area. The second numerical investigation examines the urban heat island, urban roughness effect and sea breeze structure over the region. In support of these numerical studies, high-resolution, 1 km grid size simulations are performed.

The U.S. Environmental Protection Agency, National Exposure Research Laboratory (EPA/NERL) has an instrumentation cluster that facilitates high-resolution temporal measurements near the surface. This ensemble consists of three portable trailers that support the Aerovironment Model 4000 miniSODAR, Aerovironment Model 2000 SODAR and a three-level 10 m micrometeorological tower. This cluster was deployed in lower Manhattan, New York in November 2001 to support the EPA and State Climate Office of North Carolina's study of pollutant exposure over lower Manhattan following the September 2001 disaster. To supplement these observations, the data from five ASOS stations; Newark New Jersey, Teterboro New Jersey, Central Park New York, JFK Airport New York and LaGuardia Airport New York, are also analyzed. The emphasis

here is on diagnosing the synoptic scale flow regimes favored over New York City during the autumn of 2001. Additionally, using the 10 m micrometeorological tower and the two SODARS, roughness length will be calculated for the different flow regimes observed over the region. ASOS and 10 m tower observations will be used to study the effect, if any; the urban heat island has on the temperature structure and wind fields during the different flow regimes. The 10 m wind field study centers around a high ground-level pollution event observed between 13 November 2001 and 15 November 2001 over lower Manhattan. This period was characterized by light and variable winds on the 13th, with a more southwesterly component developing on the 14th and 15th. Specific relations are investigated between the effects of roughness length variations on the 10-m wind flow, as well as the development and inland propagation of the sea breeze front. The ability of the ARPS and MM5 models to accurately represent these features is studied (A more detailed description of the model domains and set up is discussed in Chapter 3). The models output data are compared to the 10 m tower and ASOS surface observations with supplemental surface layer data coming from the SODARS.

Lastly the ARPS model is used to study the effects of the urban heat island and roughness length variations on the boundary layer structure and its diurnal evolution over New York City. This simulation employs the 1 km USGS surface characteristics and 30 second terrain information to define the lower boundary. A 48-hr case study for the 1 km domain is presented. The domain is initialized from the 32-km ARPS Data Assimilation System (ADAS). A 5 km intermediate domain is utilized to ensure that accurate lateral and upper boundary conditions are ingested into the 1 km simulation. Observations from the independent cluster and ASOS network are used to evaluate the model simulation.

The 10 m tower data and ASOS data are used for comparison with the model simulation of 10 m wind speed and direction associated with the sea breeze front and roughness induced deflections. The SODAR data are used to examine the vertical structure of the lower boundary layer and for comparison to the simulation of the sea breeze structure and urban heat island effect.

1.3 RESEARCH LAYOUT

The following is a brief description of the organization of this thesis. Information on the instrumentation cluster, and a review of the ASOS data used in this study are provided in Chapter 2. Details of both the mesoscale models, ARPS and MM5, and how, and why, they were configured for this study are presented in Chapter 3. Results of the observational analysis over New York City are discussed in Chapter 4. A comparison of the ARPS and MM5 simulations of surface meteorology is presented in Chapter 5. Results from the ARPS simulation of the sea breeze structure and inland propagation as well as the effects of urban heat island and roughness length variations on the low-level wind flow are discussed in Chapter 6. Summary and conclusions of this research are presented in Chapter 7.

CHAPTER 2

INSTRUMENTATION AND DATA

Numerous data sources were used in support of this study. These data include ASOS data and an independent instrumentation cluster maintained by the U.S. Environmental Protection Agency (EPA) and State Climate Office of North Carolina. The following section will detail the independent instrumentation cluster, followed by a description of the ASOS data.

2.1 INSTRUMENTATION AND DATA DESCRIPTION

Table 2.1a provides a technical description of the Aerovironment Model 4000 miniSODAR used in this study. The miniSODAR is a high-resolution surface layer (15 to 200 m range at 5 meter intervals, 10 min averaged) wind sampler. It transmits sound at a frequency of 4500 Hz, which helps to mitigate environmental noise interference (Crescenti, 1998), leading to a better representation of the surface layer wind distribution and variance. The miniSODAR has a wind speed uncertainty of <0.50 m/s and a wind direction uncertainty of +/- 5 deg. A previous study that evaluated the performance of ground based instruments, including the miniSODAR found a high correlation with tower measurements (Crescenti, 1999). SODAR systems, including the miniSODAR, use sound to sample the boundary layer, emitting a pulse and receiving scatter from gradients of temperature and moisture. Turbulent mixing in the boundary layer often causes these gradients. Frequency shifts (Doppler effect) between the transmitted and returned signal are translated as moving parcels of air, where the velocity is directly related to the frequency shift. Algorithms extract other related parameters such as

Table 2.1a Specifications of the Model 4000 (miniSODAR) used in this study.

Frequency (Hz)	Vertical Range (m)	Resolution (m)	Sampling Period (min)	Measurements
4500 Hz	15-250 m	5 m	10 Min Average	u,v wind comp.

Table 2.1b Specifications of the Model 2000 SODAR used in this study.

Frequency (Hz)	Vertical Range (m)	Resolution (m)	Sampling Period (min)	Measurements
2000 Hz	60-700 m	30 m	10 Min Average	u,v wind comp.

Table 2.1c Specifications of the 10 m Micrometeorological Tower used in this study.

Measurement	Instrument	Levels	Sampling Period
Wind Velocity	Young Model 05701 Anemometer	2, 5, 10 m	10 Min Avg.
Temperature	Gill aspirated Model 43408	2, 10 m	10 Min Avg.
Relative Humidity	Gill aspirated Model 43408	2, 10 m	10 Min Avg.

standard deviations of the wind components, vertical velocity, and return signal intensity (reflectivity).

Table 2.1b provides a technical description of the Aerovironment Model 2000 SODAR used in this study. The Aerovironment Model 2000 SODAR, measures the same wind properties as the miniSODAR from 60 to 600 m at 30 m intervals, and averaged over a 10 min period. The Model 2000 SODAR has a wind speed error of <0.50 m/s and a wind direction uncertainty of +/- 5 deg. This unit provides important data from the convective mixed layer, provides an independent source for comparison with the miniSODAR, and provides mixing height measurements below 600 m. This unit is also capable of assessing boundary layer structure and evolution after sunrise and before sunset.

Table 2.1c shows a technical description of the 10 m micrometeorological tower used in this study. The 10 m micrometeorological tower has instruments that measure wind (Young Model 05701 anemometer) at 2, 5 and 10 m along with temperature and relative humidity (Gill aspirated Model 43408) at 2 and 10 m. The wind direction is accurate to within +/- 5 deg, while the wind speed is accurate to within 0.25 m/s at all levels. The temperature sensors are accurate to within 0.2 C at all levels. This “ground truth” instrumentation is important and valuable for evaluating the accuracy of the SODAR data, and provides the lower level observations that are not sampled by either SODAR. The temperature observations are also important, especially the difference between 2 and 10 m that can provide valuable information on the static stability of the surface layer. All tower data used in this study are sampled each second, averaged and stored at 10 min intervals. The instrument cluster was activated on November 08, 2001 providing approximately one month of independent data during this study period. A plan view

showing the location of the instrumentation cluster with respect to lower Manhattan is shown in Figure 2.1.

Hourly surface observations from five National Weather Service Automated Surface Observing System (ASOS) stations are also used in this study. The stations are Newark Airport, Teterboro Airport, Central Park, LaGuardia Airport, and John F. Kennedy Airport. Quality assured hourly ASOS data were acquired from the National Climatic Data Center (NCDC) for the study period. The ASOS 10 m wind and 2 m temperature data are recorded every minute and are representative of the previous 5 min average. The data are recorded at the bottom of the hour, approximately 51 minutes past each hour. Figure 2.2 shows the location of the five ASOS sites used in this study. Figure 2.3 shows a high-resolution photograph of lower Manhattan on 12 September 2001. The smoke plume from the World Trade Center disaster site is evident on the photograph. The instrumentation cluster was located on Pier 25 in lower Manhattan and is labeled MIC 3 on the photograph for reference.

Figure 2.1 Plan view of the Lower Manhattan area, showing the location of NERL's 10 m Tower and two SODARs.

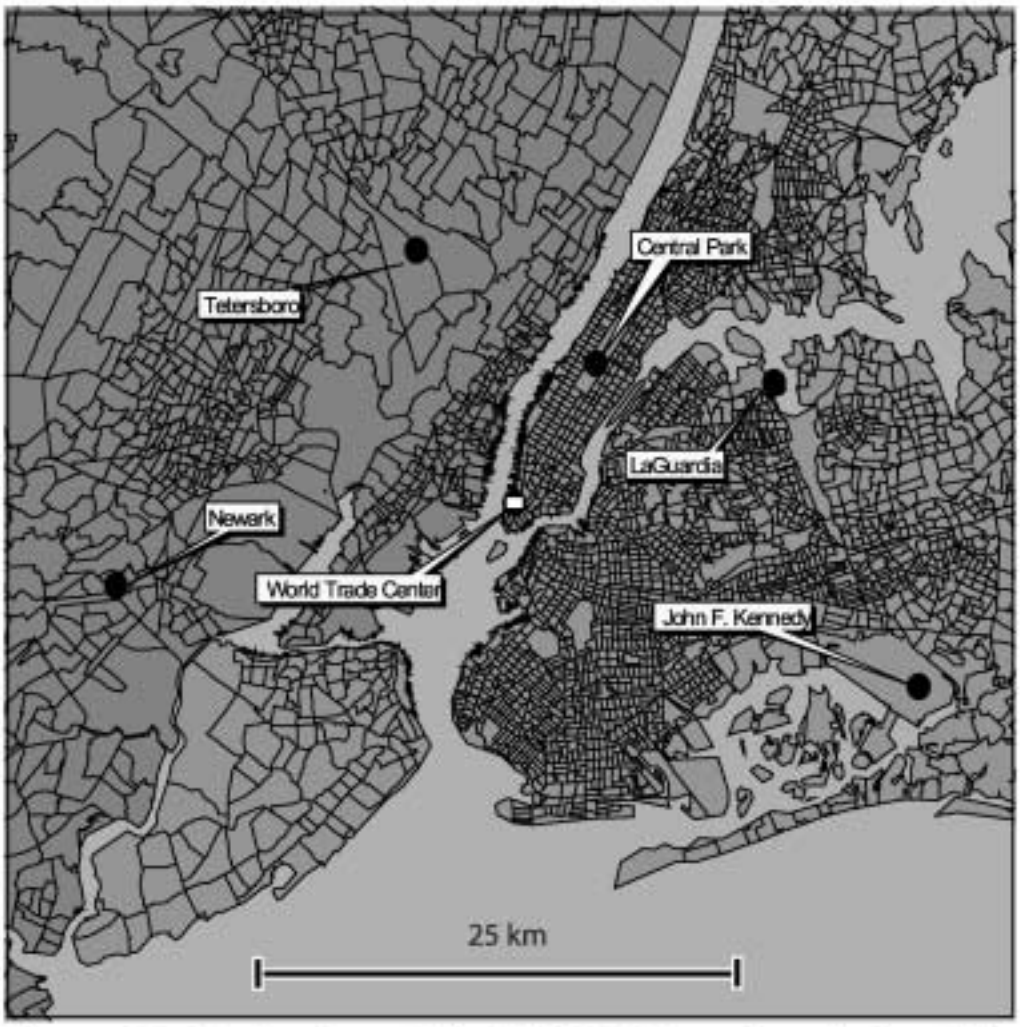

Figure 2.2 A plan view of the NWS ASOS stations depicted by solid black circles and the WTC observation site, labeled at the southern tip of Manhattan Island.

Figure 2.3 High resolution photograph of lower Manhattan on 12 September 2001. The instumentation cluster used in this study was located on Pier 25 (labeled MIC3 on the map).

CHAPTER 3

NUMERICAL SIMULATIONS

3.1 OVERVIEW OF THE MM5 MODELING SYSTEM

Two numerical weather prediction models were selected for simulating mesoscale boundary layer structure over New York City, the MM5 and ARPS. In this chapter, information and details on the configuration of the MM5 and ARPS models will be presented. These details include general model characteristics, model setup, and a detailed review of the physical parameterizations used in each numerical simulation.

The fifth-generation NCAR/ Penn State Mesoscale Model (MM5) is the latest version of a mesoscale model first used and developed at The Pennsylvania State University in the early 1970's. MM5 is a primitive equation model that uses a non-dimensional terrain-following σ-vertical coordinate system. Over the years, the model has been developed so that it now includes multiple-nests, nonhydrostatic dynamics, and a four dimensional data assimilation (FDDA) capability. Model performance has also been enhanced with the development of numerous physics options and the flexibility to run the model on several computer platforms, including SGI and Linux.

A flow chart showing the MM5 modeling system is shown in Figure 3.1. The flow chart breaks the MM5 modeling system into three components: 1. Main Programs, 2. Data Sets, and 3. Additional Capabilities. TERRAIN, REGRID, RAWINS, INTERPF, and MM5 are the main programs included in the MM5 model. Programs TERRAIN and REGRID interpolate terrestrial and isobaric atmospheric data in a latitude-longitude mesh to a variable high-resolution model domain. Projection options for the model domain

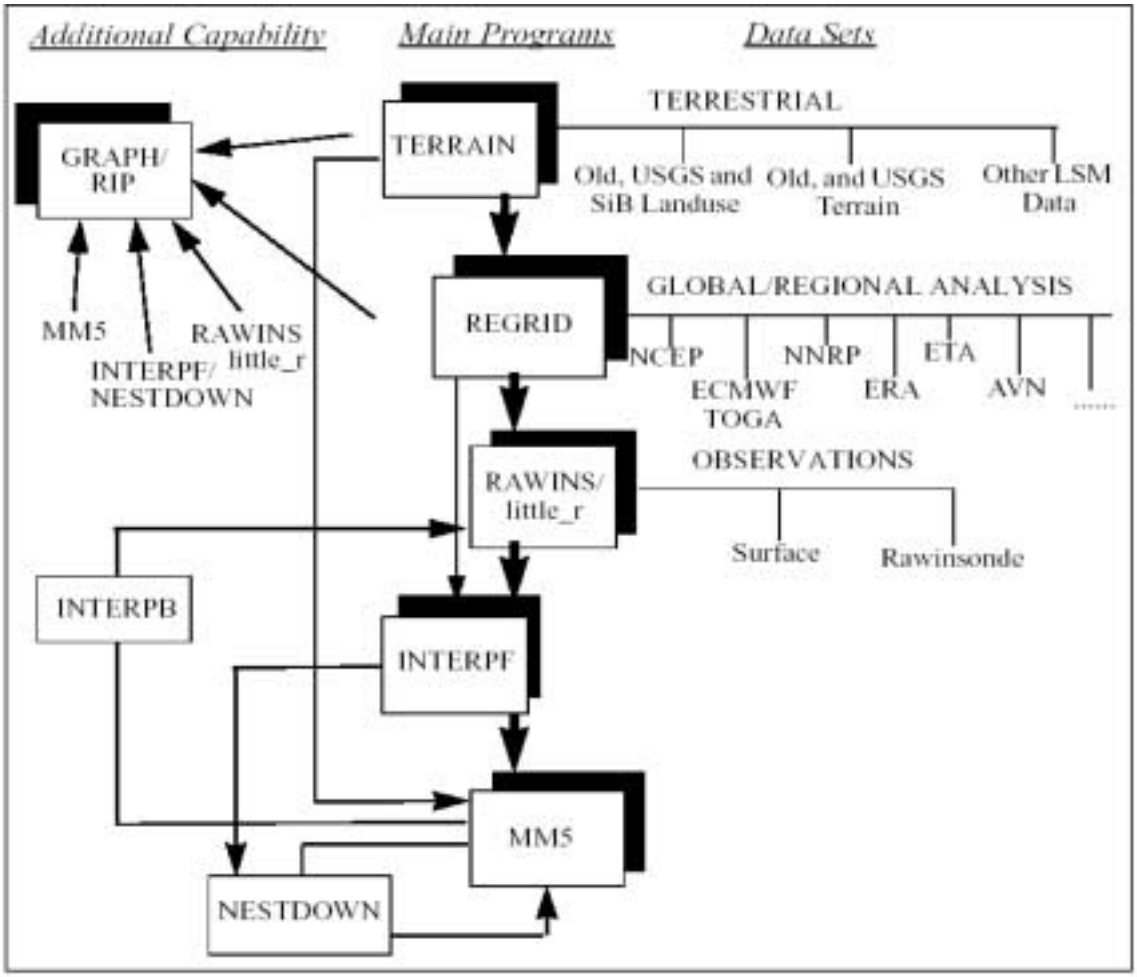

Figure 3.1 MM5 flow chart showing the main components of the MM5 modeling system.

include Mercator, Lambert Conformal, or Polar Stereographic. Mesoscale detail is added to the REGRID data with surface and upper air observations from the standard global network of surface and rawinsonde stations in the RAWINS program. Atmospheric data are then interpolated from pressure levels to the vertical sigma coordinate system using the INTERPF program. MM5 is the final main program and is the numerical weather prediction component of the model. The MM5 program includes the various physics options and the governing equations.

A triple nested model domain is created in TERRAIN and used for this numerical study. The Course Grid Mesh (CGM), Medium Grid Mesh (MGM), Fine Grid Mesh (FGM) and High-resolution Grid Mesh (HRGM) covered an area of (34.70°N-46.50°N; -82.10°W - -68.00°W), (37.80°N-43.00°N; -77.90°W - -70.80°W), (39.00°N-41.50°N; -76.05°W - -72.60°W), (39.90°N-41.00°N; -75.00°W - -73.90°W), respectively as shown in Figure 3.2. The horizontal resolutions for the CGM, MGM, FGM and HRGM are 27, 9, 3 and 1 km, respectively. Furthermore, the CGM, MGM, FGM and HRGM domains comprised of (52 x 56), (64 x 70), (76 x 82) and (100 x 100) grid points, respectively. All four domains had 37 vertical σ levels (between 1000hPa and 100hPa). The inner domain is arranged so that it is centered directly over lower Manhattan.

Atmospheric data interpolated in the REGRID and RAWINS programs must be converted from pressure levels to the sigma terrain following coordinate system. The formula for the dimensionless sigma level is given by:

$$\sigma = (p - p_t)/(p_s - p_t) \qquad (3.1)$$

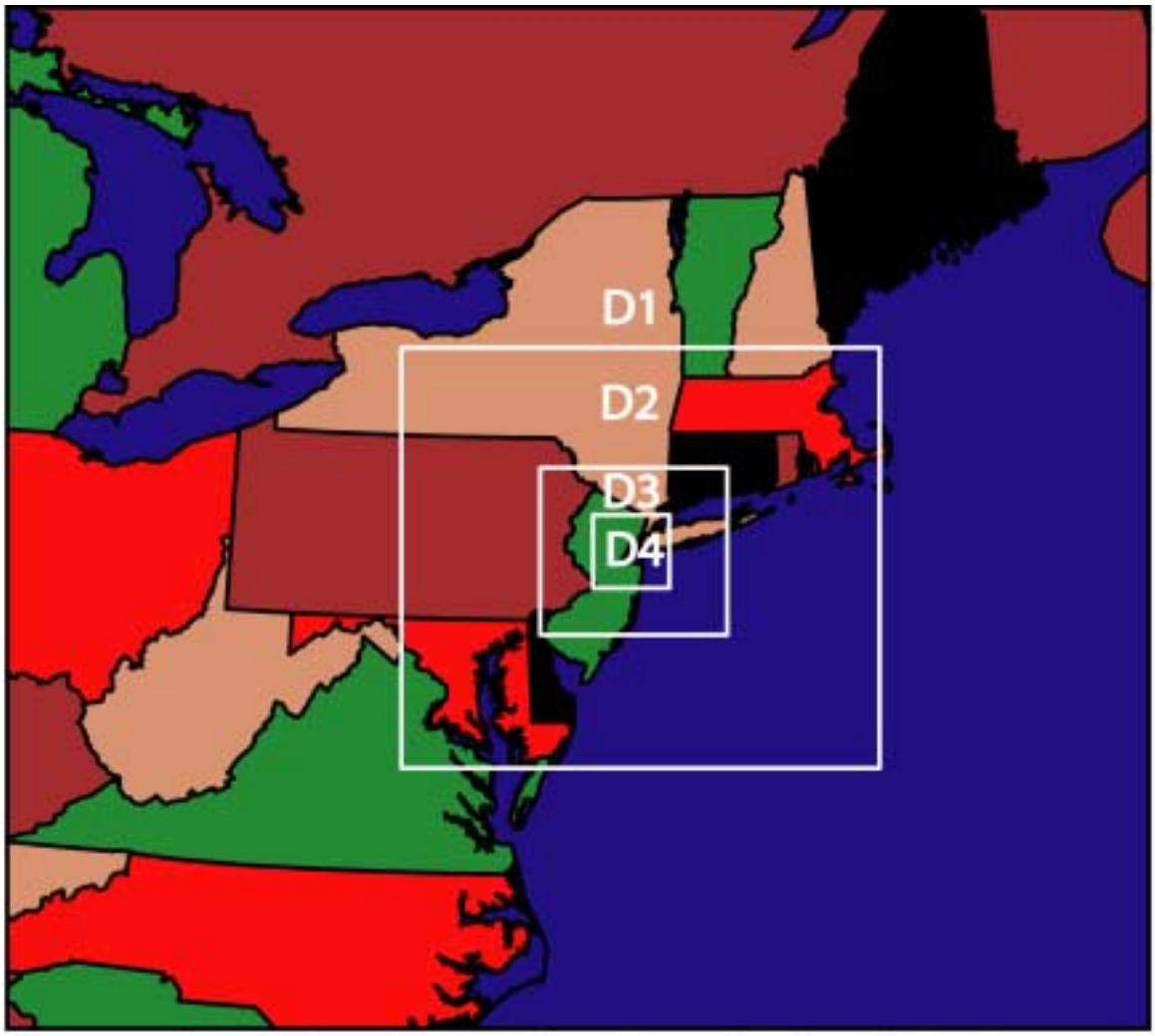

Figure 3.2 Triple-nested MM5 domain configuration used in this study. Domains are represented by the letter D. Domain 1 has a horizontal resolution of 27 km. Domain 2 has a horizontal resolution of 9 km. Domain 3 has a horizontal resolution of 3 km and Domain 4 has a horizontal resolution of 1km.

where p is the pressure, p_t is a specified constant top pressure, p_s is the surface pressure. Vertical sigma levels used for this study are shown in Table 3.1. All model domains have 37 vertical σ levels between 1000 mb and 100 mb with 18 of the levels below 850 hPa or 1.5 km.

3.2 INITIALIZATION AND BOUNDARY CONDITIONS

Eta model analyses, produced by the National Center for Environmental Prediction (NCEP) and archived by the National Center for Atmospheric Research (NCAR) were used to prescribe initial conditions. The resolution of the archived data is approximately 40 km. The above data are interpolated onto the model grid to serve as initial values and to provide lateral boundary conditions for the simulation. The analysis corresponding to 00 UTC 13 November 2001 was utilized as the initial condition. The model was integrated up to a period of 60h until 12 UTC 15 November 2001. This period was chosen because high values of ground-level pollutants were observed over the region. Additionally, the instrumentation cluster was fully operational to provide additional observational data to validate the numerical simulations.

MM5 uses data from the United States Geological Survey (USGS) database for terrain and landuse initialization. 10 min (19 km) global terrain and landuse files were used for the outermost domain while 5 min (9 km) global terrain and landuse files were used for the second domain. The third domain used 30 sec (.9 km) terrain and landuse

TABLE 3.1 Vertical sigma levels used in the MM5 simulation. Note that there are 18 sigma levels below 850 hPa to represent the planetary boundary layer.

Levels	Pressure(hPa)	Sigma	Levels	Pressure(hPa)	Sigma
1	1000	1.000	20	820	0.800
2	995	0.994	21	800	0.778
3	990	0.989	22	780	0.756
4	985	0.983	23	760	0.733
5	980	0.978	24	740	0.711
6	975	0.972	25	700	0.667
7	970	0.967	26	650	0.611
8	965	0.961	27	600	0.556
9	955	0.950	28	550	0.500
10	945	0.939	29	500	0.444
11	935	0.928	30	450	0.389
12	925	0.917	31	400	0.333
13	915	0.906	32	350	0.278
14	905	0.894	33	300	0.222
15	895	0.883	34	250	0.167
16	880	0.867	35	200	0.111
17	865	0.850	36	150	0.056
18	850	0.833	37	100	0.000
19	835	0.817			

data as did the innermost, (1 km) domain. Initialized topography for the model inner (1 km) domain is shown in Figure 3.3. A heterogeneous landuse is observed within the model region with the most interesting features being the urbanized landuse associated with the major urban corridor of the northeastern United States. A great deal of water is also present in the domain because of the Atlantic Ocean. The complex landuse and land-ocean interface will test the models ability to perform in a diverse landscape. Initialized terrain files include landuse files with 24 categories as shown in Table 3.2. The landuse categories determine values for albedo, moisture availability, emissivity, roughness length, and thermal inertia. Roughness length over the urban and built up region was changed from 0.5 m to 1.5 m to account for the highly urbanized landscape associated with New York City. The roughness length over the urban area was changed to better match observationally based estimations of roughness lengths presented in Chapter 4 of this thesis. Variables for landuse are given different values for summer and winter to account for changes in the landuse characteristics. The landuse file used for initializing the model innermost domain is shown in Figure 3.4. Some of the predominant landuse types present in the model outer domain include water (category 16), urban and built-up land (1), cropland/ grassland mosaic (5), and woodland grassland mosaic (6). This heterogeneous landuse pattern presents a challenge for the model to performance.

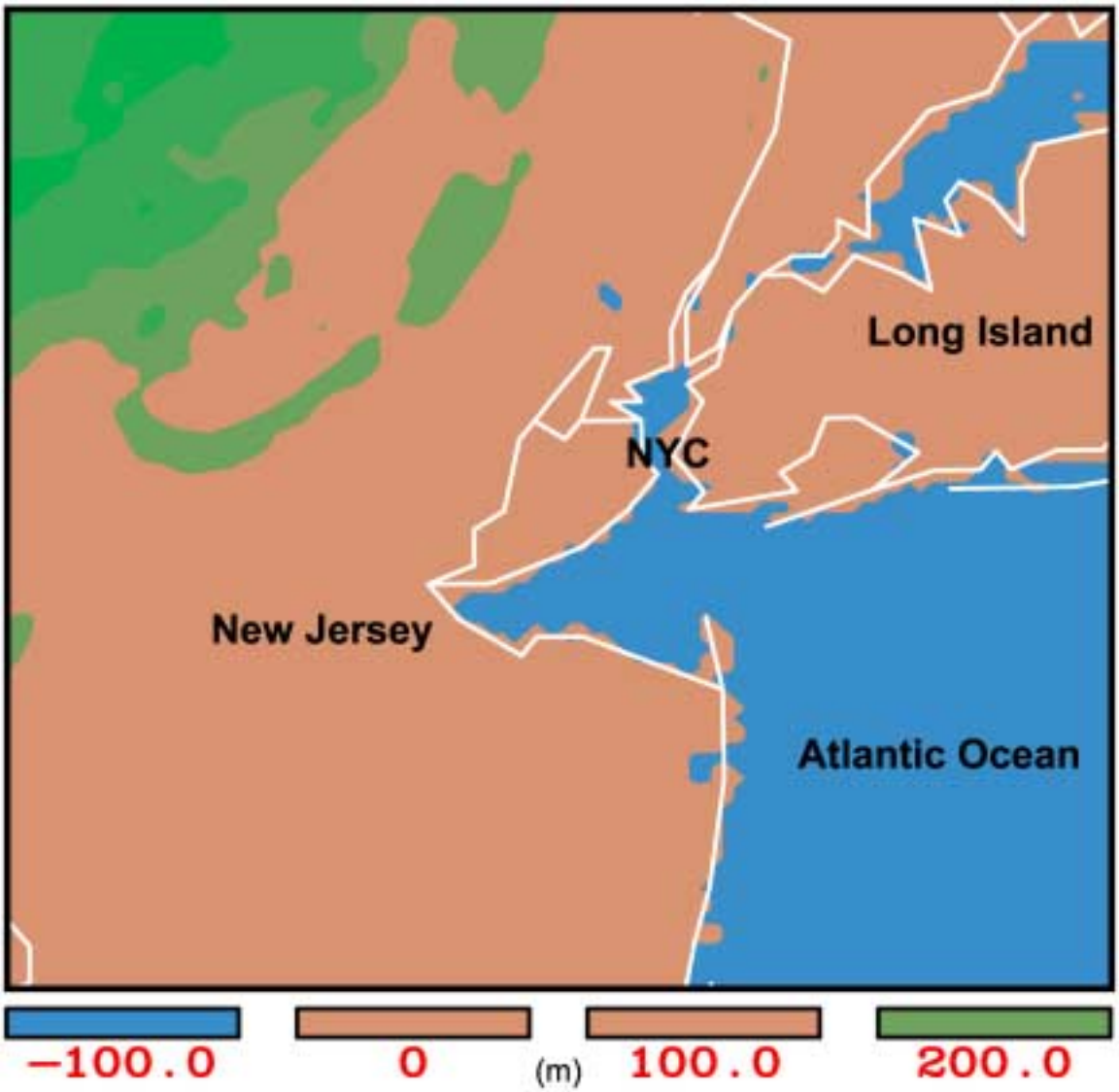

Figure 3.3 Plan view of the MM5 models .9 km topography data for the inner (1 km) domain over the New York city (NYC) area. The topography data is shaded in meters (m) above.

Table 3.2 USGS 24 category landuse input data for the MM5 simulation used in this study. Please note that all values were set to default except the roughness length over an urban area, which was adjusted from 75 cm to 150 cm.

Vegetation Integer Identification	Vegetation Description	Albedo (%)		Moisture Availability (%)		Emissivity (% at 9 mm)		Roughness Length (cm)		Thermal Inertia cal cm^2 k^-1 s^-1/2	
		Sum	Win	Sum	Win	Sum	Win	Sum	Win	Sum	Win
1	Urban	18	18	10	10	88	88	150		.03	
2	Drylnd Crop	17	23	30	60	92	92	15		.04	
3	Irrg. Crop	18	23	50	50	92	92	15		.04	
4	Mix. Dry. Irr	18	23	25	50	92	92	15		.04	
5	Crop./Grs.	18	23	25	40	92	92	14		.04	
6	Crop./Wood	16	20	35	60	93	93	20		.04	
7	Grassland	19	23	15	30	92	92	0.12		.03	.04
8	Shrubland	22	25	10	20	88	88	10		.03	.04
9	Mix Shrb.Gr	20	24	15	25	90	90	11		.03	.04
10	Savanna	20	20	15	15	92	92	15		.03	
11	Decid. Brdlf	16	17	30	60	93	93	50		.03	
12	Decid. Needl	14	15	30	60	94	93	50		.04	.05
13	Evergn.Brdlf	12	12	50	50	95	95	50		.04	.05
14	Evergn.Needl	12	12	30	60	95	95	50		.05	
15	Mixed Forest	13	14	30	60	94	94	50		.04	.05
16	Water Bodies	8	8	100	100	98	98	.01		.04	.06
17	Herb. Wetlnd	14	14	60	75	95	95	20		.06	
18	Wood. Wtlnd	14	14	35	70	95	95	40		.06	
19	Bar.Sps.Veg	25	25	2	50	85	85	10		.05	.06
20	Herb.Tundra	15	60	50	90	92	92	10		.02	
21	Wood.Tundra	15	50	50	90	93	93	30		.05	
22	Mixed.Tundra	15	55	50	90	92	92	15		.05	
23	Bare.Grd.Tndr	25	70	2	95	85	95	0.1	5	.02	.05
24	Snow/Ice	55	70	95	95	95	95	5		.05	

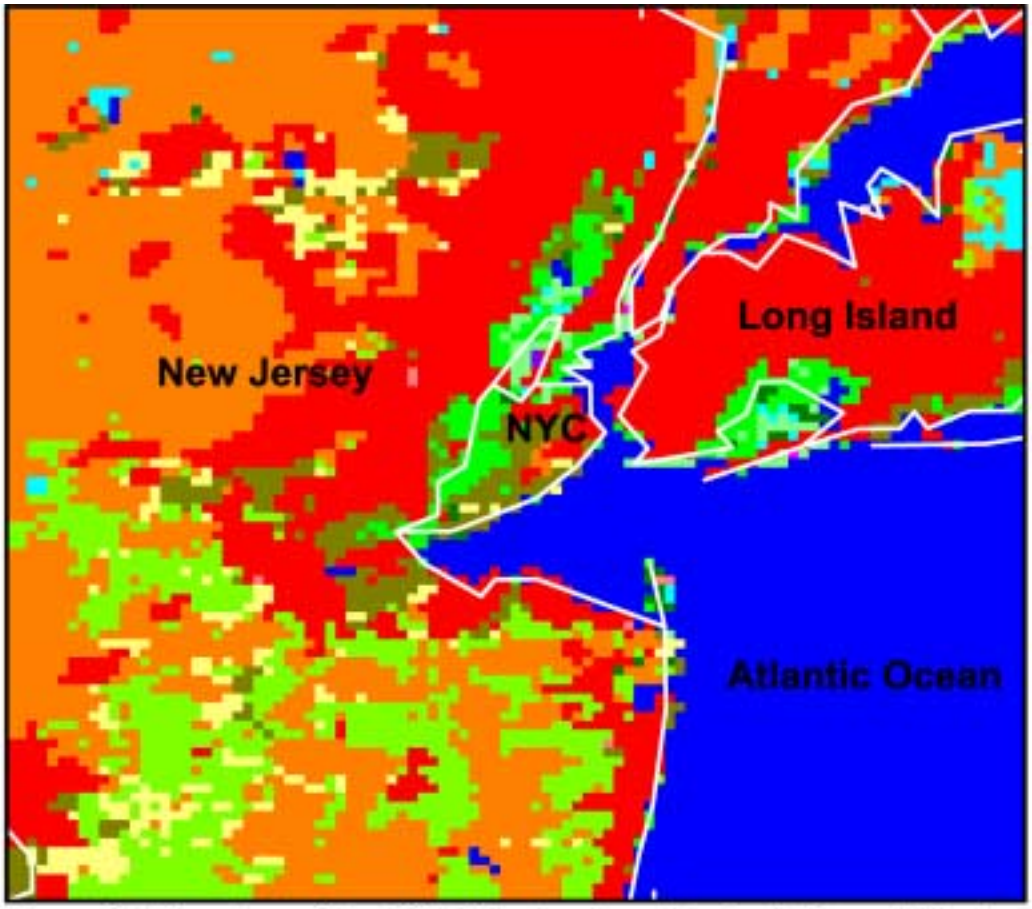

Figure 3.4 Plan view of the MM5 .9 km landuse data for the inner (1 km) domain. Dominant landuse categories over the New York City (NYC) area include water (blue shading), urban and built-up commercial (red shading), cropland and grassland mosaic (dark green shading) and woodland/grassland mosaic (light green).

3.3 MODEL GOVERNING EQUATIONS

The model's governing equations are found in the MM5 program, which is the numerical weather prediction part of the mesoscale modeling system. MM5's nonhydrostatic equations and physics options allow for research on large and small scales. Large-scale atmospheric phenomena such as monsoons and tropical systems and small-scale events such as fronts, land-sea breezes, and urban heat islands can all be simulated using MM5. Refer to the *List of Symbols* section of this thesis for a more complete listing of the following numerical variables. Equations 3.2 through 3.9 detail the governing equations used in the MM5 model. The governing equations will be separated into their respective components and identified below. The equations for the nonhydrostatic model's basic variables excluding moisture in terms of terrain following coordinates (x, y, *s*) are as follows:

Pressure

$$\frac{\partial p'}{\partial t} - \rho_0 g w + \gamma p \nabla \cdot \mathbf{V} = -\mathbf{V} \cdot \nabla p' + \frac{\gamma p}{T}\left(\frac{\dot{Q}}{c_p} + \frac{T_0}{\theta_0} D_\theta\right) \tag{3.2}$$

Momentum (x-component)

$$\frac{\partial u}{\partial t} + \frac{m}{\rho}\left(\frac{\partial p'}{\partial x} - \frac{\sigma}{p^*}\frac{\partial p^*}{\partial x}\frac{\partial p'}{\partial \sigma}\right) = -\mathbf{V} \cdot \nabla u + v\left(f + u\frac{\partial m}{\partial y} - v\frac{\partial m}{\partial x}\right) - ew\cos\alpha - \frac{uw}{r_{earth}} + D_u \tag{3.3}$$

Momentum (y-component)

$$\frac{\partial v}{\partial t} + \frac{m}{\rho}\left(\frac{\partial p'}{\partial y} - \frac{\sigma}{p^*}\frac{\partial p^*}{\partial y}\frac{\partial p'}{\partial \sigma}\right) = -\mathbf{V} \cdot \nabla v - u\left(f + u\frac{\partial m}{\partial y} - v\frac{\partial m}{\partial x}\right) + ew\sin\alpha - \frac{vw}{r_{earth}} + D_v \tag{3.4}$$

Momentum (z-component)

$$\frac{\partial w}{\partial t} - \frac{\rho_0}{\rho}\frac{g}{p^*}\frac{\partial p'}{\partial \sigma} + \frac{g p'}{\gamma p} = -\mathbf{V}\cdot\nabla w + g\frac{p_0}{p}\frac{T'}{T_0} - \frac{g R_d}{c_p}\frac{p'}{p} + e(u\cos\alpha - v\sin\alpha) + \frac{u^2+v^2}{r_{earth}} + D_w \tag{3.5}$$

Thermodynamics

$$\frac{\partial T}{\partial t} = -\mathbf{V}\cdot\nabla T + \frac{1}{\rho c_p}\left(\frac{\partial p'}{\partial t} + \mathbf{V}\cdot\nabla p' - \rho_0 g w\right) + \frac{\dot{Q}}{c_p} + \frac{T_0}{\theta_0}D_\theta \tag{3.6}$$

Advection terms can be expanded as

$$\mathbf{V}\cdot\nabla A \equiv mu\frac{\partial A}{\partial x} + mv\frac{\partial A}{\partial y} + \dot{\sigma}\frac{\partial A}{\partial \sigma} \tag{3.7}$$

where

$$\dot{\sigma} = -\frac{\rho_0 g}{p^*}w - \frac{m\sigma}{p^*}\frac{\partial p^*}{\partial x}u - \frac{m\sigma}{p^*}\frac{\partial p^*}{\partial y}v \tag{3.8}$$

Divergence term can be expanded as

$$\nabla\cdot\mathbf{V} = m^2\frac{\partial}{\partial x}\left(\frac{u}{m}\right) - \frac{m\sigma}{p^*}\frac{\partial p^*}{\partial x}\frac{\partial u}{\partial \sigma} + m^2\frac{\partial}{\partial y}\left(\frac{v}{m}\right) - \frac{m\sigma}{p^*}\frac{\partial p^*}{\partial y}\frac{\partial v}{\partial \sigma} - \frac{\rho_0 g}{p^*}\frac{\partial w}{\partial \sigma} \tag{3.9}$$

3.4 MODEL PHYSICAL SCHEMES

Table 3.3 shows the MM5 physics configuration used in this study. The model simulation for this research uses surface layer similarity for the constant flux layer and the Eta Mellor-Yamada (Eta M-Y) planetary boundary layer (PBL) parameterization scheme for the mixed layer (Betts and Chen 1997). The Eta M-Y is a 2.5 level 1.5-order TKE closure model used in NCEP's operational Eta model.

Table 3.3 MM5 physics configuration used in this study.

PBL Model	Explicit Moisture Physics	Cumulus Physics	Radiation Physics	Land Surface Model
Eta Mellor-Yamada	Simple Ice	Kain-Fritsch (27, 9 km only)	Cloud Radiation	NOAH

The scheme requires a prediction equation for the turbulent kinetic energy (TKE), and parameterization of TKE sources and sinks for each model layer. Prediction of the TKE gives better representation of mixing by sub-grid scale eddies that develop as a result of vertical wind shear. Since the diffusion rates at each model layer in the PBL are determined by the wind, moisture, and temperature conditions at the layer's top and bottom interfaces, the PBL closure is considered to be **local**. The mixing that is emulated in each time step only takes place through the interface between adjacent model layers. The scheme also requires a soil model that calculates ground temperature at multiple levels.

The model uses explicit equations for cloud water, rainwater, ice and water vapor. The Simple Ice scheme was used to account for the ice phase processes. There is no supercooled water and immediate melting of snow below the freezing level.

The Kain-Fritsch cumulus parameterization scheme was used account for sub-grid scale convection (Kain *et al*., 1993) in the 27 and 9 km domains, while the innermost domains, 3 and 1 km, used only explicit moisture physics to account for precipitation processes. The Kain-Fritsch parameterization is a complex cloud-mixing scheme that is capable of solving for entrainment and detrainment processes. The scheme also removes the available buoyant energy in the relaxation time. Updraft and downdraft properties are also predicted. The influence of shear effects on the precipitation efficiency is also considered by the Kain-Fritsch scheme. No precipitation was observed over the region during the study period presented.

A cloud-radiation scheme was used to account for the interaction of shortwave and longwave radiation with clouds and the clear air. The scheme provides an important

contribution in simulating the atmospheric temperature tendencies. Surface radiation fluxes are also considered in this scheme.

The NOAH Land Surface Model (LSM) was used to represent land surface processes. **NOAH** stands for **N**ational Centers for Environmental Prediction (NCEP), **O**regon State University (Dept of Atmospheric Sciences), **A**ir Force (both AFWA and AFRL - formerly AFGL, PL) and **H**ydrologic Research Lab land surface model. The NOAH LSM is the latest high-resolution land surface model developed and implemented by NCAR and NCEP scientists (Ek et al. 2003). The NOAH (LSM) predicts soil temperature and soil moisture at 4 levels (10, 30, 60 and 100 cm). Soil water/ice, canopy water and snow cover are also predicted. The soil heat flux explicitly includes contributions from both the snow and non-snow covered portions of a model gridbox. The scheme is capable of resolving diurnal temperature variations that result in a more rapid response from the surface temperature. The NOAH LSM is an updated version of the Oregon State University (OSU) LSM and will soon (Fall 2003) be fully implemented into the operational Eta model developed and run by NCEP. The NOAH LSM was implemented with revised equations for bare soil evaporation and soil thermal conductivity.

3.5 OVERVIEW OF THE ARPS MODELING SYSTEM

ARPS (Advanced Regional Prediction System) is a mesoscale meteorological model developed by the Center for Analysis and Prediction of Storms (CAPS); a group formed by atmospheric scientists at the University of Oklahoma in 1989. The National Science Foundation provided funding for this group. Their objective was to develop a mesoscale meteorological model that will be capable of modeling storm scale phenomena

for both research and operational interests. ARPS was selected for this research because of its advanced physical and numerical schemes. The ARPS model is written in FORTRAN code, which is compatible with most computational platforms. The ARPS also has options to simulate idealized cases, typically used for research applications. The ARPS modeling suite includes both preprocessing and post processing programs to create terrain, landuse characterization, external boundary conditions as well as output options for various environmental visualization software packages including Grads, Vis-5D and many others. In addition to the above features, the ARPS model contains a preprocessing code to assimilate a variety of observations including National Weather Service WSR-88D radar, satellite data and wind profiler data.

ARPS is a non-hydrostatic, fully compressible primitive equation model suitable for simulating weather phenomena ranging in size from several meters to several kilometers (Xue et al. 1995). The ARPS uses a terrain following vertical coordinate system with options for stretched or equal spacing while the horizontal grid spacing is equal in both the x and y directions. Additional grid options for 1-D, 2-D or 3-D simulations are included. Prognostic variables include 3-D wind components, potential temperature, pressure, sub-grid scale TKE and moisture related variables (specific humidity, cloud ice, graupel and hail).

3.6 NUMERICAL DETAILS

3.6.1 NUMERICAL METHODS

There are a variety of integration and numerical techniques available in the ARPS model, and the options used in this study are presented below. Time integration for the model simulations is split into large and small time steps. The small time step is used to compute acoustically active terms such as pressure and vertical velocity perturbations. A fully implicit scheme is used for this integration, which allows computational stability constraints to limit only the large time step. All other variables are forecasted using a large time step with a fully explicit, three-level, leapfrog method with Asselin time filter option. Spatial derivatives are estimated using 2^{nd} order accurate finite difference except for advection terms, which are accurate to the 4^{th} order. Numerical noise is dampened using computational smoothing. The ARPS simulation uses a 4^{th} order-mixing coefficient in both the horizontal (x-y) and vertical (z) direction.

3.6.2 ARPS MODEL PHYSICS

Table 3.4 shows the ARPS model physics used in this simulation. The ARPS simulation uses a 1.5-order TKE turbulence closure scheme developed by Sun and Chang (1986). In this scheme a budget equation for subgrid scale TKE is solved which includes buoyancy, shear production, advection (diffusion and transport) and viscous dissipation. The Lin-Tao 3 Category Ice (Lin et al. 1983) explicit moisture scheme is included along with the Kain Fritsch cumulus parameterization (Kain and Fritsch, 1993) in the 32 km domain. Implicit moisture physics are not used in the 5 and 1 km simulations.

Table 3.4 ARPS physics configuration used in this study.

Explicit Moisture Physics	Cumulus Physics	Radiation Physics	Land Surface Model	PBL Model	Mixing Height Estimation	Mixing	Domain Setup
Lin et al.	Kain-Fritsch	Goddard Longwave	Noilhan Planton	Sun and Chang	Solved Directly by TKE	Non-Local	32,5,1 km

Radiation physics are simulated using the atmospheric radiation transfer parameterization developed at NASA/Goddard Space Flight Center, which is tailored for use in the ARPS model. This scheme includes equations for both short wave (Chou, 1990, Chou, 1992) and long wave (Chou and Suarez, 1994) radiation processes. Refer to Xue et al. (1995), Xue et al. (2000) and Xue et al. (2001) for further details related to the above formulations. The Noilhan-Planton Land Surface Model is used to represent land surface processes over the region.

3.6.3 ARPS DYNAMICAL FRAMEWORK

The ARPS model is a nonhydrostatic mesoscale prediction model appropriate for use on scales ranging from a few meters (microbursts) to hundreds of kilometers (hurricanes). It is based on compressible Navier-Stokes equations describing atmospheric flow, and uses a generalized terrain-following coordinate system. The governing equations of the ARPS include momentum, heat (potential temperature), mass (pressure), water substances, turbulent kinetic energy (TKE), and the equation of state. These equations are represented in a curvilinear coordinate system, which is orthogonal in the horizontal. The governing equations used in the ARPS model are the result of a direct transformation from the Cartesian coordinate system, and are expressed in a fully conservative form. ARPS solves prognostic equations for u, v, w, q', p' and q y, which are the x, y and z components of the Cartesian velocity, respectively. Additionally, ARPS solves for the perturbation potential temperature and perturbation pressure, and six categories of water substance (water vapor, cloud water, rainwater, cloud ice, snow, and hail). A list of the governing equations in the ARPS model is outlined below. Refer to the *List of Symbols*

section of this Thesis for a more complete listing of the following numerical variables. Equations 3.10 through 3.16 details the governing equations used in the ARPS model. The governing equations will be separated into their respective components and identified below.

(3.10) Equation of state for an atmosphere containing water constituents

$$\rho = p\, Rd\ \ T\ \ (1 - qve + qv\ )(1 + qv + qliquid + qice\ water\ )$$

(3.11) Momentum (x-component)

$$\frac{\partial u^*}{\partial t} = -\left[u^* \frac{\partial u}{\partial \xi} + v^* \frac{\partial u}{\partial \eta} + W^* \frac{\partial u}{\partial \zeta} \right]$$
$$- \left[\frac{\partial}{\partial \xi} \left\{ J_3 (p' \alpha Div^*) \right\} + \frac{\partial}{\partial \zeta} \left\{ J_1 \ (p' \alpha Div^*) \right\} \right]$$
$$+ \left[\rho^* f v - \rho^* f w \right] + \sqrt{G}\, D_u ,$$

(3.12) Momentum (y-component)

$$\frac{\partial v^*}{\partial t} = -\left[u^* \frac{\partial v}{\partial \xi} + v^* \frac{\partial v}{\partial \eta} + W^* \frac{\partial v}{\partial \zeta} \right]$$
$$- \left[\frac{\partial}{\partial \eta} \left\{ J_3 (p' \alpha Div^*) \right\} + \frac{\partial}{\partial \zeta} \left\{ J_2 \ (p' \alpha Div^*) \right\} \right]$$
$$- \rho^* f u + \sqrt{G}\, D_v ,$$

(3.13) Momentum (z-component)

$$\frac{\partial w}{\partial t} - \frac{\rho_0}{\rho}\frac{g}{p^*}\frac{\partial p'}{\partial \sigma} + \frac{g p'}{\gamma p} = -\mathbf{v}\cdot\nabla w + g\frac{p_0}{p}\frac{T'}{T_0} - \frac{g R_d}{c_p}\frac{p'}{p} + e(u\cos\alpha - v\sin\alpha) + \frac{u^2+v^2}{r_{earth}} + D_w$$

(3.14) Thermodynamics Equation

$$\frac{\partial}{\partial t}(\rho^* \theta \dot{E}) = \pm\left[u^* \frac{\partial \theta \dot{E}}{\partial \xi} + v^* \frac{\partial \theta \dot{E}}{\partial \eta} + W^{c*} \frac{\partial \theta \dot{E}}{\partial \zeta}\right] \pm\left[\rho^* w \frac{\partial \bar{\theta}}{\partial z}\right] + \sqrt{G}\, D_\theta + \sqrt{G}\, S_\theta .$$

(3.15) Divergence can be expanded from

$$\frac{\partial}{\partial t}(J_3 p\dot{E}) = -\left[(J_3 u)\frac{\partial p\dot{E}}{\partial \xi} + (J_3 v)\frac{\partial p\dot{E}}{\partial \eta} + (J_3 W^c)\frac{\partial p\dot{E}}{\partial \zeta}\right] + J_3 \bar{\rho} g w - \bar{\rho} c_s^2\left[\frac{\partial}{\partial \xi}(J_3 u) + \frac{\partial}{\partial \eta}(J_3 v) + \frac{\partial}{\partial \zeta}(J_3 W^c)\right] + J_3 \bar{\rho} c_s^2\left[\frac{1}{\theta}\frac{d\theta}{dt} - \frac{1}{E}\frac{dE}{dt}\right],$$

Divergence can be expanded from

$$\frac{\partial}{\partial t}(Div^*) = \alpha \nabla^2 (Div^*) + \ldots$$

to include advection

(3.16) Conservation equations of water phase mixing ratios

$$\frac{\partial}{\partial t}(\rho^* q_\psi) = \pm\left[u^* \frac{\partial q_\psi}{\partial \xi} + u^* \frac{\partial q_\psi}{\partial \eta} + W^{c*} \frac{\partial q_\psi}{\partial \zeta}\right] + \frac{\partial(\rho^* V_{q_\psi} q_\psi)}{\partial \zeta} + \sqrt{G}\, D_{q_\psi} + \sqrt{G}\, S_{q_\psi}$$

3.6.4 INITIALIZATION AND BOUNDARY CONDITIONS

Initialization and boundary conditions are some of the most important aspects of numerical modeling. ARPS is very flexible, with numerous options for initial conditions and boundary conditions. Options are embedded to define an idealized initial state including: constant static stability, constant potential temperature and even a single sounding. These options allow for idealized simulations including density currents (Xue et al., 1998), storm cells, and seabreeze fronts (Gilliam et al., 2003). Additional options allow ARPS to be initialized using more realistic data from many of the available operational models including Global Forecast System model (GFS), Eta, Rapid Update Cycle (RUC), ARPS and COAMPS data. This research takes advantage of the realistic initialization using the 32 km ARPS model analysis, provided by the CAPS group, to generate an intermediate 5 km ARPS domain centered over New York City.

Boundary conditions (BC) are necessary for all limited domain models including such models as the MM5, ARPS and Eta models. In ARPS, five options are available for lateral boundary conditions. These include wall BC, periodic BC, zero gradient BC, open (radiative) BC and external BC from another model. The external BC option is used in this study. For the 1 km simulations over New York City, the 5 km simulation provides initial and boundary conditions. The inner ARPS domain is shown in Figure 3.5. The inner domain is (50 x 50) grid points with 37 vertical sigma levels. The ARPS landuse data are shown in Figure 3.6. The data are regridded to evenly fit onto the ARPS grid. The predominant landuse characteristics are identical to that found in the MM5 model and the reader is referred to the MM5 discussion above. Roughness length over the urban and built up region was changed from 0.5 m to 1.5 m to account for the highly urbanized

landscape associated with New York City and to match roughness length estimations presented in Chapter 4 of this thesis. An ARPS preprocessing program, *ext2arps,* extracts the values of the prognostic variables at specified time intervals for the outer edges of the grid domain. A linear interpolation is performed between the extracted time periods so that boundary condition values are available for each time step.

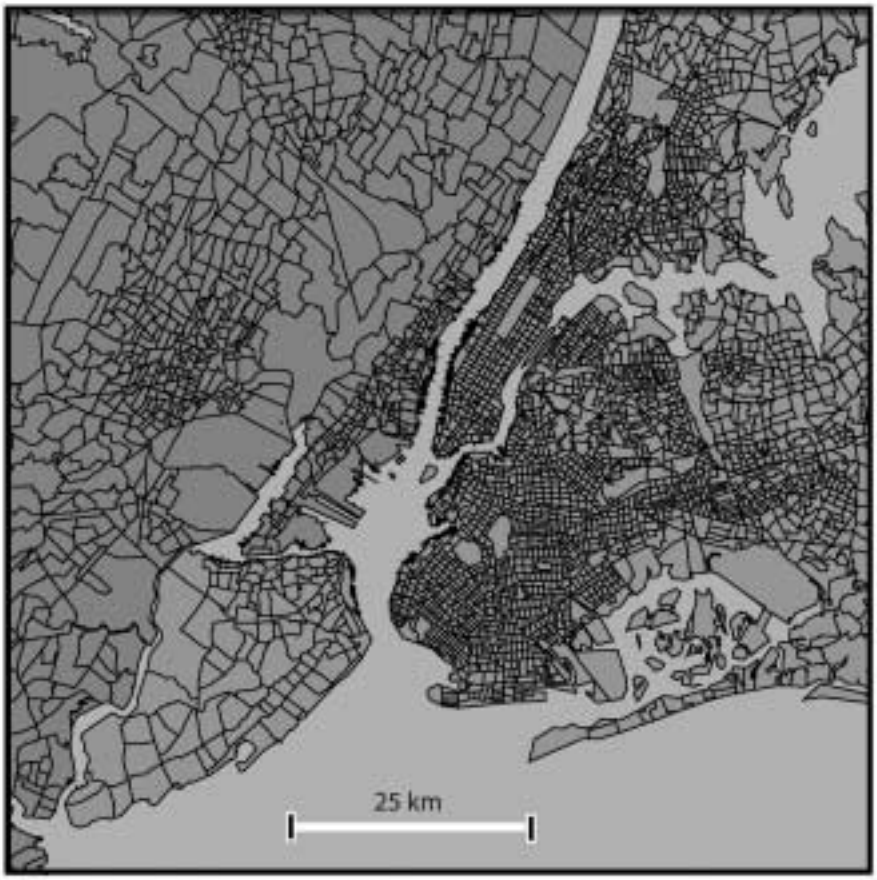

Figure 3.5 Plan view of the ARPS model domain over the New York City area. Horizontal resolution is 1 km.

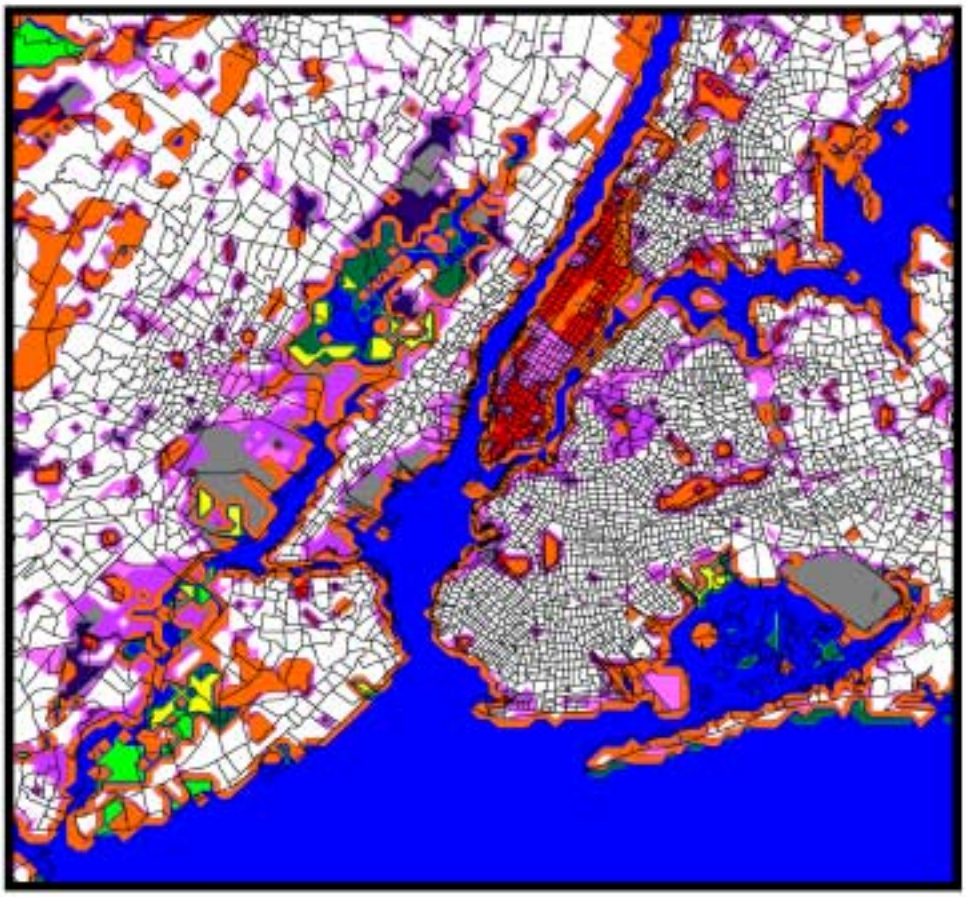

Figure 3.6 USGS landuse parameterization for the New York City ARPS domain. Landuse specification is at a grid spacing .9 km in the ARPS simulation. Please refer to **Table 3.2** for more landuse characterstics.

CHAPTER 4

OBSERVATIONAL ANALYSIS

4.1 INTRODUCTION

A detailed observational analysis over the New York City area is one of the objectives of this study. This study spans the time period from 10 September 2001 through 10 April 2002, with the focus being 10 September 2001 through 10 December 2001 in this research. Observations from five National Weather Service (NWS) ASOS sites will be used in this study as detailed in Chapter 2. A plan view of the New York City area with the ASOS locations overlayed in white is shown in Figure 2.2. Additional data from an instrumentation cluster, deployed by the EPA and The State Climate Office of North Carolina (SCO), near the WTC recovery site in lower Manhattan will be analyzed. Figure 2.1 shows a plan view of the lower Manhattan area with the location of the EPA/SCO instrumentation systems overlayed in black. The cluster consisted of two Sound Detection and Ranging (SODAR) systems and a three-level micrometeorological tower. The instruments were activated on November 08, 2001, providing several months of micro-meteorological data during this study period. Data from the SODAR and 10 m micro-meteorological tower are archived in the SCO. The following section will give a brief overview of the format and structure of this database.

4.2 BOUNDARY LAYER MONITORING DATABASE

The State Climate Office of North Carolina maintains a complete database for the independent instrumentation cluster used in this study. Various meteorological parameters can be accessed from the database, including multilevel temperature, wind and relative humidity data from the 10 m micro-meteorological tower. Additionally, multilevel u, v and w wind velocity components as well as component standard deviations from the Model 2000 and Model 4000 SODARs can be accessed from the database. The data are updated twice a day through a PERL-driven ftp script. Several platforms are available to access the database, including an interactive webpage, as well as a user customized MySQL query interface. The database is a private, password-protected system, quality controlled and maintained by The State Climate Office of North Carolina.

4.3 OVERVIEW OF INSTRUMENTATION

The instrumentation cluster used in this study consisted of two SODARs and a 10 m micro-meteorological tower. The SODAR's consisted of the Aerovironment Model 4000 (miniSODAR) and the Aerovironment Model 2000 SODAR. The miniSODAR is a high-resolution surface layer (15 to 200 m range at 5 meter intervals, 10 min averaged) wind sampler. It transmits sound at a frequency of 4500 Hz. The Model 2000 SODAR measures the same wind properties as the miniSODAR from 60 to 600 m at 30 m intervals, and averaged over a 10 min period. The 10 m micrometeorological tower has instruments that measure wind (Young Model 05701 anemometer) at 2, 5 and 10 m along

with temperature and relative humidity (Gill aspirated Model 43408) at 2 and 10 m and is averaged over a 10 min period.

Hourly surface observations from five National Weather Service Automated Surface Observing System (ASOS) stations are also used in this study. Quality controlled hourly ASOS data were acquired from the National Climatic Data Center (NCDC) for the study period. The ASOS 10 m wind and 2 m temperature data are recorded every minute and are representative of the previous 5 min average. The data are recorded at the bottom of the hour, approximately 51 minutes past each hour.

4.4 SYNOPTIC ANALYSES

The synoptic conditions over a three-month study period (September 11, 2001 - December 15, 2001) have been classified for each day into one of seven climatological flow regimes that normally exists during the fall season, or classified as “other” for complicated synoptic occurrences. Seasonal weather patterns affect the local meteorology and dispersion of pollutants in NYC. Over NYC the mesoscale boundary layer structure and stability vary both seasonally and during different synoptic flow situations. Climatologically, a weather system passes on average every 4-6 days (Brown and SethuRaman, 1981) during the fall season. This cycle, starting after a cold front passage, typically includes a day of moderate to strong (>4-5 m/s) N-NW winds; followed by a transition day where the wind decreases as it veers from northerly to northeasterly. Next, the region experiences a day where high pressure is centered near or directly over the area and winds become light and variable. Following this, the high pressure system moves east and winds turn southerly but remain light for a day, then as another frontal

boundary approaches from the west, southwest winds increase to moderate levels. Based upon this evolution, all days during the study period have been categorized as one of these flow regimes, except for a limited few that could not be justly grouped into the above classification. These "other" days were mostly situations when either a strong low pressure system impacted the area or frontal boundaries oscillated over the region, resulting in drastic wind shifts. Figure 4.1a shows a pie chart illustrating the synoptic flow regimes observed over the New York City region between 10 September 2001 and 10 December 2001. Seven synoptic flow regimes, along with an “other” category for complex flow patterns, are analyzed in Figure 4.1a. The categories are southerly, westerly and northerly with these further divided by the estimated flow strength (light or strong). The light and strong flow classification was determined by the critical wind speed of 4.0 m s^{-1} that has been linked to the urban heat island (Bornstein and Johnson, 1977) and sea breeze development (Arritt, 1993). The flow strength and direction were subjectively determined by examining six-hourly synoptic charts provided by the NCEP and surface observations. The data is then classified based on a daily average of the wind speed and direction. The range of wind flow for northerly regimes was defined as flow from 310º to 20º, westerly flow from 250º to 300º and southerly flow from 180º to 250º. Additionally, a light and variable and an “other” classification were included. Four flow regimes dominated: light southerly (18%), strong southerly (18%), strong westerly flow (17%), and light and variable flow (16%). These regimes occurred on 70 % of the days. The remaining periods were light westerly (9%), light northerly (6%), strong northerly (7%) and other (9%), respectively. A wind rose valid 10 September 2001 through 10 December 2001 is shown in Figure 4.1b.

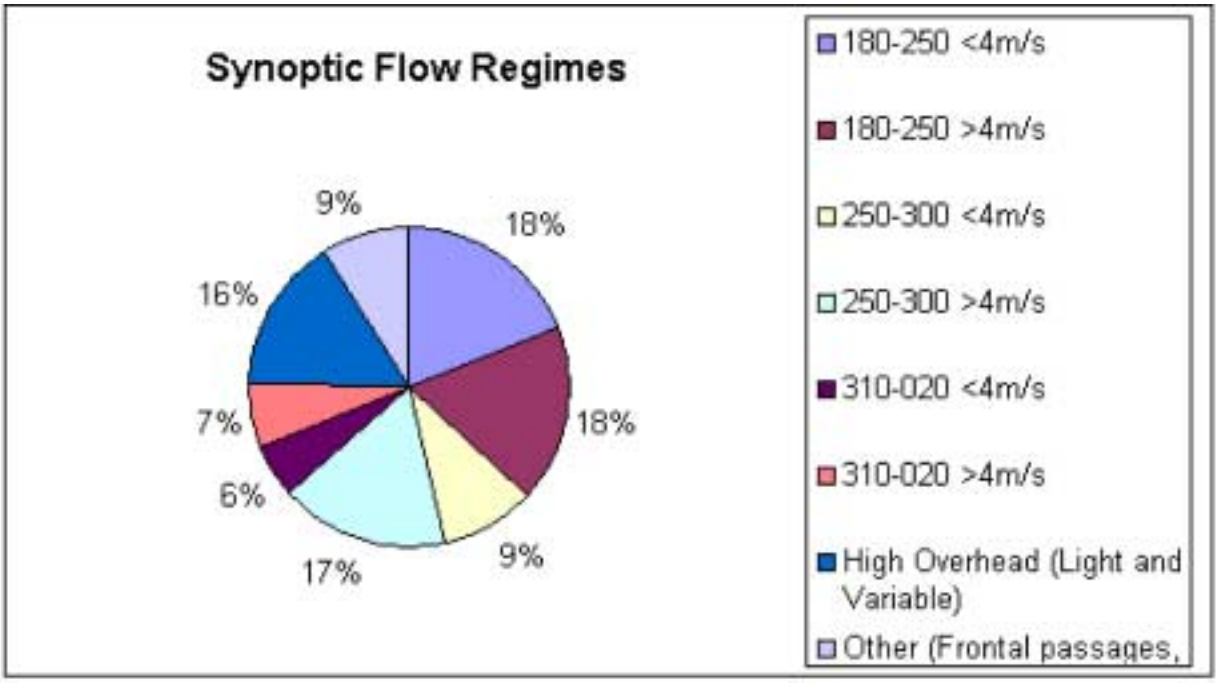

Figure 4.1a Pie chart illustrating the synoptic flow regimes observed over the New York City region between 10 September 2001 and 10 December 2001. Seven synoptic flow regimes are identified above along with an "other" category for very complex flow patterns.

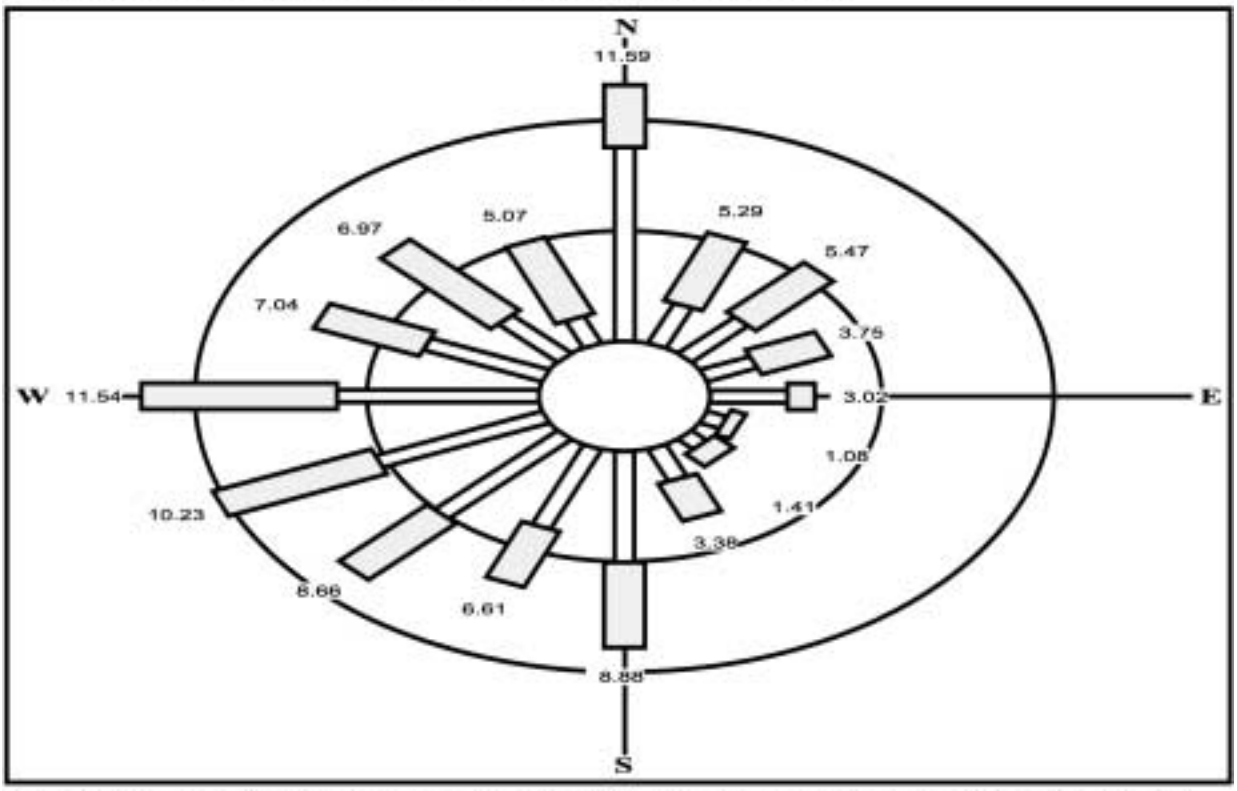

Figure 4.1b Wind Rose showing the distribution of wind speed and direction over the New York City area valid 10 September 2001 through 10 December 2001. Distribution rings are contoured every 5%.

Hourly observations from Newark, Central Park, LaGuardia and JKF ASOS sites valid 10 September 2001 through 10 December 2001 were used to create the wind rose. Distribution rings are labeled every 5% with wind speed ranges defined as above and below 4 m/s, which was discussed above. The wind rose shows that a large percentage (35 %) of wind speeds greater than 4 m/s came from a direction between southwest and northwest. Additionally, the wind rose shows that lighter winds were typically observed when the synoptic flow was out of the north and northeast.

4.5 EFFECTS OF SURFACE ROUGHNESS LENGTH ON WIND FLOW OVER LOWER MANHATTAN

Large aerodynamic roughness length variations are often observed over highly urbanized terrain, such as New York City. These variations can significantly affect the surface wind flow, causing a reduction in speed, turning of the wind flow, or both. The effect of the urbanized terrain on the surface wind flow over New York City is highly dependent on the mesoscale scale flow direction. In order to quantify this effect, aerodynamic roughness length will be calculated over lower Manhattan and separated into one of four flow regimes. These flows regimes will include 0-89º, 90-179º, 180-269º and 270-359º. The 0-89º flow moves over the urban core of central Manhattan before reaching the WTC site, while the 90-179º flow moves over the urban core of lower Manhattan before reaching the WTC site. The 180-269º flow moves over the Staten Island and the Hudson River before reaching the WTC site while the 270-359º flow moves over the Hudson River and portions of Manhattan Island before reaching the WTC site. Data from the independent 10 m tower over lower Manhattan are used to identify

each flow regime. Additionally, the MiniSODAR, located in the vicinity of the 10 m tower, will be used in the aerodynamic roughness length calculation. The 10 m tower and miniSODAR became operational on 8 November 2001. The wind velocity data for the separate flow regimes is averaged over the last month of the study period, November 10 through December 10, 2001. Wind speed and direction are averaged separately over 24 hr periods (00 UTC to 00 UTC), then classified into the appropriate flow regime based on the above conditions. Four 24 hr periods were observed for the 0-89 deg flow regime, while six 24 hr periods were classified in the 90-179 deg flow classification. Ten 24 hr periods were classified into 180-269 deg flow regime, while twelve 24 hr periods were classified into the 270-359 deg flow regime. The data were averaged over 24 hr periods to mitigate the affects of missing data from the miniSODAR. Several methods are available to determine z_o. One of the most common methods of empirically estimating roughness length is based on the logarithmic wind profile equation (4.1) below, where u_* is the friction velocity, d_o is the zero-plane displacement and k is the von Karman constant which is considered a universal constant for all surface or wall layers, and is empirically estimated to be 0.40 (Arya 1988).

$$U/u_* = (1/k) \ln (z-d_o/z_o) \qquad (4.1)$$

Here, we calculate roughness length graphically by plotting ln z versus U and extrapolating the best-fitted straight line down to the point where U=0, its intercept on the ordinate axis being ln z_o. In the derivation of equation (4.1), $z_o << z$. 10 m wind data from the independent tower will be used in this calculation, supplemented by low level wind data from the high resolution miniSODAR.

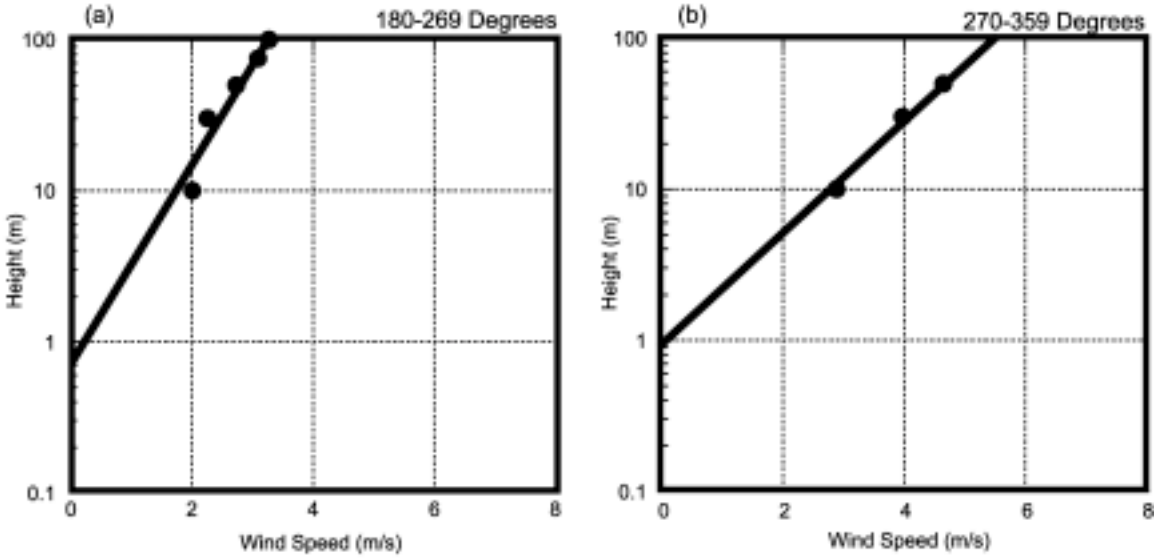

Figure 4.2 Averaged aerodynamic roughness length (m) calculated for two independent flow directions covering the period 10 November 2001 through 10 December 2001. **(a)** shows the 180-269 degree flow direction, while **(b)** shows the 270-359 degree flow direction.

Figure 4.2 shows averaged aerodynamic roughness length (m) calculated for the two selected ranges of wind, covering the period 10 November 2001 through 10 December 2001. Several assumptions were made in the roughness length estimations. It was assumed that $z > h_{o,}$ where h_o is the height of the roughness elements. The 10 m level must satisfy the criteria that $z>>zo$ and $z > h_{o.}$ However, the roughness elements in lower Manhattan are on the order of hundreds of meters, so the above criteria are not entirely satisfied for wind directions from 0 to 179 degrees. This period was chosen because high levels of ground level pollutants, including PM-2.5, were observed over the region during this period. Monthly averaged wind velocity values were calculated and then broken up into the four ranges of flow directions. Figure 4.2a shows the averaged aerodynamic roughness length for the 180-279 degree flow directions, while Figure 4.2b shows the same for the 270-359 degree wind directions. Figure 2.1 shows details of the WTC site and locations of instrumentation cluster in lower Manhattan. Due to the lack of wind data from height levels well above the average height of building in Manhattan, the roughness length cannot be determined for the 0-89 and 90-179 degree wind direction sectors. For the 180-269 degree flow directions, the average aerodynamic roughness length was 0.7 m, while for the 270-359 degree flow direction, the average aerodynamic roughness length was 0.9 m. Both of these lower values seem reasonable, as the flow pattern between 180 and 359 degrees moved over the Hudson River before being measured by the instrumentation cluster. Much lower values of aerodynamic roughness length, less than 0.01 m, are often observed over the water, however the flow off the water in lower Manhattan is still being influenced by various near-surface features, including waterfront office buildings, boat depots and even large ships and barges. The calculated

aerodynamic roughness lengths agree well with the Davenport-Wieringa roughness length classifications (Stull 1988). This scheme classifies centers of large towns and cities, such as New York City, as chaotic with aerodynamic roughness lengths greater 2 m.

Another important surface layer parameter is the kinematic shear stress, which is used to define the friction velocity (u_*). Friction velocity is a scaling velocity, and is shorthand for $\sqrt{(\tau / p)}_{z=0.}$ Values of u_* range from near zero during calm winds and stable conditions to greater than 1 m/s during strong winds. The kinematic shear stress or u_* also increases with increasing surface roughness, and for a given speed at some reference level in the surface layer, it is expected to attain largest values over large city centers, such as Manhattan. Using the averaged aerodynamic roughness lengths estimated above, and the monthly averaged tower data, an average friction velocity has been calculated for the same four ranges of flow directions as specified above. The study period is the same as above, 10 November 2001 through 10 December 2001. Friction velocity can be determined from the slopes of fitted lines in Figure 4.2; alternatively it can be calculated using equation (4.1), which can be expressed as

$$u_{*} = (k * U_{10}) / \ln(z_R - d_o / z_o) \qquad (4.2)$$

k is the von Karman constant, generally accepted at 0.4, while U_{10} is the surface (10 m) wind speed.

Table 4.1 Average friction velocity (m/s) for roughness length (m) for two independent flow classifications. The average period is 10 November 2001 through 10 December 2001.

Flow Direction	**180-269 Degrees**	**270-359 Degrees**
Friction Velocity (m/s)	**0.30 m/s**	**0.48 m/s**
Roughness Length	**0.7**	**0.9**

z_R is the surface wind speed measurement height (10 m), while d_o is the zero-plane displacement height and z_o is the aerodynamic roughness length. Table 4.1 shows the averaged friction velocity for the two flow regimes. From Table 4.1, the average friction velocity for the 180-269 degree flow directions was 0.30 m/s, while that for the 270-359 degree flow direction was 0.48 m/s. Since friction velocity is dependent on both wind speed and aerodynamic roughness length, the above estimated values reflect the variability of both the roughness length and the mean wind speeds with different ranges of flow directions that prevailed during the observational period.

4.6 CASE STUDY I: 13 NOVEMBER 2001 THROUGH 15 NOVEMBER 2001

This section analyzes the observations during the period 00 UTC (19 LT) 13 November 2001 through 00 UTC (19 LT) 16 November 2001. High-pressure controlled the weather over much of the contiguous United States on 13 November 2001. Given the light synoptic-scale flow, local scale meteorological influences were pronounced on 13 November 2001 over the New York City region. The surface high-pressure center moved slowly off the Mid-Atlantic coast on the 14 and 15 November resulting in a light to moderate southwesterly near-surface wind flow across NYC. A more detailed synoptic review for this period is presented in Chapter 5. This period was selected to study the influences of near-surface wind flow moving off the water on the temperature and wind fields over the WTC site in lower Manhattan.

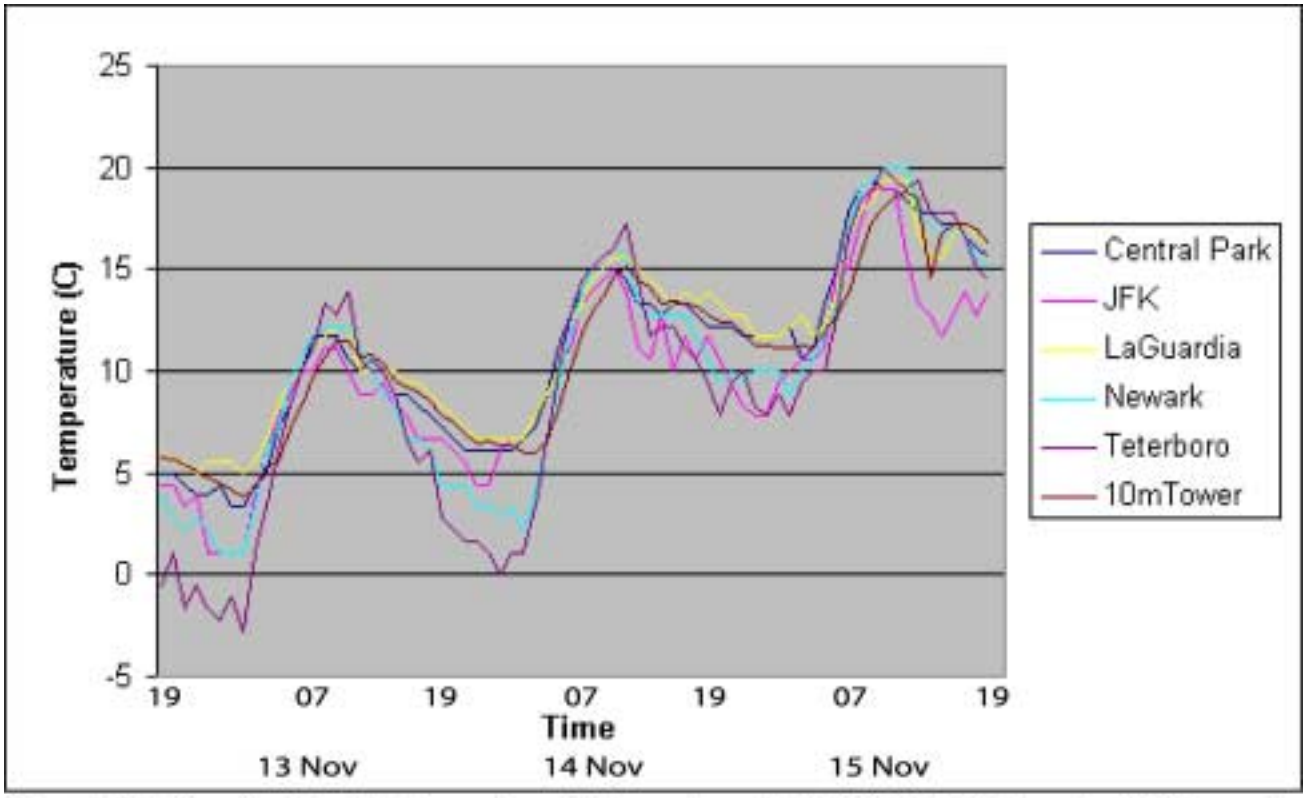

Figure 4.3 Surface (2 m) dry bulb temperature (c) time series valid 00 UTC (19 LT) 13 November 2001 through 00 UTC (19 LT) 16 November 2001. Five National Weather Service ASOS stations and the 10 m micrometeorological tower data are shown in color shading.

Table 4.2 Average surface temperature, wind speed and direction valid 00 UTC (19 LT) 13 November 2001 through 00 UTC (19 LT) 16 November 2001.

Station Name	Mean Temperature (C)	Mean Wind Speed ($m\ s^{-1}$)	Mean Wind Direction
JFK ASOS	9.70	4.32	226
LaGuardia ASOS	11.55	3.61	235
Central Park ASOS	11.08	2.80	235
Newark ASOS	10.15	3.48	209
Teterboro ASOS	9.29	2.30	221
10 m Micro Tower	10.75	3.87	238

Surface observations from five National Weather Service ASOS sites and a 10 m micrometeorological tower located in lower Manhattan (location of the instrumentation cluster was shown in Figure 2.1) have been used in this study. Additional near-surface wind data are obtained from the Model 4000 miniSODAR located in lower Manhattan. The ASOS sites include Central Park, LaGuardia Airport, JFK Airport, Newark Airport and Teterboro (the location of the ASOS sites are shown in Figure 2.2). A surface (2 m) dry bulb temperature C time series for the period 00 UTC (19 LT) 13 November 2001 through 00 UTC (19 LT) 16 November 2001 is shown in Figure 4.3. The daily maximum temperatures appear to be increasing throughout the study period, with an average maximum value of about 12 C observed by the stations on 13 November and the maximum value near 20 C observed on 15 November. Additionally, Central Park and LaGuardia appeared to stay warmer during the nighttime hours, as their temperatures remained nearly 2 C warmer than the other stations, including Newark, Teterboro and JFK. The 10 m micrometeorological tower in lower Manhattan was in between these extremes. The warmer temperatures observed during the nighttime in Central Park and LaGuardia were likely associated with the urban heat island, as one effect of the urban heat island is to keep surface temperatures within the urban core warmer during the nighttime hours. Table 4.2 shows the averaged surface temperature C, wind speed and direction, during the period 00 UTC (19 LT) 13 November 2001 through 00 UTC (19 LT) 16 November 2001, for the six stations used in this study. The mean temperature over the study period at Central Park and LaGuardia was between 1 and 2 C higher than the mean temperature over JFK, Newark and Teterboro, respectively. The 10 m micrometeorological tower in lower Manhattan had a mean temperature of 10.75 C,

which was less than the mean temperatures at Central Park and LaGuardia of 11.08 and 11.55 C but greater than the mean temperatures of 10.15, 9.70 and 9.15 C observed at Newark, JFK and Teterboro, respectively. Central Park, LaGuardia and the 10 m micrometeorological tower in lower Manhattan were located within the highly built-up urban core of New York City, and were likely influenced by the affects of the urban heat island, which kept their temperatures warmer at night than surrounding rural locations.

Figure 4.4a shows a surface (10 m) wind speed (m/s) time series for 00 UTC (19 LT) 13 November 2001 through 00 UTC (19 LT) 16 November 2001. The wind speeds from JFK and the 10 m micrometeorological tower in lower Manhattan were greater than the wind speeds observed from the other locations during much of the study period. A possible explanation for this is that both JFK and 10 m tower were located close to water. With synoptic conditions creating near-surface southwesterly winds, both locations experienced wind fields that moved over water and were less influenced by the highly urbanized area of the region before being measured. Additionally, the wind speeds at Central Park were 1-2 m/s lower than surrounding stations during much of the study period. Central Park is located in the center of Manhattan Island where the wind speeds were greatly influenced by the highly built up terrain of the region. Table 4.2 shows average values of surface temperature, wind speed and wind direction, during the period 00 UTC (19 LT) 13 November 2001 through 00 UTC (19 LT) 16 November 2001, for the six stations used in this study. The average wind speed at Central Park was 2.80 m/s, while the average wind speed at JFK and the 10 m tower were 4.32 and 3.87 m/s, respectively. The average wind speeds at LaGuardia, Newark and Teterboro where 3.61, 3.48 and 2.30, respectively.

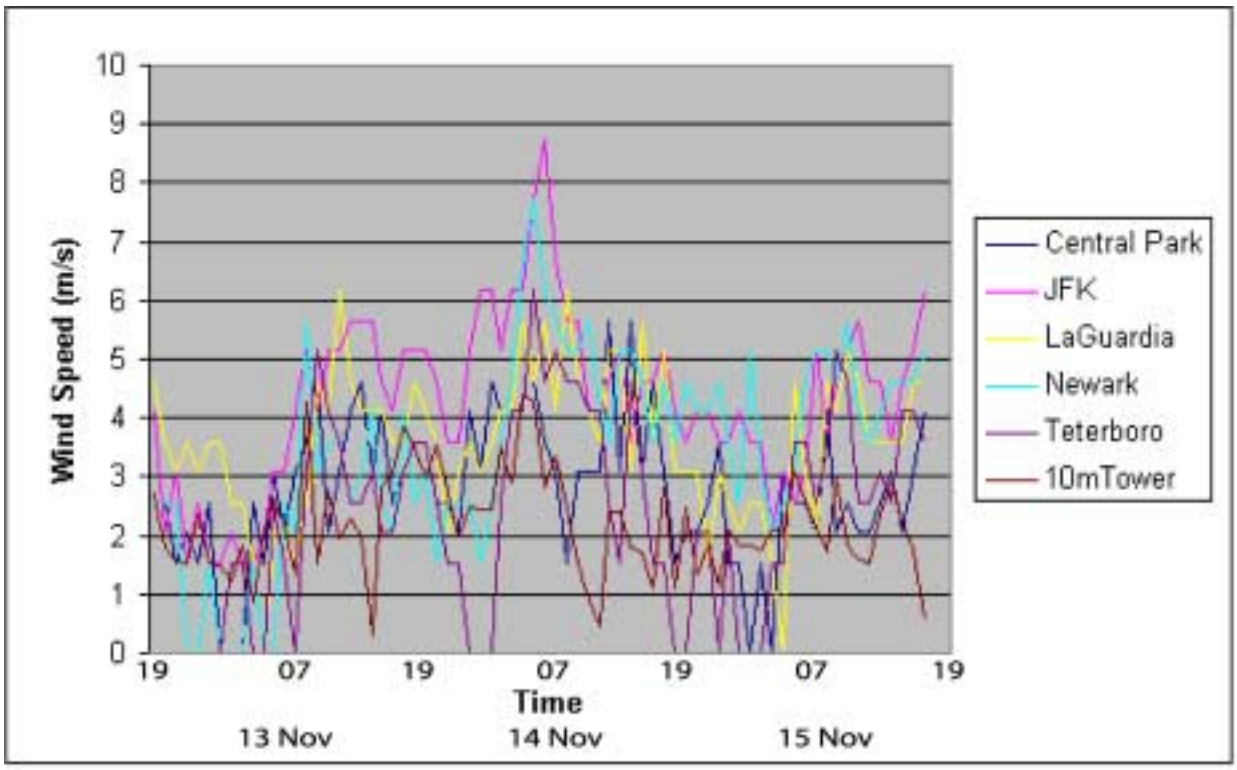

Figure 4.4a Surface (10 m) wind speed (m/s) time series valid 00 UTC (19 LT) 13 November 2001 through 00 UTC (19 LT) 16 November 2001. Five National Weather Service ASOS stations and the 10 m micrometeorological tower data are shown in color shading.

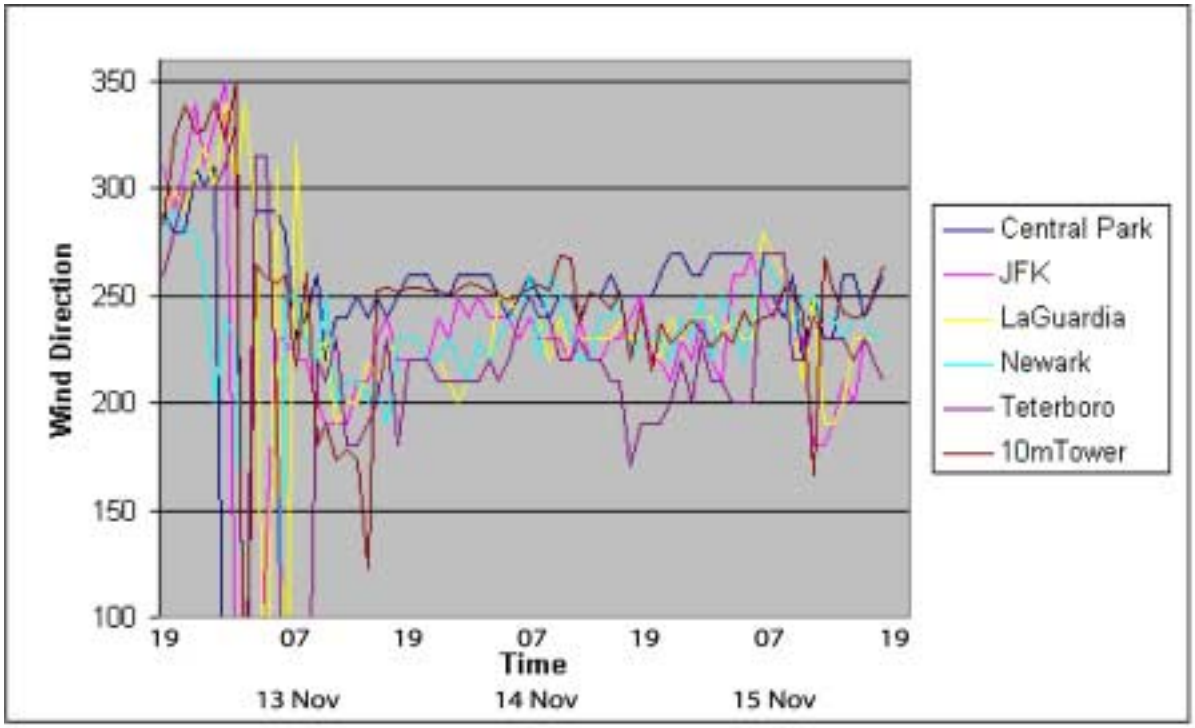

Figure 4.4b Surface (10 m) wind direction time series valid 00 UTC (19 LT) 13 November 2001 through 00 UTC (19 LT) 16 November 2001. Five National Weather Service ASOS stations and the 10 m micrometeorological tower data are shown in color shading.

With the exception of Teterboro, Central Park had the lowest mean wind speed during the study period. This was likely a result of near-surface winds decelerating as they encountered the taller buildings on Manhattan Island.

Figure 4.4b shows a surface (10 m) wind direction time series for 00 UTC (19 LT) 13 November 2001 through 00 UTC (19 LT) 16 November 2001. North to northwesterly winds are observed over the region between 00 UTC (19 LT) 13 November and 10 UTC (05 LT) 13 November before becoming more westerly and southwesterly after 18 UTC (13 LT) 13 November. This near-surface wind shift may be the result of the passage of a sea breeze front through the region and will be discussed in greater detail in Chapter 5 of this thesis. Throughout the rest of the study period, the wind directions are generally between 200 and 250 degrees. Tables 4.2 shows averaged surface temperature, wind speed and direction, for 00 UTC (19 LT) 13 November 2001 through 00 UTC (19 LT) 16 November 2001, for the six stations used in this study. The mean wind directions were all between 209 and 238 degrees throughout the study period, indicative of a well-established southwesterly synoptic flow pattern.

Figure 4.5 shows a time series plot from the Model 4000 miniSODAR profile in lower Manhattan (Figure 2.1) for the period 12 UTC (07 LT) 13 November 2001 through 12 UTC (07 LT) 14 November 2001. Wind barbs are shown in standard notation. The lowest (15 m) observation is typically unreliable, so it should be ignored. The miniSODAR showed west to west southwesterly winds around 20 m between 15 UTC (10 LT) and 18 UTC (13 LT) 13 November. At approximately 19 UTC (14 LT) the 20 m winds became more southerly, and were likely associated with the passage of a sea breeze front.

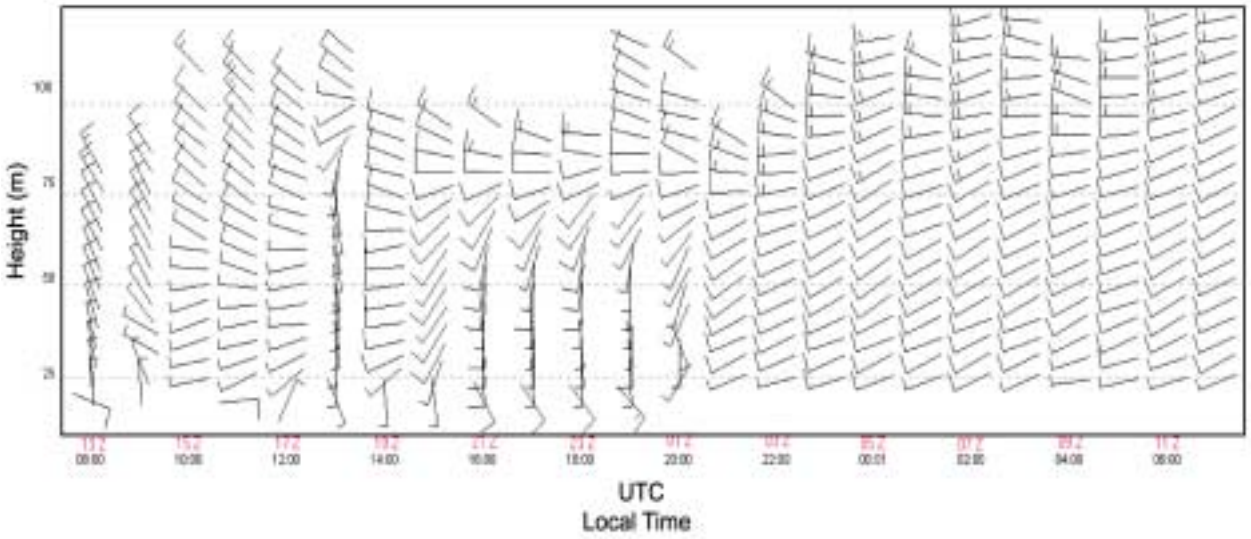

Figure 4.5 Model 4000 miniSODAR profile at the WTC Instrumentation site in lower Manhattan on November 13-14, 2001. Wind barbs use the standard knots notation. The lowest (15 m) observation is typically unreliable, so it should be ignored. Time is shown in both local and UTC time formats.

Another interesting feature was the vertical profile of nearly uniform wind speed and direction between 03 UTC (22 LT) 14 November and 12 UTC (07 LT) 14 November over lower Manhattan. Such a wind profile is often associated with a daytime convectively mixed boundary layer. Near-surface west-southwesterly winds was advecting air into lower Manhattan that previously crossed over Staten Island. This apparent mixed layer may be the result of urban heat island induced static instability, originating over Staten Island, allowing greater turbulent mixing in the nocturnal boundary layer. However, mechanical mixing may also be contributing to this apparent mixed layer.

Some conclusions from this case study are now presented. The mean temperature over the study period at Central Park and LaGuardia was between 1 and 2 C higher than the mean temperature over JFK, Newark and Teterboro, respectively. The 10 m micrometeorological tower in lower Manhattan had a mean temperature of 10.8 C, which was less than the mean temperatures at Central Park and LaGuardia of 11.1 and 11.6 C, respectively, but greater than the mean temperatures of 10.2, 9.7 and 9.2 C observed at Newark, JFK and Teterboro, respectively. Central Park, LaGuardia and the 10 m micrometeorological tower were located within the highly developed urban core of New York City, and were likely influenced by the formation of the urban heat island. The urban heat island often leads to warmer nighttime temperatures over the urban center than the surrounding rural locations. The wind speeds at JFK and the 10 m micrometeorological tower in lower Manhattan appeared to be greater than the wind speeds observed from the other locations during much of the study period. With synoptic conditions creating near-surface southwesterly winds, both locations experienced wind

fields that moved over water and were not influenced by the highly urbanized terrain of the region before being measured. Teterboro had the lowest mean wind speed, 2.30 m/s and Central Park had the second lowest mean wind speed of 2.80 m/s during the study period. This was likely a result of near-surface winds decelerating as they encountered higher roughness lengths associated with Manhattan Island. Observations from a miniSODAR over lower Manhattan were also studied. The miniSODAR showed west to west southwesterly winds around 20 m between 15 UTC (10 LT) and 18 UTC (13 LT) 13 November. At approximately 19 UTC (14 LT) the 20 m winds became more southerly, and were likely associated with the passage of a sea breeze front. Another interesting feature was the vertical profile of nearly uniform wind speed and direction between 03 UTC (22 LT) 14 November and 12 UTC (07 LT) 14 November over lower Manhattan. This apparent mixed layer may be the result of urban heat island induced static instability, originating over Staten Island, allowing greater turbulent mixing in the nocturnal boundary layer.

4.7 CASE STUDY II: 30 JANUARY 2002 THROUGH 02 FEBRUARY 2002

This section analyzes surface and boundary layer observations during the period 00 UTC (19 LT) 30 January 2002 through 00 UTC (19 LT) 02 February 2002. A winter storm was rapidly developing on 30 January 2002 over the Midwest as a 990 hPa low pressure system moved toward the north and east. Cold, high pressure was stationary over Maine, reinforced by strong confluent flow at 300 hPa. Figure 4.6 shows a synoptic scale surface analysis of mean sea level pressure (hPa) valid 12 UTC 20 January 2002.

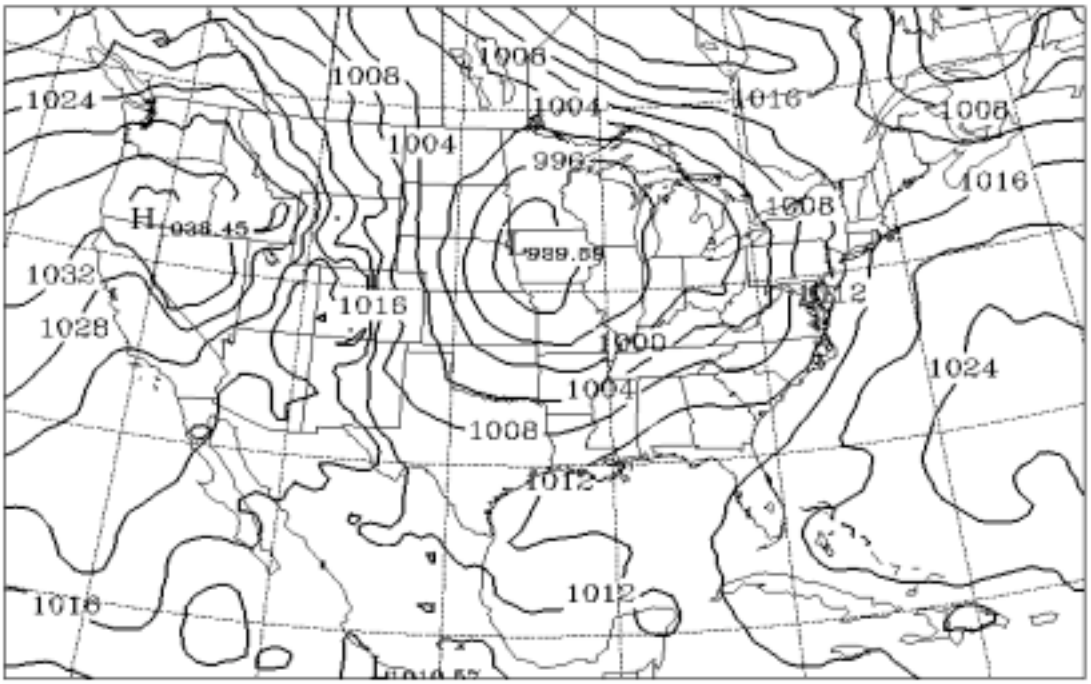

Figure 4.6 Mean sea level pressure (hPa) analysis valid 12 UTC 30 January 2002. Pressure systems are labeled in standard meteorological format.

Strong east to southeasterly winds were observed over the New York City area, where some light snow fell on 31 January 2002. High pressure moved into the area early on 01 February 2002. This period was selected to study the influences of near-surface wind flow moving from the city on the temperature and wind field over the WTC site in lower Manhattan. Surface observations from five National Weather Service ASOS sites and a 10 m micrometeorological tower located in lower Manhattan (The location of the Instrumentation Cluster is shown if Figure 2.1) will be used in this study. Additional near-surface wind data were obtained from the Model 4000 miniSODAR.

Figure 4.7 shows a surface temperature time series for 00 UTC (19 LT) 30 January 2002 through 00 UTC (19 LT) 02 February 2002. Between 00 UTC (19 LT) 30 January and 12 UTC (07 LT) 30 January surface temperatures over the region were observed to be between 12 and 16 C. Between 13 UTC (08 LT) and 15 UTC (10 LT) 30 January, surface temperature observations lowered from 16 C to 4 C. This dramatic temperature fall is likely associated with the passage of the back-door cold front analyzed on synoptic weather maps. Area temperatures remained between 4 and 5 C until 12 UTC (07 LT) 01 February. Between 12 UTC (07 LT) 01 February and 17 UTC (12 LT) temperatures rose from 5 to 10 C. Table 4.3 shows averaged surface temperature, wind speed and direction for the selected period 00 UTC (19 LT) 30 January 2002 through 00 UTC (19 LT) 02 February 2002, for the six stations used in this study. The mean temperatures at Central Park and Newark were slightly higher than the average temperatures over the other stations used in this study. Central Park and Newark had averaged temperatures of 6.70 and 6.66 C, while LaGuardia, JFK, Teterboro and the 10 m tower had mean temperatures of 6.65, 6.64, 6.33 and 6.65 C, respectively.

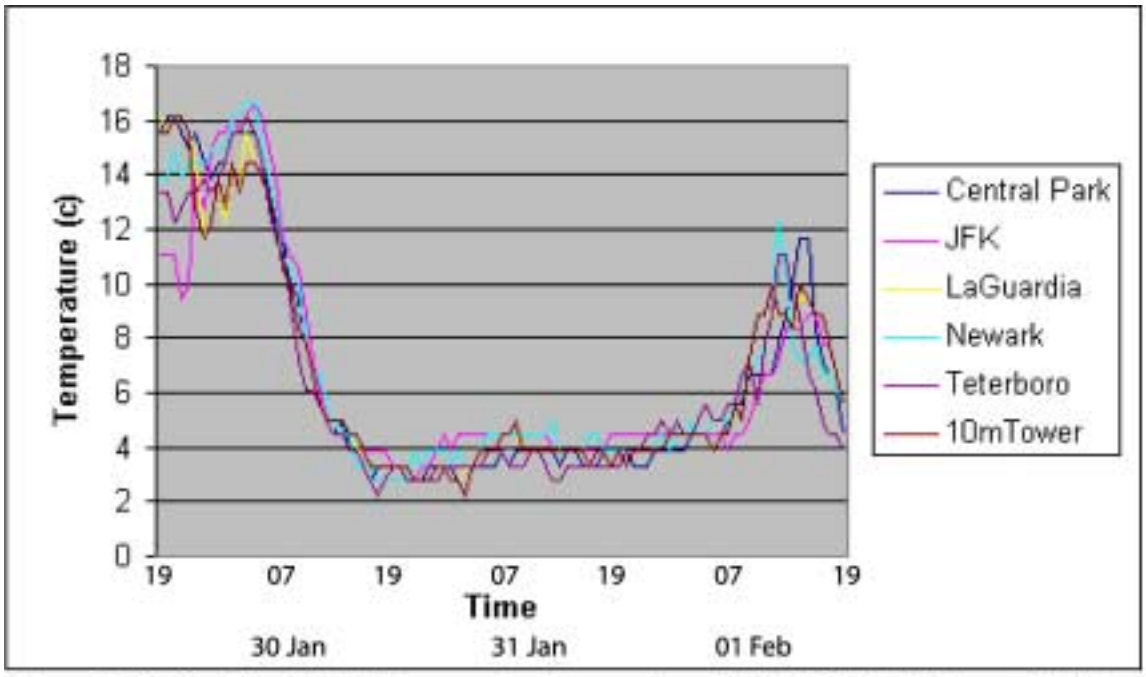

Figure 4.7 Surface (2 m) dry bulb temperature time series valid 00 UTC (19 LT) 30 January 2002 through 00 UTC (19 LT) 02 February 2002. Five National Weather Service ASOS stations and the 10 m micrometeorological tower data are shown in color shading.

Table 4.3 Averaged surface temperature, wind speed and direction valid 00 UTC (19 LT) 30 January 2002 through 00 UTC (19 LT) 02 February 2002.

Station Name	Mean Temperature (C)	Mean Wind Speed ($m\ s^{-1}$)	Mean Wind Direction
JFK ASOS	6.64	4.96	133
LaGuardia ASOS	6.65	5.41	128
Central Park ASOS	6.70	3.65	86
Newark ASOS	6.66	4.72	129
Teterboro ASOS	6.33	3.57	135
10 m Micro. Tower	6.65	5.35	131

Figure 4.8a shows a surface (10 m) wind speed time series for the period 00 UTC (19 LT) 30 January 2002 through 00 UTC (19 LT) 02 February 2002. Regional wind speed observations were between 2 and 8 m/s throughout most of the study period. However, toward the end of the period, around 18 UTC (13 LT) 01 February, wind speeds increased sharply from between 0 and 3 m/s to greater than 10 m/s. This increase in speed was associated with a cold front that moved through the region around 12 UTC (07 LT) 01 February 2002. Table 4.3 shows that the mean wind speeds at Central Park and Teterboro were significantly lower than the mean wind speeds at the other stations. The mean wind speeds at Central Park and Teterboro were 3.65 and 3.57 m/s, respectively, while those at LaGuardia, the 10 m tower in lower Manhattan, JFK and Newark were 5.41, 5.35, 4.96 and 4.72 m/s, respectively. The wind speed in Central Park was likely lower as a result of the increased roughness length associated with Manhattan Island. Figure 4.8b shows a surface (10 m) wind direction time series for 00 UTC (19 LT) 30 January 2002 through 00 UTC (19 LT) 02 February 2002. Between 00 UTC 30 January and 12 UTC (07 LT), regional wind directions ranged from 200 to 350 degrees. After 12 UTC (07 LT) 30 January the wind direction changed from around 350 degrees to 40 degrees. This wind shift matches up with the increased wind speeds observed in Figure 4.8a and is likely associated with the passage of a back-door front. The wind direction remained between about 20 and 100 degrees from 15 UTC (10 LT) 30 January through 17 UTC (12 LT) 01 February when the wind direction changed from 50 degrees to 340 degrees following a cold frontal passage.

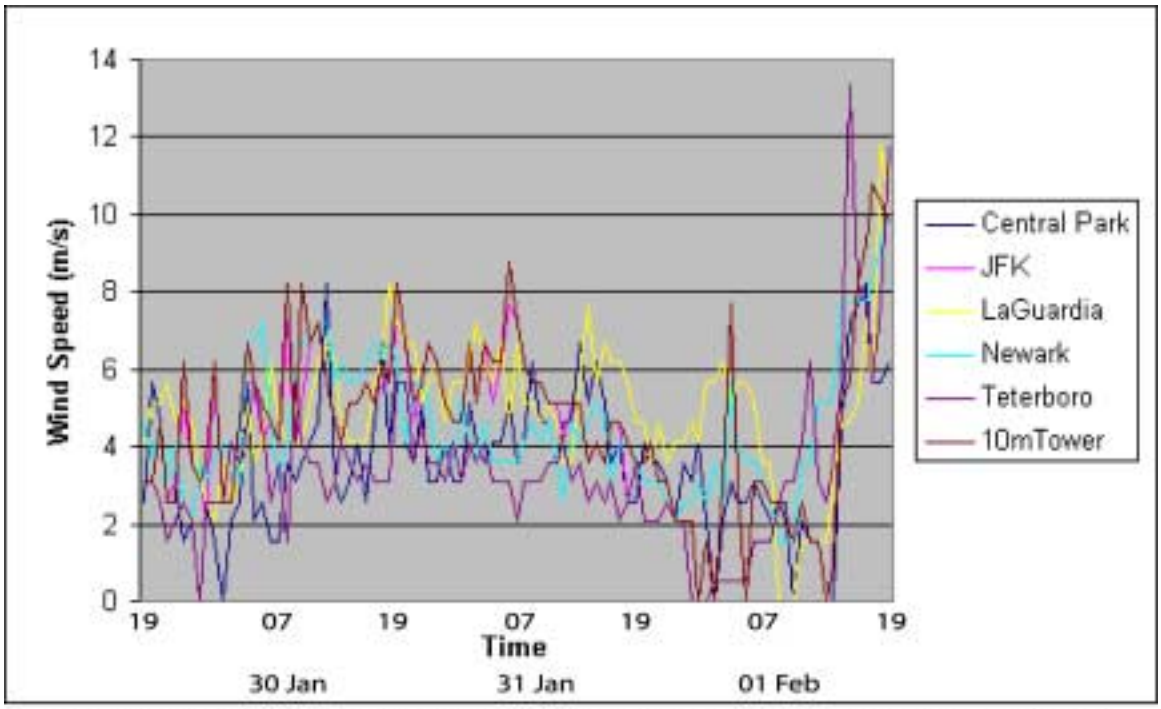

Figure 4.8a Surface (10 m) wind speed time series valid 00 UTC (19 LT) 30 November 2002 through 00 UTC (19 LT) 02 February 2002. Five National Weather Service ASOS stations and the 10 m micrometeorological tower data are shown in color shading.

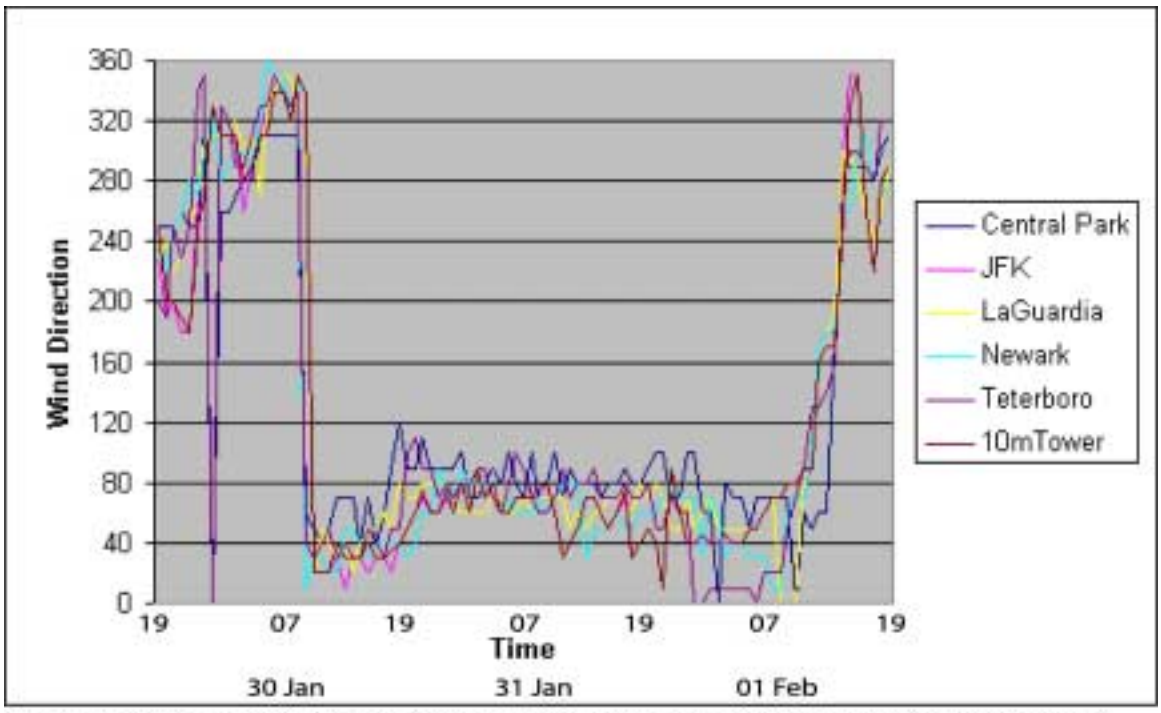

Figure 4.8b Surface (10 m) wind direction time series valid 00 UTC (19 LT) 30 January 2002 through 00 UTC (19 LT) 02 January 2002. Five National Weather Service ASOS stations and the 10 m micrometeorological tower data are shown in color shading.

Table 4.3 shows that with the exception of Central Park, the mean wind directions observed were between 128 and 135 degrees. The complex terrain and high roughness lengths likely interrupted the near-surface wind flow leading to a much different mean wind direction than the other locations in the region.

Figure 4.9a shows a Model 4000 miniSODAR vertical wind profile (m/s) over lower Manhattan at 05 UTC (00 LT) 31 January 2002. The vertical profile showed a shallow layer of near constant wind speeds between 2.2 and 2.7 m/s. This layer extended up to 180 m and had characteristics of a convectively mixed layer. Above 180 m, the winds speeds increase more rapidly to greater than 3.5 m/s. This may be associated with the capping inversion. Figure 4.9b shows a Model 4000 miniSODAR vertical wind direction distribution valid 05 UTC 31 January 2002. The wind direction is from between 130 and 160 degrees between 20 and 200 m, the maximum height of available data from the miniSODAR. With boundary layer wind directions between 130 and 160 degrees, the near-surface wind field traveled through the urban core of New York City before reaching the WTC site in lower Manhattan. The mixed layer between 40 m and 180 m may be associated with the urban heat island over lower Manhattan. The urban heat island creates boundary layer instability during the night, which helps develop a shallow mixed layer (Stull, 1988). The vertical profiles shown in Figures 4.9a and 4.9b show the formation of a shallow mixed layer, approximately 150 m deep, over lower Manhattan, although large wind direction shear is suggestive of a stable nocturnal boundary layer. Mechanical TKE generation may also be contributing to the observed shallow mixed-layer, which develops as a result of the low-level wind flow encountering the high roughness associated with NYC.

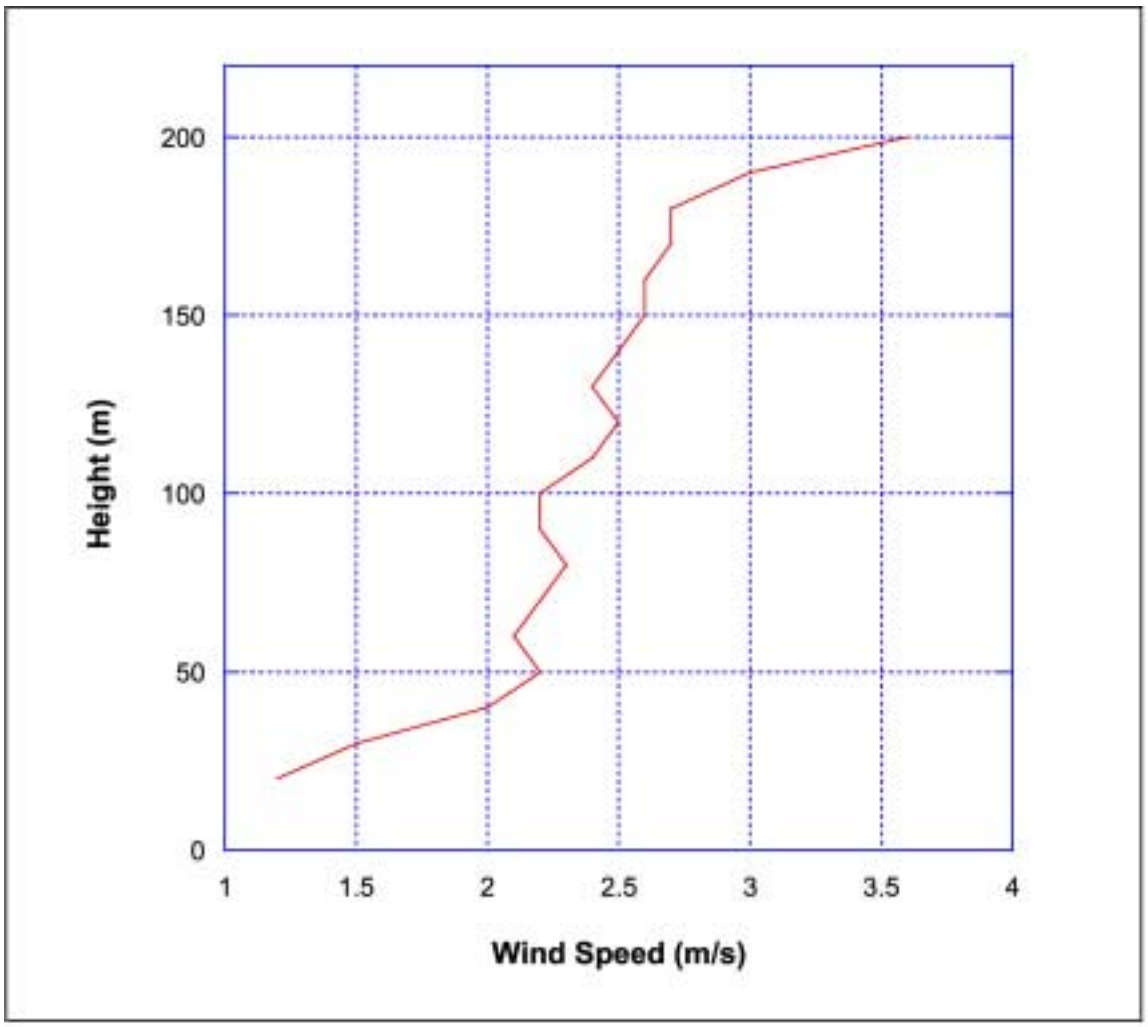

Figure 4.9a Model 4000 miniSODAR vertical wind profile (m/s) over lower Manhattan valid 05 UTC (00 LT) 31 January 2002. The near surface wind direction was from the east-southeast.

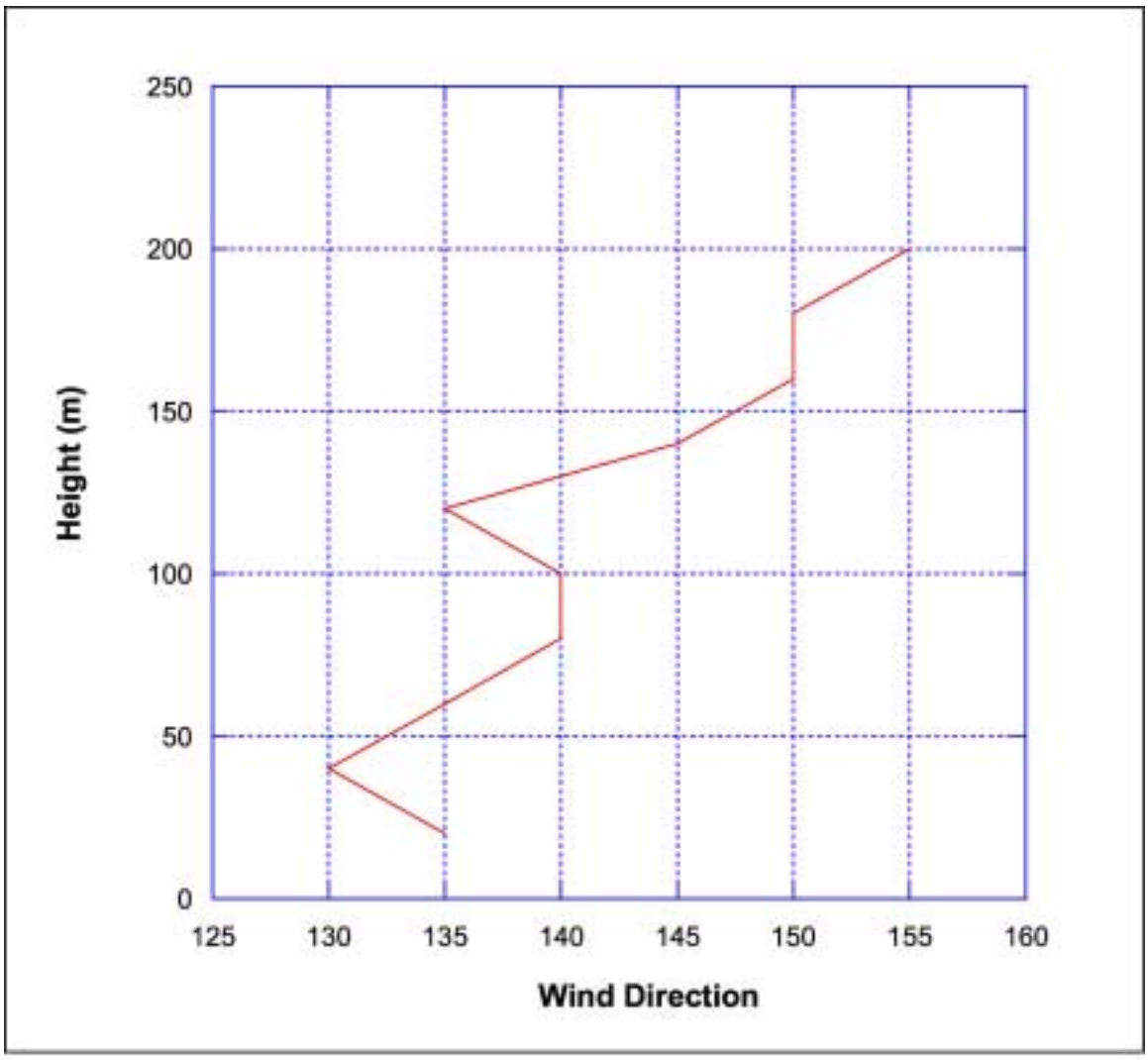

Figure 4.9b Model 4000 miniSODAR wind direction profile over lower Manhattan valid 05 UTC (00 LT) 31 January 2002.

A summary of this case study is now presented. Between 00 UTC (19 LT) 30 January and 12 UTC (07 LT) 30 January surface temperatures over the region were observed between 12 and 16 C. Between 13 UTC (08 LT) and 15 UTC (10 LT) 30 January, surface temperature observations lowered from 16 C to 4 C. Area temperatures remained between 4 and 5 C until 12 UTC (07 LT) 01 February. Between 12 UTC (07 LT) 01 February and 17 UTC (12 LT) temperatures rose from 5 to 10 C. The mean temperatures at JFK and Teterboro were significantly higher than the averaged temperatures for the other stations used in this study. JFK and Teterboro had averaged temperatures of 3.22 and 3.16 C, respectively, while LaGuardia, Central Park, Newark and the 10 m tower had mean temperatures of 2.16, 2.07, 2.06 and 2.13 C, respectively. It is suggested that JFK may have remained warmer during this period as a result of its proximity to Atlantic Ocean, which was observed to be 5 C. Regional wind speed observations were between 2 and 8 m/s throughout most of the study period. However, toward the end of the study period, around 18 UTC (13 LT) 01 February, wind speeds increased from between 2 and 4 m/s to greater than 10 m/s. The mean wind speed at Central Park and Teterboro were significantly lower than the mean wind speeds at the other stations. The mean wind speeds at Central Park and Teterboro were 3.65 and 3.57 m/s, respectively, while the mean wind speeds at LaGuardia, the 10 m tower in lower Manhattan, JFK and Newark were 5.41, 5.35, 4.96 and 4.72 m/s, respectively. The wind speed in Central Park was likely lower as a result of the increased roughness length associated with Manhattan Island. Between 00 UTC 30 January and 12 UTC (07 LT), regional wind directions range from 200 to 350 degrees. After 12 UTC (07 LT) 30 January the wind direction changed from around 350 degrees to 40 degrees. This wind shift matches up with the increased

wind speeds observed in Figure 4.7a and is likely associated with the passage of a back-door front. With the exception of Central Park, the mean wind directions observed were between 128 and 135 degrees. Central Park had a mean wind direction of 87 degrees. The complex terrain and high roughness lengths associated with Manhattan Island likely interrupted the near-surface wind flow, leading to a much different mean wind direction than the other locations in the region. Observations from the Model 4000 miniSODAR in lower Manhattan were also analyzed in this study. The vertical profile from the miniSODAR showed a shallow layer of wind speeds between 2.2 and 2.5 m/s. This layer extended up to 180 m and had characteristics of a convectively mixed layer. With boundary layer wind directions between 130 and 160 degrees, the near-surface wind field traveled through the urban core of New York City before reaching the WTC site in lower Manhattan. The mixed layer between 40 m and 180 m may be associated with the urban heat island over lower Manhattan.

4.8 SUMMARY

In this chapter, an observational study of the mesoscale boundary layer structure over the New York City area is presented. The “climatological” flow regimes observed over New York City region were identified during a three-month period, 10 September 2001 through 10 December 2001. Four flow regimes dominated: light southerly (18%), strong southerly (18%), strong westerly flow (17%), and light and variable flow (16%). These regimes occurred on 70 % of the days. The remaining periods were light westerly (9%), light northerly (6%), strong northerly (7%) and other (9%), respectively.

Additionally, using the surface layer wind profile data during a selected period of one month, the effects of wind direction on the calculated roughness lengths over lower Manhattan were analyzed. Roughness lengths (z_o) were calculated using 10 m tower and miniSODAR data, and separated into four wind direction regimes. Large values of z_o, up to 10 m may be expected, but could not be determined for the 0-89 degree and 90-179 degree flow directions, respectively, as the flow coming from 0 and 179 degrees encountered the urban core of Manhattan before moving over the instrumentation cluster. Smaller values of z_o, 0.7 and 0.9 m, were obtained for the 180-269 and 270-359 degree flow directions, respectively. These values seem reasonable, as the flow coming from 180 and 359 degrees moved over the Hudson River before being measured by the instrumentation cluster. Much lower values of aerodynamic roughness length, less than 0.01 m, are often observed over the water, however the flow off the water in lower Manhattan is still being influenced by various near-surface features, including waterfront office buildings, boat depots and even large ships and barges. The calculated aerodynamic roughness lengths agree well with the Davenport-Wieringa roughness length classifications (Stull 1988).

Friction velocities were also calculated using the same logarithmic wind profile used for calculating roughness lengths. The average friction velocity for the 180-269 degree flow directions was 0.30 m/s while that for the 270-359 degree flow directions was 0.48 m/s. The friction velocity depends on both the roughness length and average wind speed at some reference height.

Two case studies were conducted to study the effects of the near-surface wind flow on the development of the urban heat island over lower Manhattan. Case Study I analyzed

the mesoscale meteorology over New York City using surface observations from the National Weather Services' ASOS network as well as data from the instrumentation cluster, 10 m tower and miniSODAR, located in lower Manhattan (See Figure 2.1). The study period was 00 UTC (19 LT) 13 November 2001 through 00 UTC (19 LT) 16 November. This period was selected to study the effects of near-surface winds moving from off the water on the development of the urban heat island over lower Manhattan. The mean temperature over the study period at Central Park, LaGuardia and the 10 m tower was between 1 and 2 C higher that surrounding locations. Central Park, LaGuardia and the 10 m micrometeorological tower were located within the highly built up urban core of New York City, and were likely influenced by the effects of the urban heat island. Wind speed observations from JFK and the 10 m micrometeorological tower in lower Manhattan were greater than wind speeds observed from the other locations during much of the study period. With synoptic conditions creating near-surface southwesterly winds, both locations experienced wind fields that moved over water and were not influenced by the highly urbanized terrain of the region before being measured. With the exception of Teterboro, 2.30 m/s, Central Park had the lowest mean wind speed during the study period, 2.80 m/s. This was likely a result of near-surface winds decelerating as they encountered higher roughness associated with Manhattan Island. Observations from a miniSODAR over lower Manhattan were also studied. The miniSODAR showed west to west southwesterly winds around 20 m between 15 UTC (10 LT) and 18 UTC (13 LT) 13 November. At approximately 19 UTC (14 LT) the 20 m winds became more southerly, and were likely associated with the passage of a sea breeze front. Another interesting feature was the vertical profile of nearly uniform wind speed and direction between 03

UTC (22 LT) 14 November and 12 UTC (07 LT) 14 November over lower Manhattan. This apparent mixed layer may be the result of urban heat island induced static instability, originating over Staten Island, causing greater turbulent mixing in the nocturnal boundary layer. Another explanation for the near uniform wind velocity may be decoupling of the boundary layer wind field in association with nocturnal stabilization.

Case Study II analyzed the mesoscale meteorology over New York City using surface observations from the National Weather Services' ASOS network as well as data from the instrumentation cluster, 10 m tower and miniSODAR, located in lower Manhattan (See Figure 2.1). The study period was 00 UTC (19 LT) 30 January 2002 through 00 UTC (19 LT) 02 February 2002. This period was selected to study the effects of near-surface winds moving from the east on the development of the urban heat island over lower Manhattan. The mean temperatures at JFK and Teterboro were significantly higher than the averaged temperatures for the other stations used in this study. It is suggested that JFK may have remained warmer during this period as a result of its proximity to Atlantic Ocean, which was observed to be 5 C. Regional wind speed observations were between 2 and 8 m/s throughout most of the study period. However, toward the end of the study period, around 18 UTC (13 LT) 01 February, wind speeds increased from between 2 and 4 m/s to greater than 10 m/s. The mean wind speed at Central Park and Teterboro were significantly lower than the mean wind speeds at the other stations. The wind speed in Central Park was likely lower as a result of the increased roughness length associated with Manhattan Island. With the exception of Central Park, the mean wind directions observed over the region were between 128 and 135 degrees. Central Park had a mean wind direction of 87 degrees. The complex terrain and high roughness associated with

Manhattan Island likely interrupted the near-surface wind flow, leading to a much different mean wind direction than the other locations in the region. Observations from the Model 4000 miniSODAR in lower Manhattan were also analyzed in this study. The vertical profile from the miniSODAR showed a shallow layer of near constant wind speeds between 2.2 and 2.5 m/s at 05 UTC (00 LT) 31 January 2002. This layer extended from 40 to 180 m and had characteristics of a convectively mixed layer. With boundary layer wind directions between 130 and 160 degrees, the near-surface wind field traveled through the urban core of New York City before reaching the WTC site in lower Manhattan. The mixed layer between 40 m and 180 m may have been associated with the urban heat island over lower Manhattan.

CHAPTER 5

NUMERICAL SIMULATIONS OF NEAR-SURFACE FLOW

5.1 INTRODUCTION

Urban boundary layers are known to have several distinguishing characteristics as compared to boundary layers over nonurban flat terrain in terms of both near-surface wind flow and turbulent energetics. These differences are associated with the increased roughness length and heat island effect associated with urban canopy. Urban areas affect the near-surface wind pattern in several ways. Previous research over New York City has shown that in passing over the urban area, near-surface wind speeds may be decreased (increased) during periods of synoptic-scale near-surface wind speeds above (below) 4 m/s (Bornstein and Johnson, 1977). Additionally, research by Bornstein and Johnson (1977) has also suggested that the origin and time of day influence the near-surface wind flow. More specifically, during nighttime heat island hours, the origin, direction, of the near-surface wind flow greatly affects the turning of the winds over the city.

This study investigates the ability of the ARPS and MM5 mesoscale models to simulate the near-surface (10 m) wind structure and evolution over the New York City Metropolitan area. Because of the highly urbanized landuse characteristics of the region, numerical simulations are extremely challenging. However, previous research has demonstrated the capability of the high-resolution ARPS model to simulate the mesoscale and microscale structure of urbanized terrain (Gilliam et al. 2001).

5.2 NUMERICAL SIMULATIONS

A triple-nested version of the fifth generation PSU-NCAR Mesoscale Model (MM5), and a single nested version of the ARPS model are employed to study the surface level (10 m) wind structure and evolution over the New York City Metropolitan Area. Each simulation had a horizontal grid spacing of 1 km with 37 vertical sigma levels. The lowest vertical sigma level in each model was 1000 hPa (~10 m). With each model sharing the same landuse data and vertical resolution, the PBL scheme employed by each model will be instrumental in simulating an accurate 10 m wind field over the study region.

Table 5.1 shows the MM5 and ARPS models' parameterizations and grid configuration used in this study. In this study, the MM5 model was parameterized using the Eta Mellor-Yamada 2.5 level, TKE closure model (Eta M-Y PBL model). In the Eta M-Y PBL model, TKE is initialized from above the PBL in order to preserve the ability of the scheme to respond quickly to large thermal instabilities in the initial conditions. This technique also allows for efficient PBL spinup (Janjic 1994). The Eta M-Y PBL model uses a level 2.5 scheme to represent surface layer fluxes and specified the roughness length based on the landuse data for each grid square. The urban canopy cannot be fully resolved in the model due to the limitations of horizontal and vertical grid resolution. Just above this layer, the Eta M-Y PBL model constitutes the horizontally homogeneous surface layer (constant flux layer). Wind speed at top of the canopy layer, and just below the surface layer is assumed zero, with a minimum first layer wind of 1 m/s allowed to avoid numerical problems. The MM5 10 m wind calculation is based on the surface layer similarity theory.

Table 5.1 ARPS and MM5 physics configurations used in this study.

Explicit Moisture Physics	Cumulus Physics	Radiation Physics	Land Surface Model	PBL Model	Mixing Height Estimation	Mixing	Domain Setup
Simple Ice	Kain-Fritsch	Cloud Radiation	Noah LSM	Eta Mellor-Yamada	Solved Directly by TKE	Local	27,9,3,1 km

MM5

Explicit Moisture Physics	Cumulus Physics	Radiation Physics	Land Surface Model	PBL Model	Mixing Height Estimation	Mixing	Domain Setup
Lin et al.	Kain-Fritsch	Goddard Longwave	Noilhan Planton	Sun and Chang	Solved Directly by TKE	Non-Local	32,5,1 km

ARPS

The ARPS models uses the Sun and Chang 1.5-order TKE turbulence closure following the non-local scheme of Sun and Chang (1986). The Sun and Chang model uses surface roughness and a stability dependent surface flux model, developed by Businger et al. (1971). The surface fluxes are of momentum, heat and moisture. The momentum flux is calculated from the first level (10 m) wind speed and wind components. The 10 m wind is calculated in a similar fashion to the Eta M-Y PBL model, with a modified surface flux model first developed by Businger et al. (1971) and updated by Deardorff (1972).

These numerical simulations will be compared with surface observations from both National Weather Service ASOS sites and an independent site in lower Manhattan Island maintained by the United States Environmental Protection Agency (EPA) and State Climate Office of North Carolina as described in the previous chapter. Additional comparisons will be made between both model simulations as well. The main purpose of this study is to evaluate the ability of high-resolution mesoscale models to accurately predict the mesoscale and microscale meteorology over the highly urbanized New York City Metropolitan area.

The MM5 and ARPS models are initialized at 00 UTC 13 November 2001 and integrated out 60 hours until 12 UTC 15 November 2001. This period was chosen because high ground-level pollutant concentrations were observed over Manhattan. Additionally, this period featured the development and inland propagation of a sea breeze front that moved through lower Manhattan after 18 UTC (13 LT) 13 November. Moreover, data from the instrumentation cluster in lower Manhattan was available to validate the ARPS and MM5 simulations during this period. Both numerical simulations will be compared with surface observations and previous research (Bornstein et. al. 1977)

to evaluate their ability to represent the 10 m wind flow over the region, including the sea breeze front. The following paragraph will outline the synoptic meteorology present over the United States during this study period.

5.3 SYNOPTIC REVIEW

High-pressure controlled the weather over much of the contiguous United States on 13 November 2001. Centered over West Virginia, the surface high pressure (1035 hPa) resulted in clear skies and calm winds over NYC. Figure 5.1 shows a surface weather analysis over the United States valid at 00 UTC, 13 November 2001. The pressure systems are labeled according to standard meteorological format. Given the light synoptic-scale flow, local scale meteorological influences were pronounced on 13 November 2001 over the New York City region. The surface high-pressure center moved slowly off the Mid-Atlantic coast on the 14 and 15 November resulting in a light to moderate southwesterly flow across NYC. Figure 5.2a shows an Eta analysis of 300 hPa wind velocity (kts) over the United States valid at 00 UTC, 13 November 2001. After reviewing the 300 hPa wind velocity (kts) structure from the Eta analysis, much of the northeastern US was located under the right front quadrant of a 130 kt jet streak. This quadrant is associated with strong ageostrophic convergence aloft, which favors subsiding air and rising pressures at the surface (This is also referred to as an indirect transverse circulation). Figure 5.2b shows the Eta analysis of 700 hPa relative humidity (%) valid at 00 UTC 13 November 2001. From this analysis of mid level relative humidity (%), much of the eastern US had less than 30% relative humidity. This situation is not conducive to significant precipitation, and is often associated with strong synoptic scale high pressure.

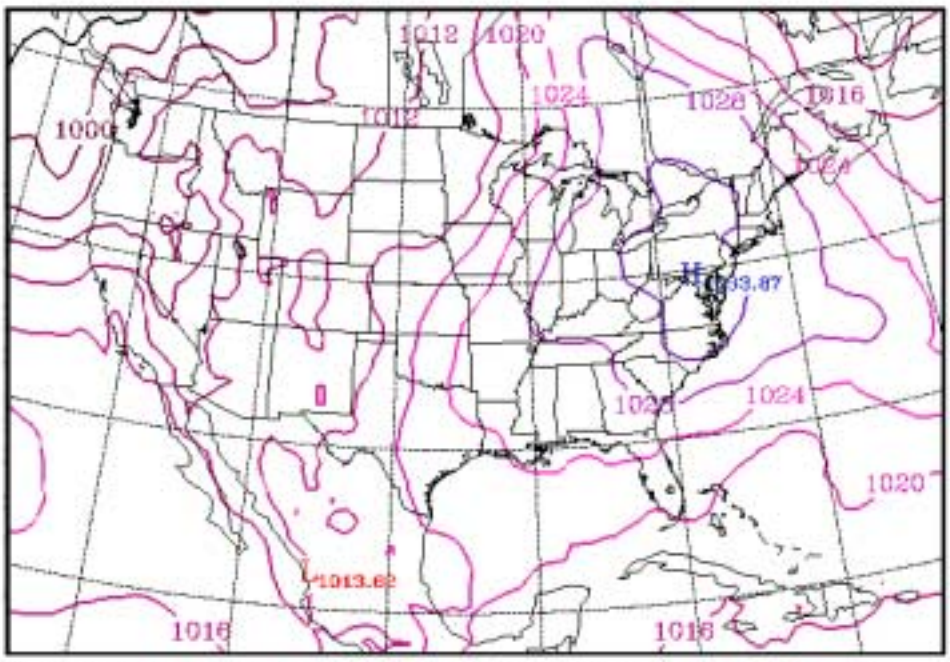

Figure 5.1 Surface analysis of the United States Valid 00 UTC (19 EST)13 November 2001. Surface pressure systems are contoured in mb.

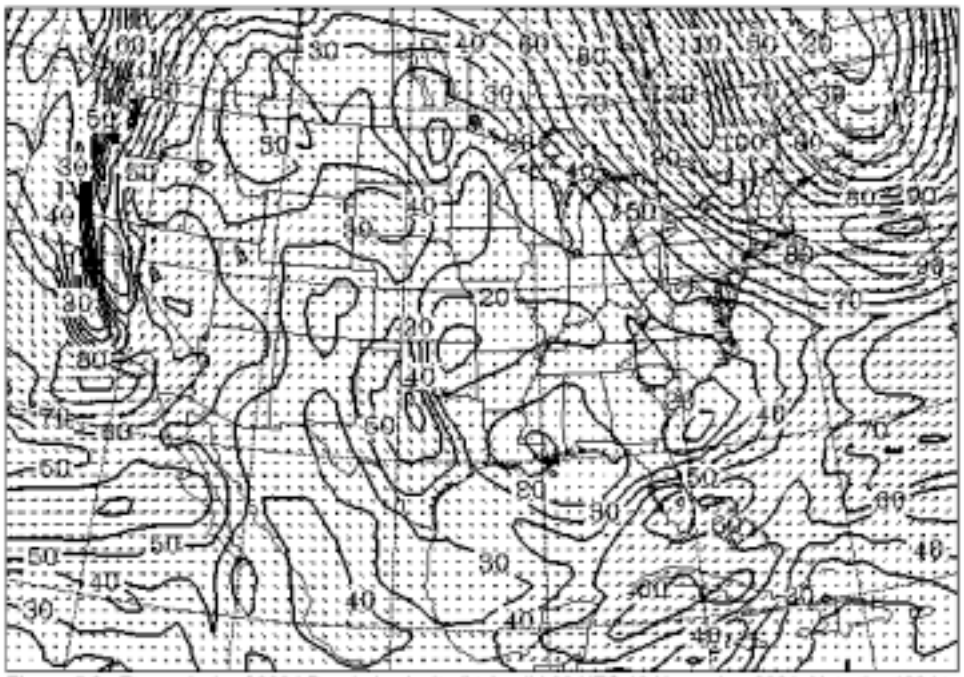

Figure 5.2a Eta analysis of 300 hPa wind velocity (kts) valid 00 UTC 13 November 2001. Note the 120 kt jet streak moving into the northeastern United States, where much of the region is under the right exit region of this jet feature, where large scale subsidence is favored.

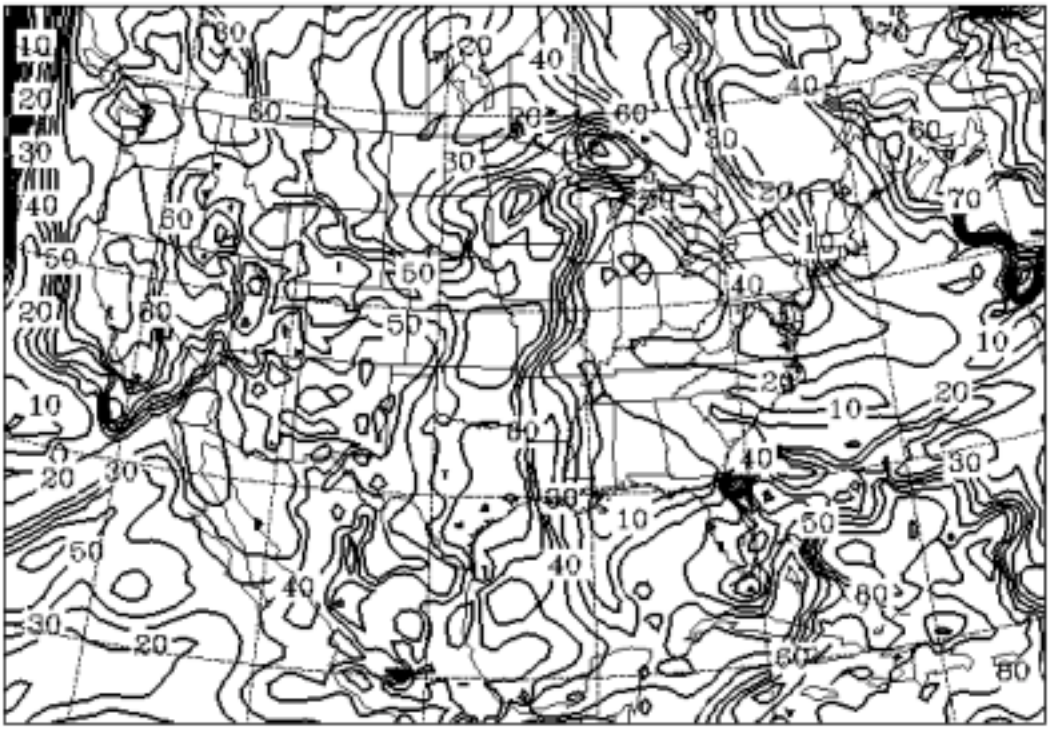

Figure 5.2b Eta analyses of 700 hPa relative humidity (%) valid 00 UTC 13 November 2001. Note the 700 hPa relative humidity values of less than 30% over much of the northeastern United States.

5.4 NUMERICAL SIMULATION RESULTS

Near-surface pollutant transport and dispersion depends on winds in the surface layer. Simulating surface wind velocity over a highly urbanized area, such as New York City, is extremely complex, as large differences in roughness length are evident over very small distances. Numerical simulations over the region are made even more challenging by the proximity of numerous water bodies and the land-water interface that is directly related to them. Internal boundary layers, following changes in roughness and temperature, are often observed over the region as well. In the following section, we will analyze the 10 m wind evolution over the New York City region between 12 UTC (07 LT) 13 November and 12 UTC (07 LT) 14 November. This period was characterized by high ground-level pollutant concentrations over Manhattan, and the development and inland propagation of a sea breeze front through lower Manhattan.

Model estimated 10-m wind direction (vectors) and speed (contoured in m/s) at 12 UTC (07 LT) 13 November are shown in Figures 5.3a (ARPS) and 5.3b (MM5). Surface wind observations are shown in red, with the barb indicating direction from and the number indicating speed (m/s). (Note: The surface winds observations are overlayed in the same format on Figures 5.3 through 5.13). The surface (10 m) wind flow over the region was generally less than 2 m/s out of the northwest. Surface observations from Teterboro and LaGuardia ASOS as well as data from the independent 10 m tower all showed winds out of the northwest between 1.3 and 2.6 m/s. Both the ARPS and MM5 simulations matched the surface observations and were very similar to each other. However the MM5 model did show wind speeds slightly lower over Manhattan, 1.5 m/s as compared to 2 m/s in the ARPS simulation.

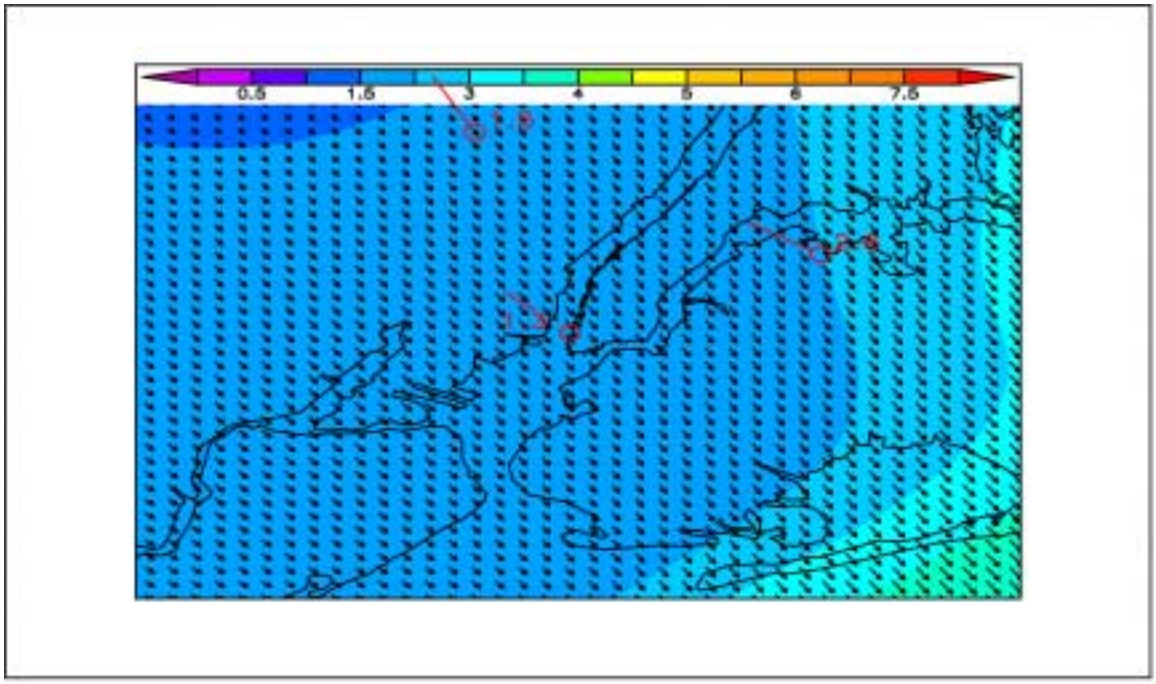

Figure 5.3a ARPS simulated 10 m wind velocity (m/s) valid 12 UTC (07 LT) 13 November 2001. Surface wind observations shown in Red with barb indicating direction from and number indicating speed (m/s).

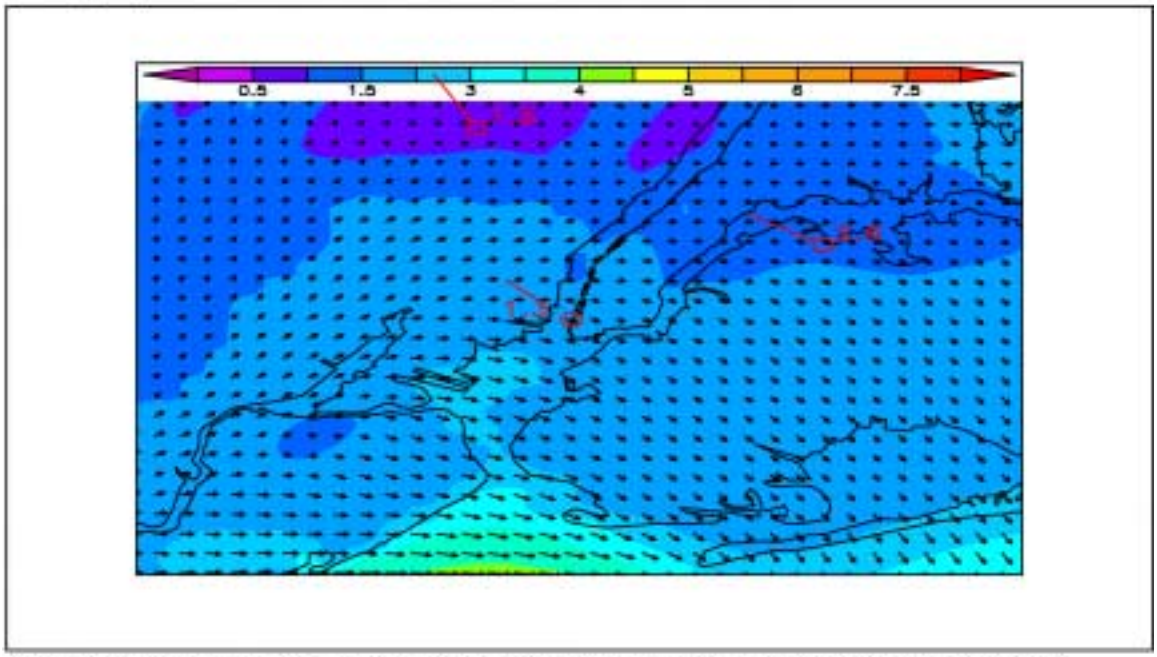

Figure 5.3b MM5 simulated 10 m wind velocity (m/s) valid 12 UTC (07 LT) 13 November 2001. Surface wind observations shown in Red with barb indicating direction from and number indicating speed (m/s).

Model estimated 10-m wind direction (vectors) and speed (contoured in m/s) at 15 UTC (10 LT) 13 November are shown in Figures 5.4a (ARPS) and 5.4b (MM5). In comparison, both the ARPS and MM5 simulations were very similar with their forecasted wind speeds and directions over the region. However, there were some subtle differences. The MM5 model had a wind speed around 0.5 m/s over lower Manhattan, while the independent tower had a surface wind speed of 1.7 m/s. The ARPS forecasted a surface wind speed between 1.5 and 2 m/s. Clearly, the ARPS magnitude appears to be better over lower Manhattan than the MM5. However, the MM5 had a surface wind direction out of the southwest over lower Manhattan, matching closely with observations. Contrary to the MM5, the ARPS simulation had a surface wind direction out of the north. These differences are believed to be the result of the flow being light and variable. Previous research has shown similar results from numerical simulations over highly urbanized areas during light and variable flow regimes (Gilliam et. al 2003).

Model estimated 10-m wind direction (vectors) and speed (contoured in m/s) at 18 UTC (13 LT) 13 November are shown in Figures 5.5a (ARPS) and 5.5b (MM5). The ARPS model had simulated wind speeds exceeding 5 m/s out of the south over portions of the New York Harbor, while the MM5 had surface wind speeds between around 2 m/s out of the south over the same region. This difference was most likely caused by the 2 C cooler sea surface temperatures initialized in the MM5 resulting in a more stable boundary layer, with less vertical momentum transfer. Observed land temperatures were 12 C, while SST's were observed near 8 C over the region. This thermal gradient was enough to allow for a sea breeze front to develop over the New York Harbor.

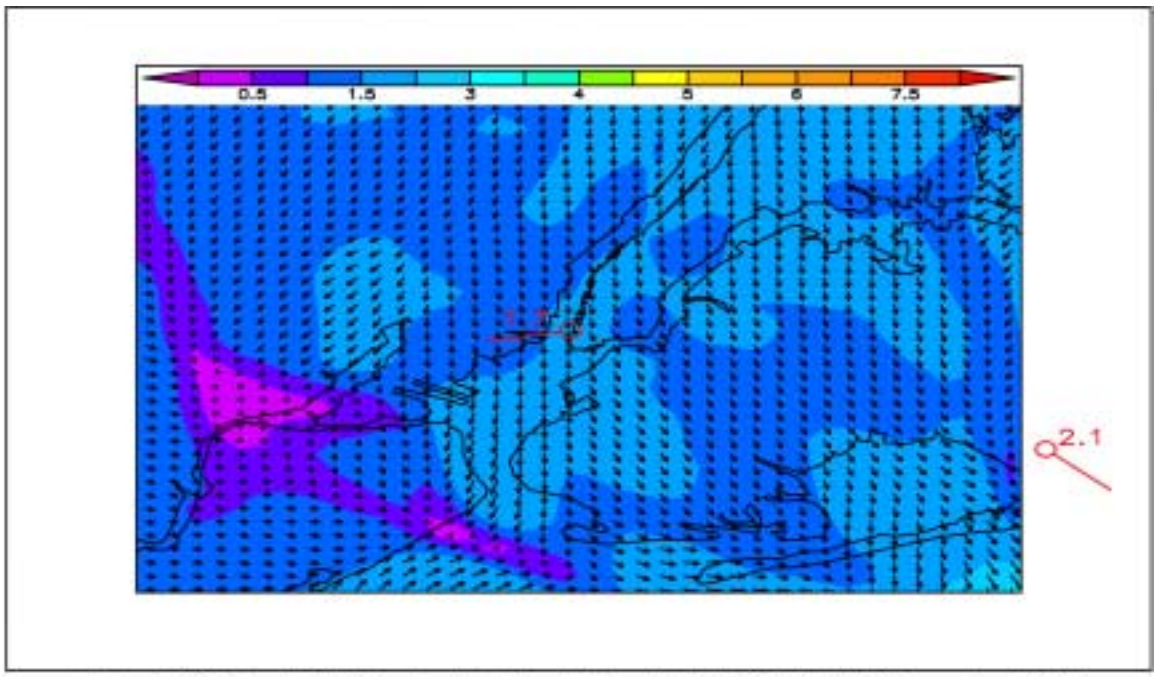

Figure 5.4a. ARPS simulated 10 m wind velocity (m/s) valid 15 UTC (10 LT) 13 November 2001. Surface wind observations shown in Red with barb indicating direction from and number indicating speed (m/s).

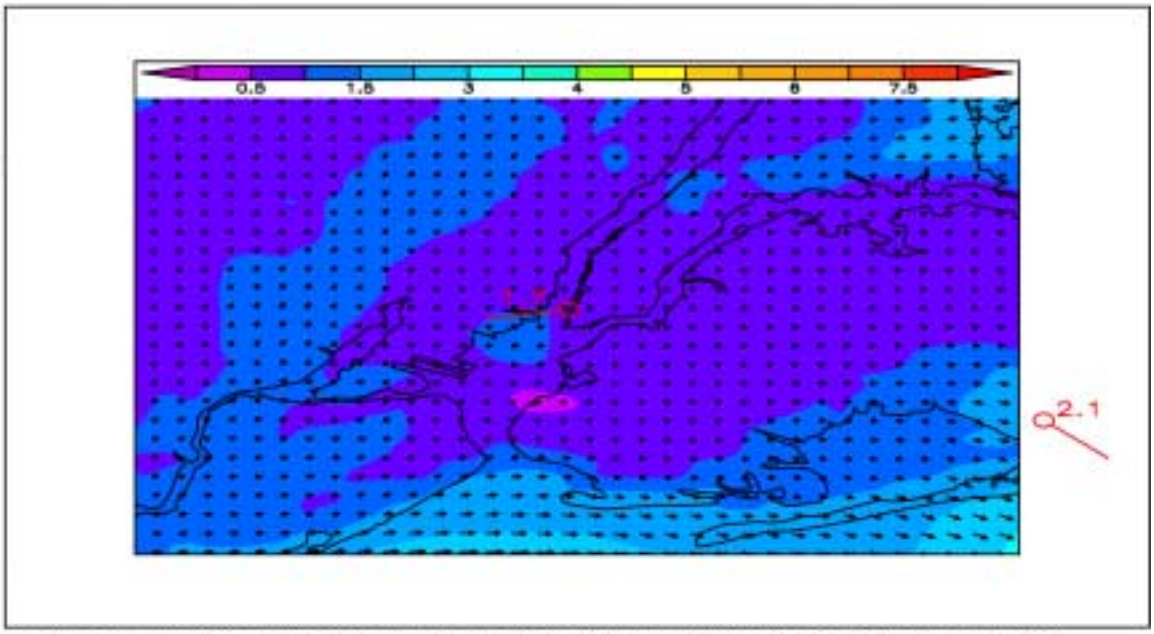

Figure 5.4b. MM5 simulated 10 m wind velocity (m/s) valid 15 UTC (10 LT) 13 November 2001. Surface wind observations shown in Red with barb indicating direction from and number indicating speed (m/s).

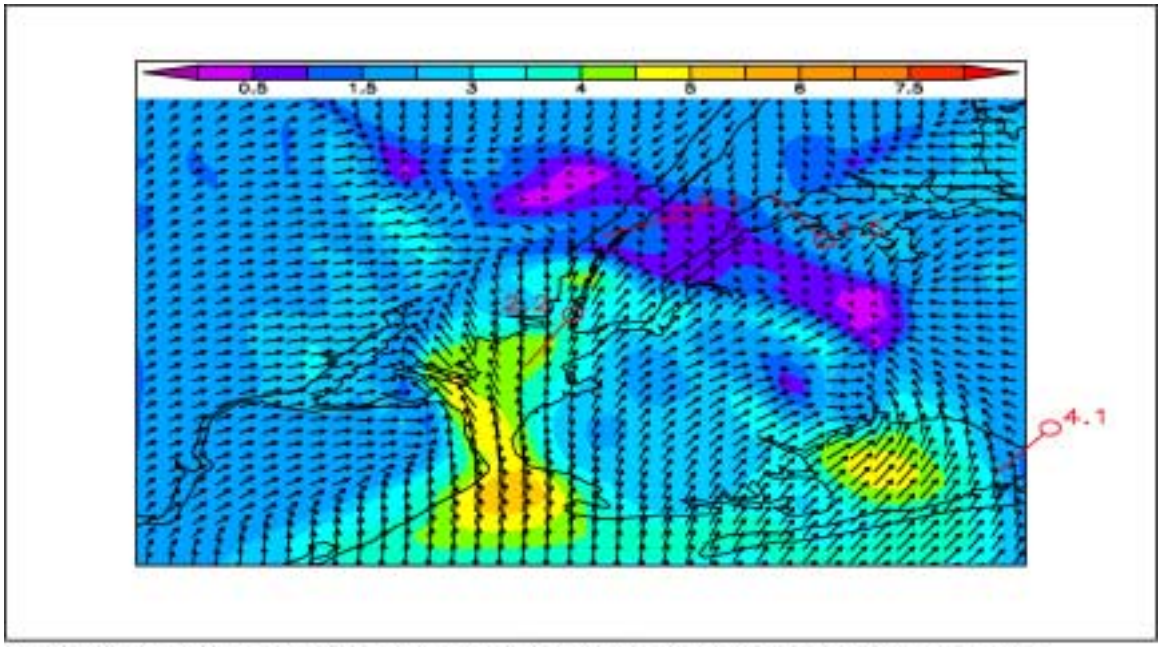

Figure 5.5a ARPS simulated 10 m wind velocity (m/s) valid 18 UTC (13 LT) 13 November 2001. Surface wind observations shown in Red with barb indicating direction from and number indicating speed (m/s).

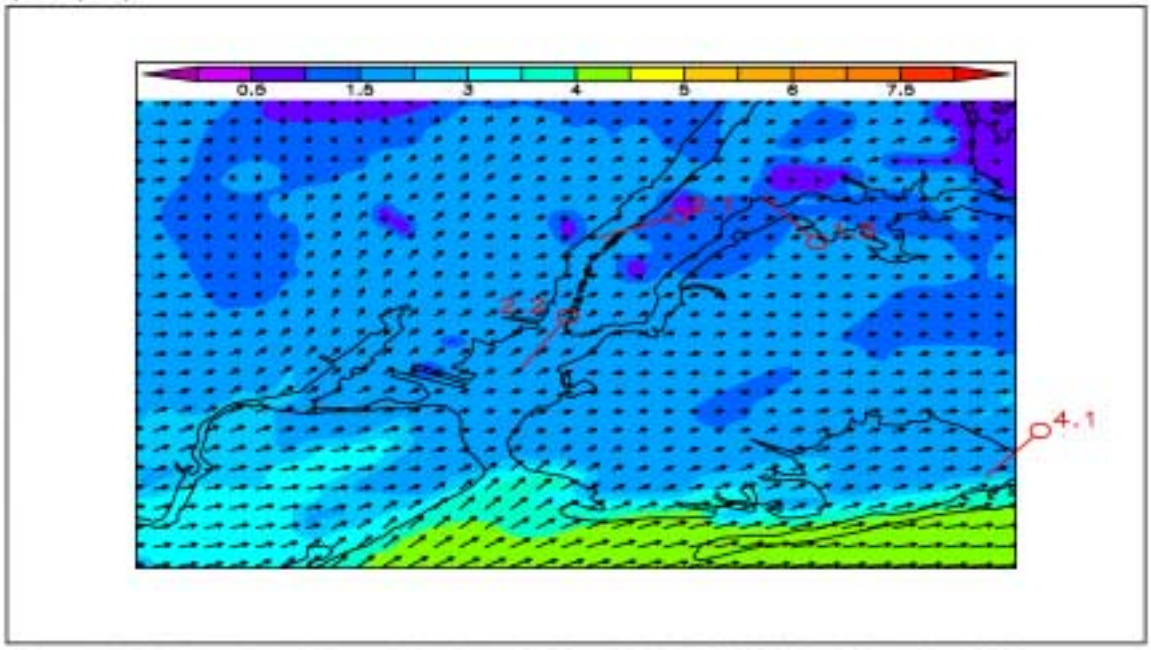

Figure 5.5b MM5 simulated 10 m wind velocity (m/s) valid 18 UTC (13 LT) 13 November 2001. Surface wind observations shown in Red with barb indicating direction from and number indicating speed (m/s).

Another interesting difference between the two simulations was the very pronounced convergence patterns predicted by the ARPS model over New Jersey and Brooklyn. The MM5 simulation did not predict these patterns, and showed generally south to southwesterly winds over the entire region. Another difference worth noting in the two simulations was the wind speed and direction over Midtown Manhattan, where the ARPS model predicted a wind direction out of the north at a speed of less than 1 m/s. Surface observations from the Central Park ASOS showed winds out of the southwest at 2 m/s, with the MM5 simulation simulating winds out of the southwest at approximately 1.5 m/s.

Model estimated 10-m wind direction (vectors) and speed (contoured in m/s) at 21 UTC (16 LT) 13 November are shown in Figures 5.6a (ARPS) and 5.6b (MM5). The model simulated wind field patterns were very close to the model simulated wind fields at 18 UTC 13 November. For example, the ARPS simulated wind field showed 5 m/s southerly winds over the New York Harbor, while the MM5 forecasted southerly winds between 1.5 and 2 m/s. As discussed above, the MM5 was initialized with 2 C cooler SST's than the ARPS simulation, which led to a more stable boundary layer and less turbulent momentum transfer. Looking more closely, both the ARPS and MM5 simulations were very similar over Manhattan and Brooklyn, although the MM5 was slightly better with wind direction observations from the LaGuardia and Central Park ASOS. Both ASOS observations showed winds blowing from the southwest and west-southwest, respectively, while the ARPS simulation showed winds out of the south. In comparison, the MM5 simulation forecasted winds out of the southwest over these stations.

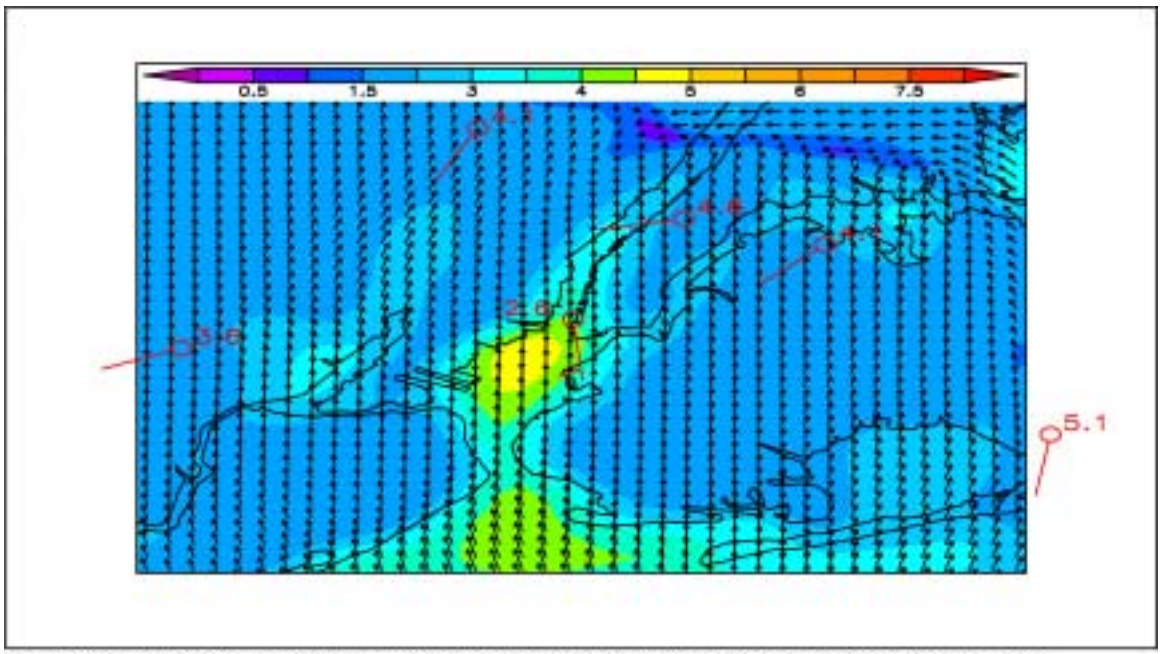

Figure 5.6a ARPS simulated 10 m wind velocity (m/s) valid 21 UTC (16 LT) 13 November 2001. Surface wind observations shown in Red with barb indicating direction from and number indicating speed (m/s).

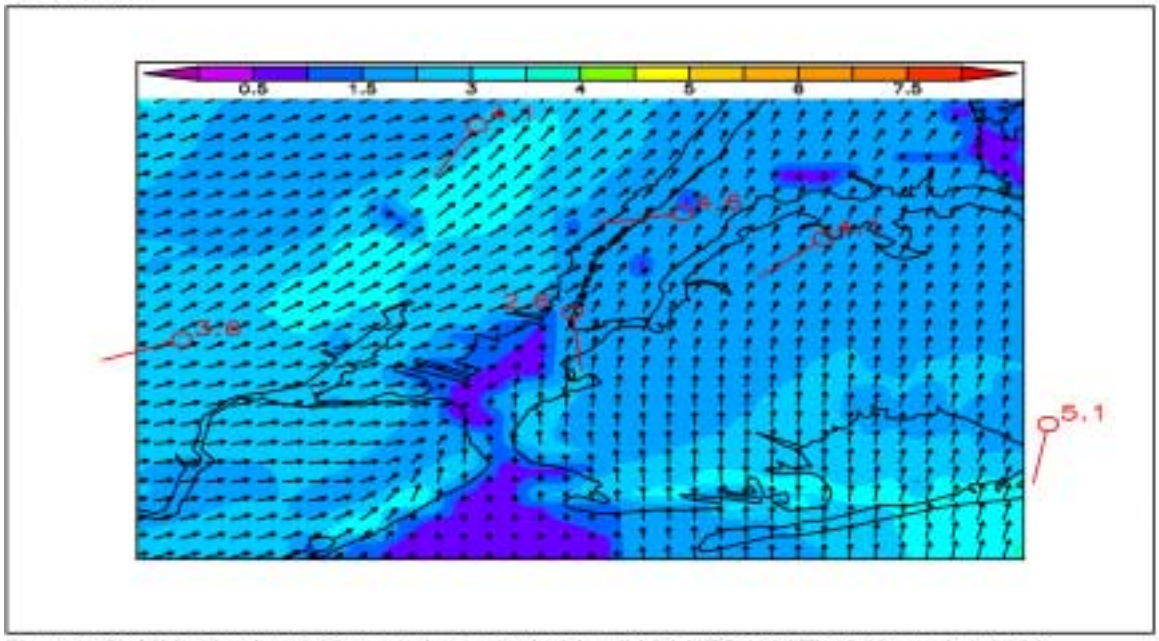

Figure 5.6b MM5 simulated 10 m wind velocity (m/s) valid 21 UTC (16 LT) 13 November 2001. Surface wind observations shown in Red with barb indicating direction from and number indicating speed (m/s).

Additionally, the ARPS model simulated a wind velocity of 1.5 m/s out of the south over Newark, New Jersey, while the MM5 simulated a wind velocity of 3 m/s out of the west-southwest over the same area. The Newark ASOS reported a wind speed of 3.6 m/s out of the west-southwest. Observations from the independent tower and wind fields from both numerical simulations showed that the sea breeze front moved through lower Manhattan between 18 UTC (13 LT) and 21 UTC (16 LT).

Model estimated 10-m wind direction (vectors) and speed (contoured in m/s) at 00 UTC (19 LT) 14 November are shown in Figures 5.7a (ARPS) and 5.7b (MM5). Under close examination, there were several noticeable differences between the ARPS simulation and the MM5 simulation. The ARPS forecasted very strong southerly winds, in excess of 7 m/s, over the New York Harbor, while the MM5 simulated southwesterly winds between 4 and 5 m/s over the same region. The independent tower, located directly adjacent to the New York Harbor over Lower Manhattan, reported a southerly wind at 2.6 m/s at this time. Another striking difference between the two simulations was found over central and upper Manhattan Island. The ARPS simulated winds moving out of the southeast at 1.0 to 1.5 m/s, while the MM5 simulated winds out of the southwest at 3.0 m/s. The Central Park ASOS observation showed winds out of the southwest at 4.1 m/s. Subtle differences between the two simulations were also evident over New Jersey. More closely, the ARPS simulation showed winds out of the south-southeast at 1.5 m/s, while the MM5 forecasted winds out of the southwest at 2 m/s. The Newark ASOS observation reported winds out of the southwest at 3.1 m/s. From the observations, it is shown that the ARPS simulation agrees with the independent 10 m tower over lower Manhattan.

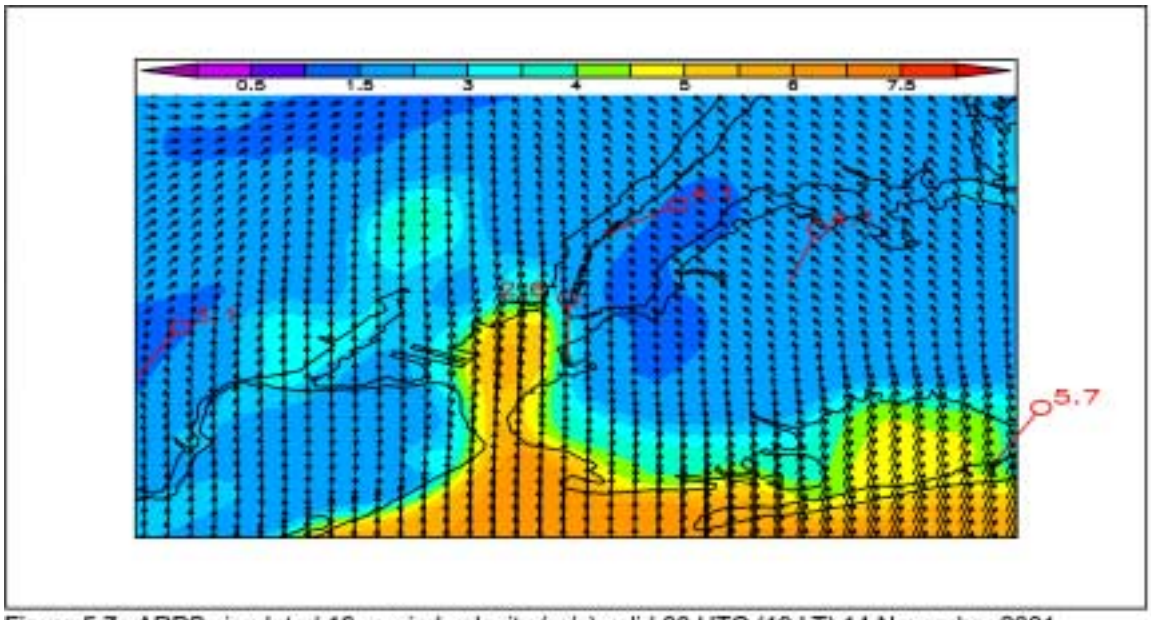

Figure 5.7a ARPS simulated 10 m wind velocity (m/s) valid 00 UTC (19 LT) 14 November 2001. Surface wind observations shown in Red with barb indicating direction from and number indicating speed (m/s).

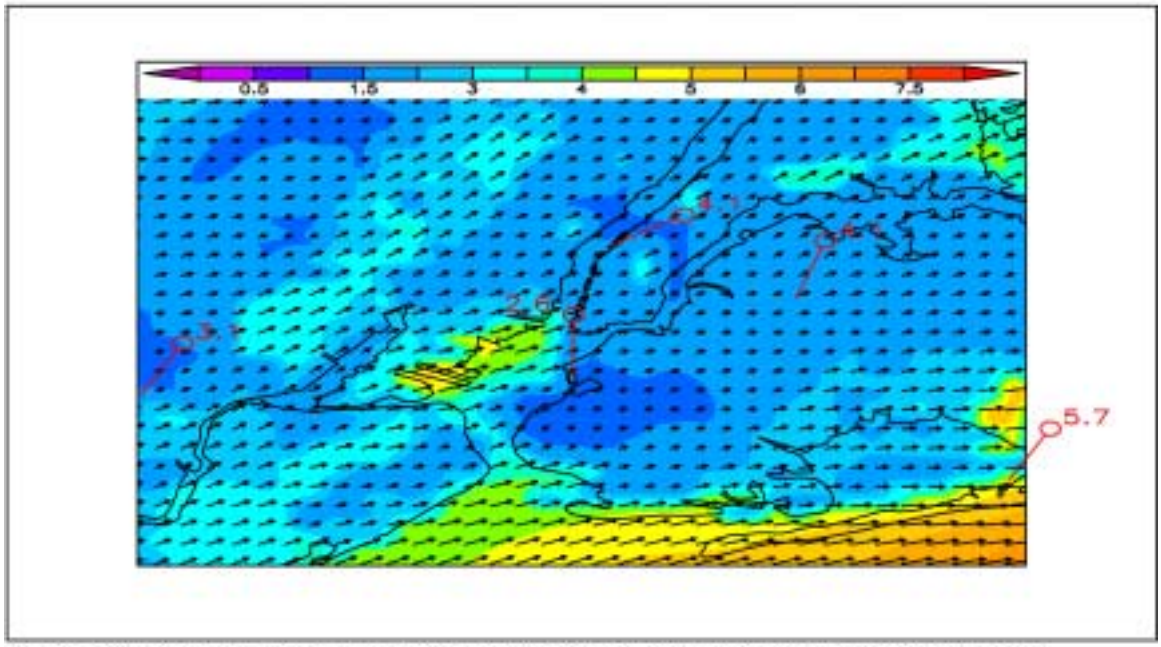

Figure 5.7b MM5 simulated 10 m wind velocity (m/s) valid 00 UTC (19 LT) 14 November 2001. Surface wind observations shown in Red with barb indicating direction from and number indicating speed (m/s).

The independent tower showed southerly winds of 2.6 m/s, while the ARPS simulation predicted southerly winds around 3 m/s. The MM5 simulation predicted southwesterly winds over lower Manhattan during this period.

Model estimated 10-m wind direction (vectors) and speed (contoured in m/s) at 03 UTC (22 LT) 14 November are shown in Figures 5.8a (ARPS) and 5.8b (MM5). All surface observations showed a general wind flow moving from southwest to northeast at this time. The MM5 simulation had a southwesterly flow forecasted over the entire domain, at varying speeds, agreeing with the surface observations. However, the ARPS simulation had a much more complex flow pattern, with winds blowing out of the southeast over portions over Brooklyn and Manhattan. For example, the ARPS simulated a 1.5 m/s southeasterly wind velocity over LaGuardia Airport, while the ASOS site measured a southwesterly wind flow at a speed of 3.6 m/s. The MM5 simulated a southwesterly wind flow at 2 m/s over the same region. Additionally, the ARPS simulated a 1.5 m/s southerly wind velocity over Central Manhattan, while the Central Park ASOS observed west-southwesterly winds at a speed of 4.1 m/s. The MM5 simulation showed southwesterly winds at speeds more than 3 m/s over the same region in central Manhattan. Looking more closely over New Jersey, both the ARPS and MM5 showed a southwesterly wind direction, agreeing with surface observations. However, there were some differences between the two simulations regarding wind speed over New Jersey. For example, the ARPS simulated a wind speed of 1.5 m/s over Teterboro, New Jersey. The MM5 simulated a 2 m/s over the same region. The Teterboro ASOS observed a 2.1 m/s wind speed at this time.

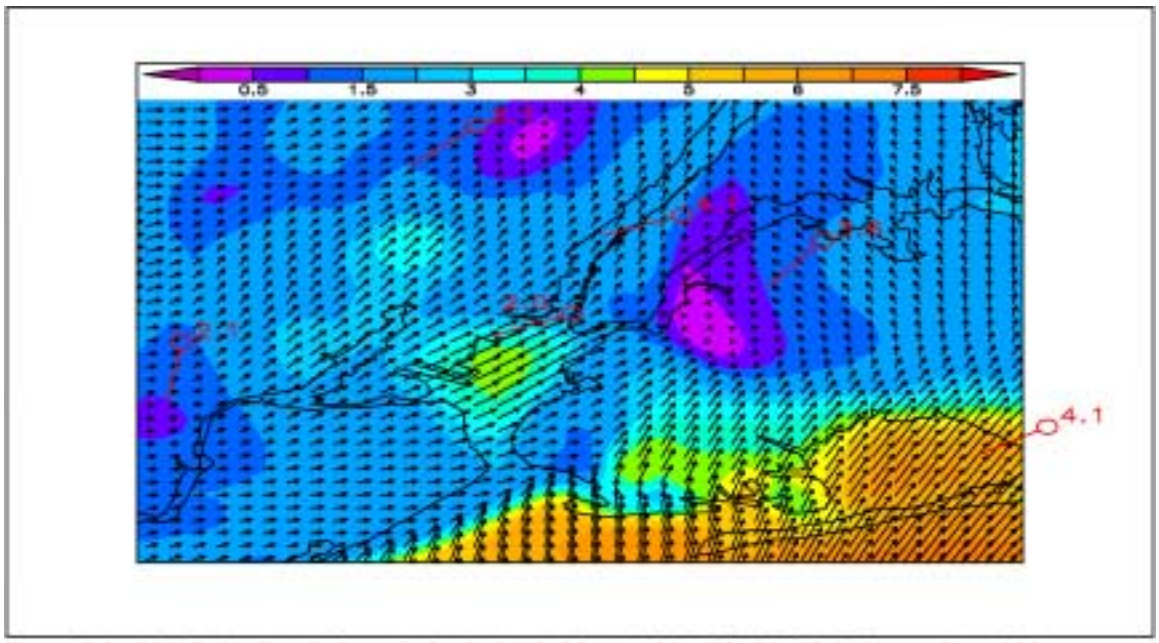

Figure 5.8a ARPS simulated 10 m wind velocity (m/s) valid 03 UTC (22 LT) 14 November 2001. Surface wind observations shown in Red with barb indicating direction from and number indicating speed (m/s).

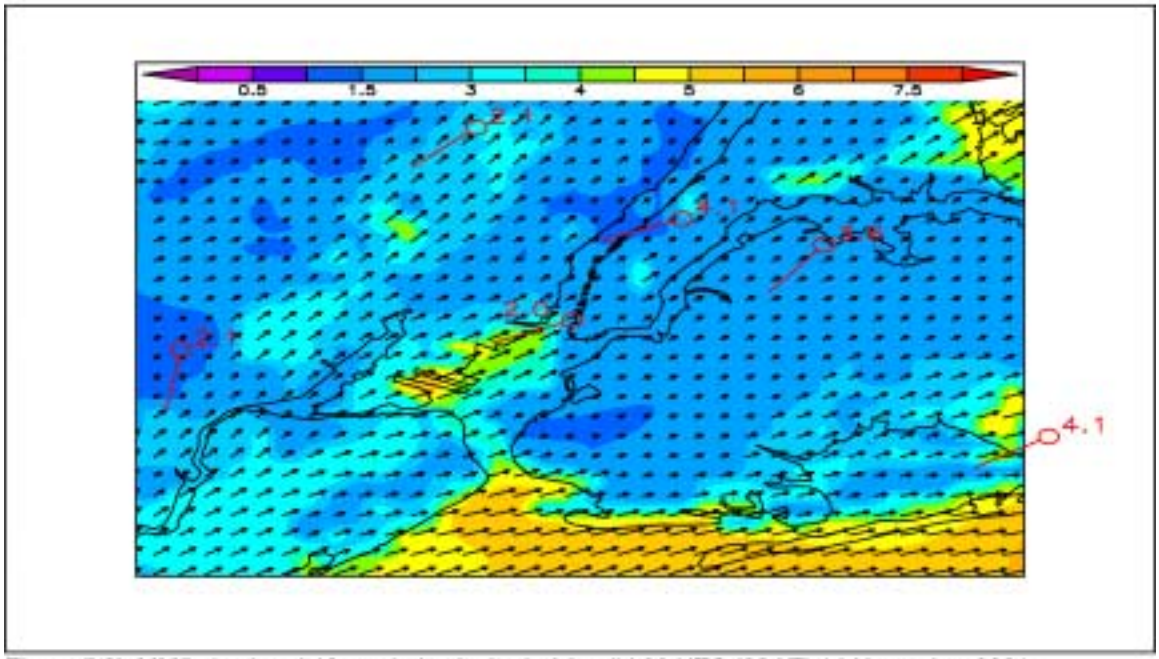

Figure 5.8b MM5 simulated 10 m wind velocity (m/s) valid 03 UTC (22 LT) 14 November 2001. Surface wind observations shown in Red with barb indicating direction from and number indicating speed (m/s).

Additionally, the ARPS simulated a wind speed of 1.25 m/s over Newark, New Jersey, while the MM5 simulated a wind speed of 1.75 m/s over the same region. The Newark ASOS observed a 2.1 m/s wind speed. The ARPS 10 m wind simulation showed more features than the MM5 simulation. Interestingly enough, both simulations showed some cyclonic turning of the 10 m wind field over the urban core of lower Manhattan, as the model simulations showed southwesterly winds becoming more southerly over portions of lower and central Manhattan Island. Observational findings by Bornstein and Johnson (1977) showed that nighttime events during stronger flow regimes (>4 m/s) were associated with distinctive roughness induced cyclonic turning in the winds over the main core of Manhattan and Brooklyn. Clearly, the ARPS and to a lesser extent the MM5 agree with the observational findings of Bornstein and Johnson.

Model estimated 10-m wind direction (vectors) and speed (contoured in m/s) at 06 UTC (01 LT) 14 November are shown in Figures 5.9a (ARPS) and 5.9b (MM5). A very similar wind field to 03 UTC (22 LT) was shown by surface observations over the region. Winds were observed blowing out of the west-southwest over much of New Jersey, Manhattan and Brooklyn. The ARPS simulation at 06 UTC (01 LT) was nearly identical to the 03 UTC (22 LT) ARPS model forecast. For example, both the 03 UTC (22 LT) ARPS simulated wind field and the 06 UTC (01 LT) ARPS simulated wind field showed southeasterly winds over much of Brooklyn and Manhattan. However, surface observations showed winds moving out of the southwest over this region. The MM5 simulation agrees well with observations, forecasting southwesterly winds at varying magnitudes over the entire study domain.

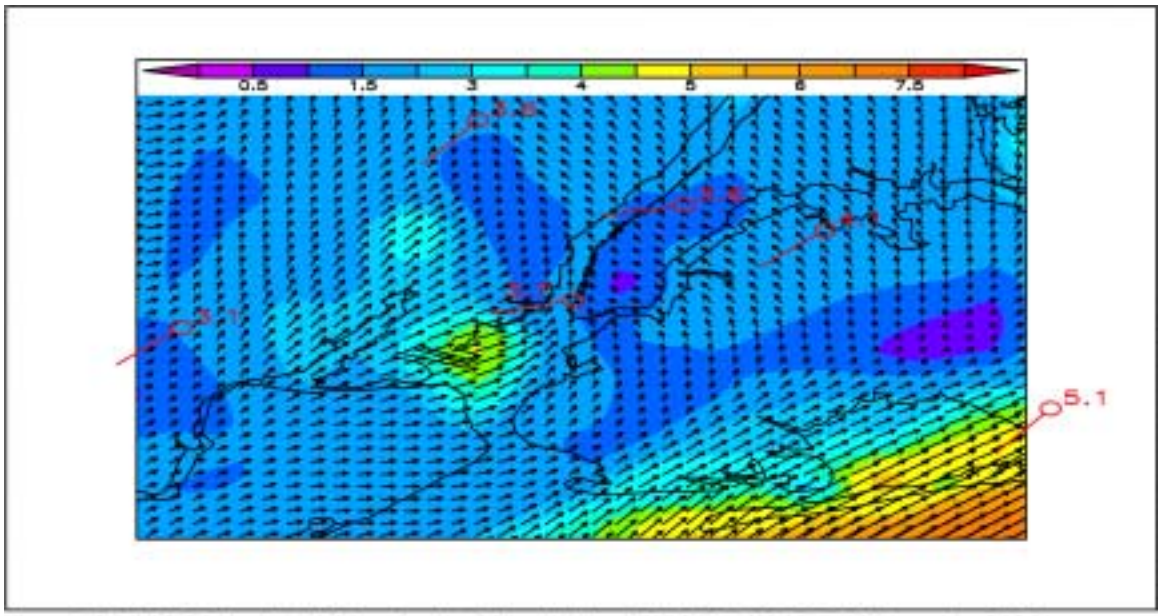

Figure 5.9a ARPS simulated 10 m wind velocity (m/s) valid 06 UTC (01 LT) 14 November 2001. Surface wind observations shown in Red with barb indicating direction from and number indicating speed (m/s).

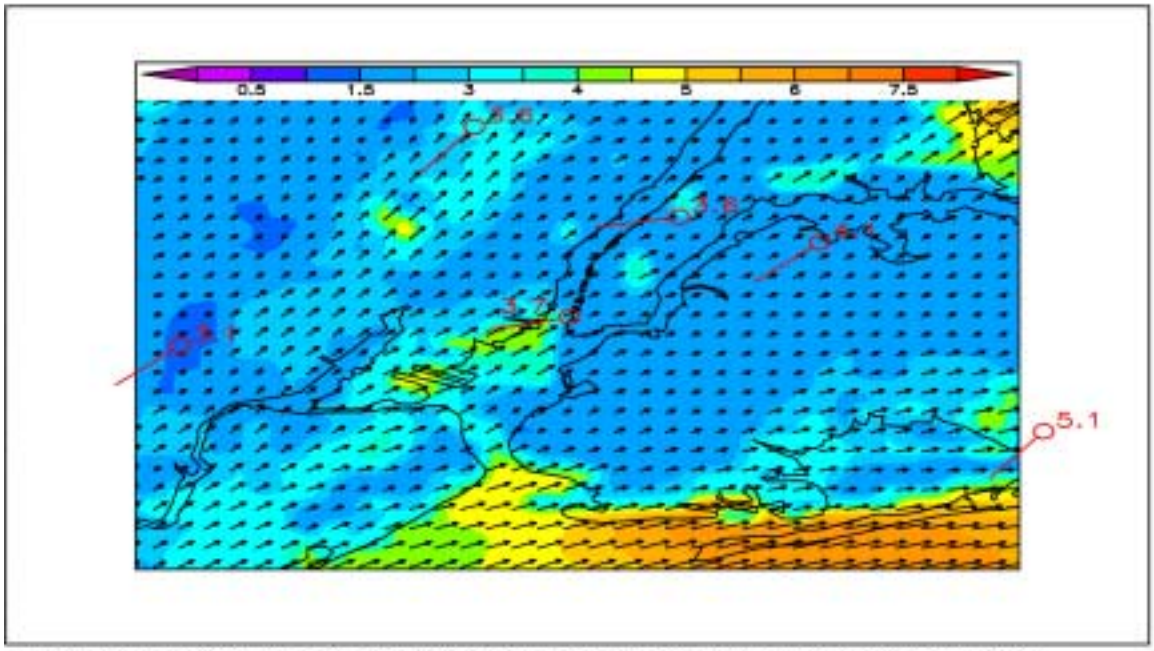

Figure 5.9b MM5 simulated 10 m wind velocity (m/s) valid 06 UTC (01 LT) 14 November 2001. Surface wind observations shown in Red with barb indicating direction from and number indicating speed (m/s).

More specifically, the MM5 forecasted 3.0 m/s southwesterly winds over Central Manhattan, while the Central Park ASOS showed winds out of the west-southwest at 3.6 m/s. However, the ARPS simulation forecasted winds out of the east-southeast at 1.5 m/s. Of interest was the enhancement in the 10 m wind field predicted by the MM5 simulation over Central Park region. Looking closely at the MM5 landuse data, Central Park was well represented in the simulation with a region of much lower roughness length, 0.5 m vs 1.5 m, over the built-up urban core. This decrease in roughness length likely contributed to the localized enhancement of the 10 m wind field. Additionally, the ARPS forecasted winds out of the south-southeast at 2 m/s over Teterboro, New Jersey, while surface observations showed winds out from the southwest at 3.6 m/s. The MM5 simulation, however, forecasted southwesterly winds at 3 m/s, agreeing well with the surface observations. The previous research by Draxler (1986) on the influence of the nocturnal UHI on the local wind fields over highly urbanized regions should be noted. Draxler argues that fast moving winds over rural areas tend to decelerate and turn cyclonically, or anticyclonically depending on large scale flow direction, as they “feel” the effects of the nocturnal UHI. Interestingly enough, the ARPS simulated the decelerating and cyclonic turning in the 10 m wind field; shown in Figure 5.9a, as the fast moving winds from the New York Harbor moved over the urbanized region.

Model estimated 10-m wind direction (vectors) and speed (contoured in m/s) at 09 UTC (04 LT) 14 November are shown in Figures 5.10a (ARPS) and 5.10b (MM5). The differences between the ARPS and MM5 simulations at 09 UTC (04 LT) were very similar to the differences between the simulations at 06 UTC (01 LT).

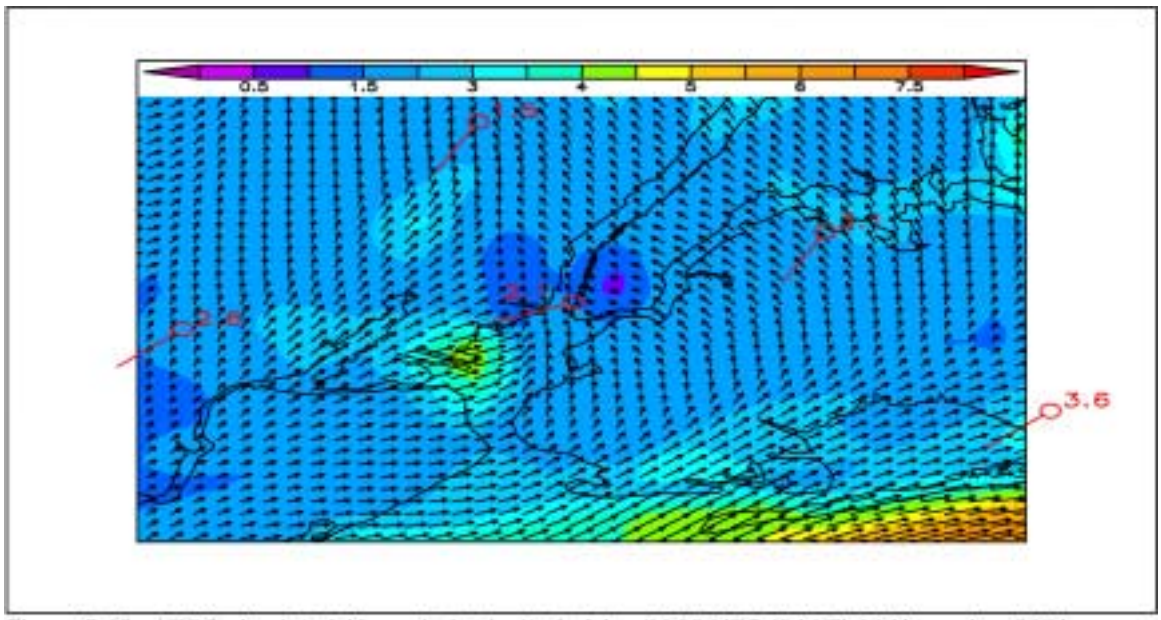

Figure 5.10a ARPS simulated 10 m wind velocity (m/s) valid 09 UTC (04 LT) 14 November 2001. Surface wind observations shown in Red with barb indicating direction from and number indicating speed (m/s).

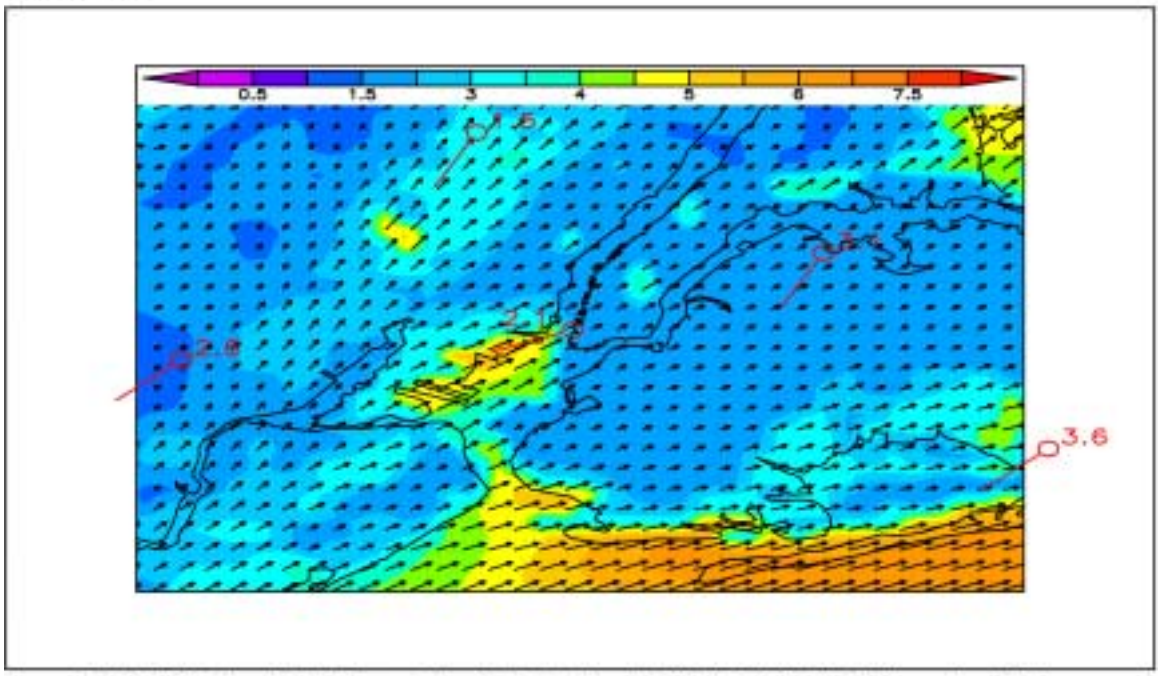

Figure 5.10b MM5 simulated 10 m wind velocity (m/s) valid 09 UTC (04 LT) 14 November 2001. Surface wind observations shown in Red with barb indicating direction from and number indicating speed (m/s).

Moreover, the 09 UTC (04 LT) surface observations were nearly identical to the 06 UTC (01 LT) surface observations, showing a southwesterly wind over the entire region. Similarly, the ARPS simulation continued to show strong cyclonic turning of the 10 m wind field over Brooklyn and Manhattan. For example, the ARPS simulation showed southeasterly winds over LaGuardia Airport, while the ASOS site showed winds out of the southwest. Additionally, the ARPS simulation produced southeasterly winds over lower Manhattan, while the independent tower has winds out of the southwest. The MM5 has southwesterly winds for both locations, matching up closely with observations. As mentioned above, the ARPS simulation does agree with previous research by Draxler (1986) who argued that fast moving winds over rural areas tend to decelerate and turn cyclonically, or anticyclonically depending on large scale flow direction, as they "feel" the effects of the nocturnal UHI.

Model estimated 10-m wind direction (vectors) and speed (contoured in m/s) at 12 UTC (07 LT) 14 November are shown in Figures 5.11a (ARPS) and 5.11b (MM5). The surface observations indicated a broad southwesterly flow over the entire region, and both the ARPS and MM5 continued to diverge in their respective wind field simulations. More specifically, the ARPS simulation continued to show strong (>4 m/s) southwesterly winds moving into Brooklyn off the Atlantic, decelerating and turning cyclonically as they interact with the UHI and roughness change. The MM5 continued to show a general southwesterly flow over the entire region. The differences in the 10 m wind simulations are likely associated with the representation of the urban heat island and roughness length heterogeneities in each of the dynamical simulations.

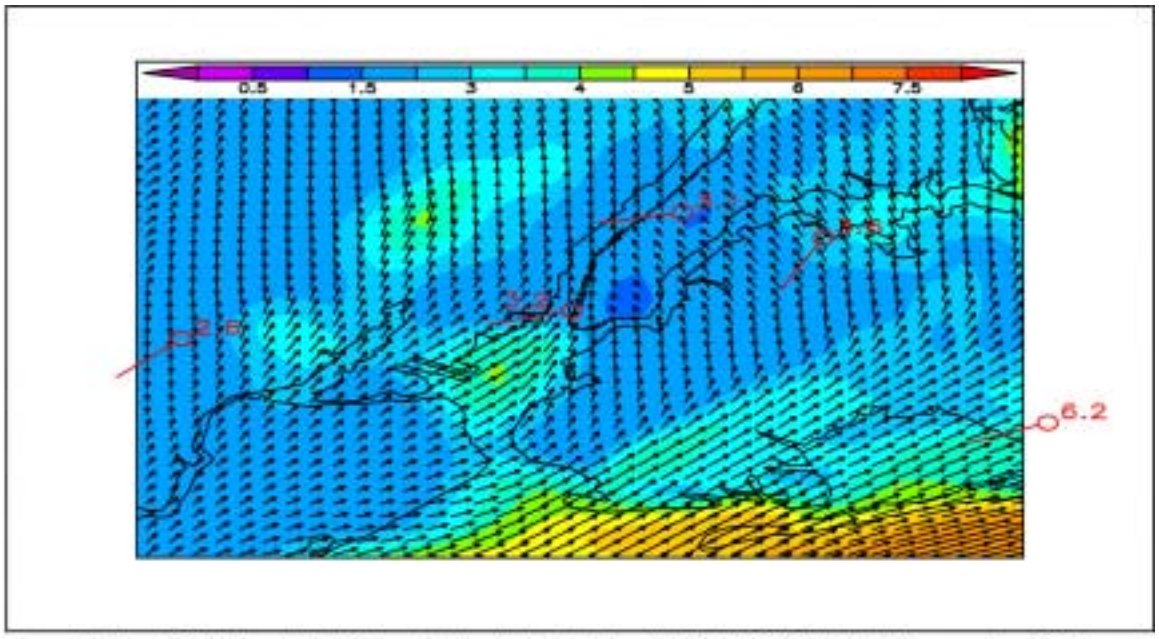

Figure 5.11a ARPS simulated 10 m wind velocity (m/s) valid 12 UTC (07 LT) 14 November 2001. Surface wind observations shown in Red with barb indicating direction from and number indicating speed (m/s).

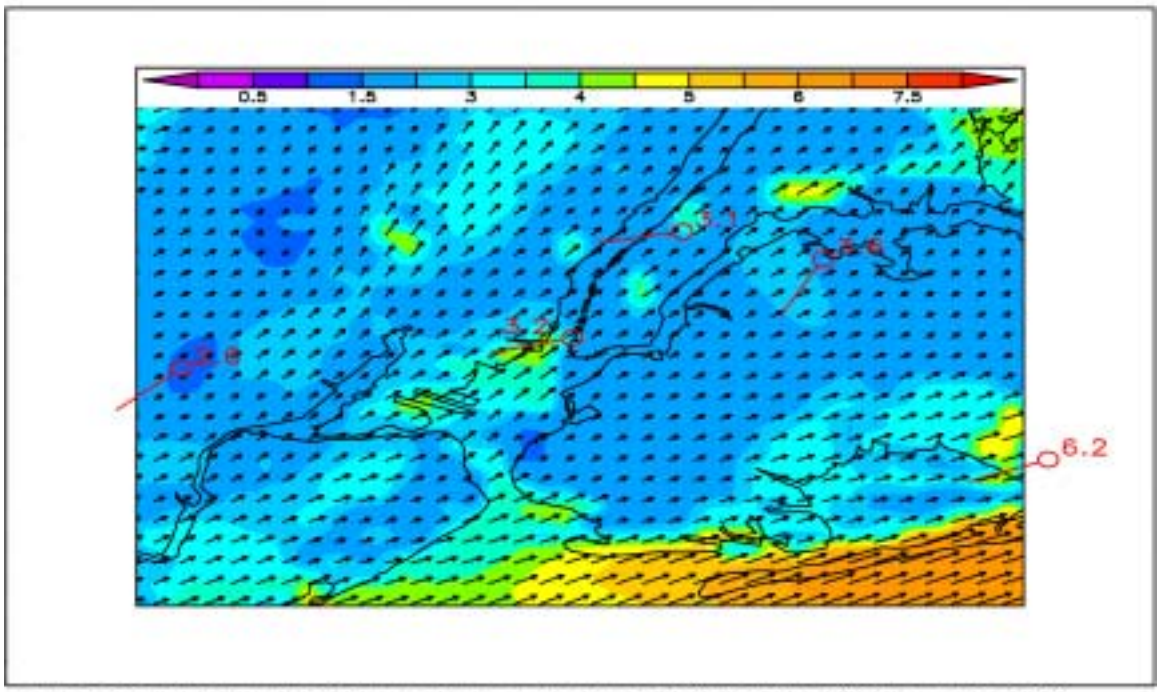

Figure 5.11b MM5 simulated 10 m wind velocity (m/s) valid 12 UTC (07 LT) 14 November 2001. Surface wind observations shown in Red with barb indicating direction from and number indicating speed (m/s).

In an effort to gain additional insight into the differences between the ARPS and MM5 simulations, 24-h averaged 10 m wind speed and direction will be examined with 24-h averaged surface observations. Model simulated 24-h average wind speed and direction, valid at 12 UTC (07 LT) 13 November until 11 UTC (06 LT) 14 November, are shown in Figures 5.12a (ARPS) and 5.12b (MM5), respectively. The 24-h averaged 10 m observations are shown in red, with the barb indicating direction from, and the number indicating wind speed (m/s). Looking closely at both simulations, it is apparent that there were some differences between the two. For example, the ARPS simulation showed 24-h averaged south-southeasterly winds over portions of Queens and Manhattan at a speed of 1.5 m/s, while 24-h averaged observations from LaGuardia and Central Park ASOS sites showed westerly winds at 3.6 and 3.1 m/s, respectively. The MM5 simulation shows 2.5 m/s southwesterly winds over both locations. It is suggested that the ARPS simulation turned the low-level wind field cyclonically over much of Brooklyn, Queens and Manhattan, as a result of influences from both the roughness length heterogeneities and nocturnal urban heat island associated with New York City. Surface observations and the MM5 simulation showed a general southwesterly flow over most of region. The exception to this was over the far eastern-most location in the domain, where the JFK Airport ASOS site observed a 24-h averaged wind direction from the southeast at 4 m/s. This is likely a result of the development of a thermal internal boundary layer developing between the land/water interfaces to the southeast of JKF Airport. Additionally, there were also some differences between the simulations noted over New Jersey. For example, the ARPS simulation showed 24-h averaged wind velocity of 1.5 m/s from a direction slightly east of due south over Teterboro.

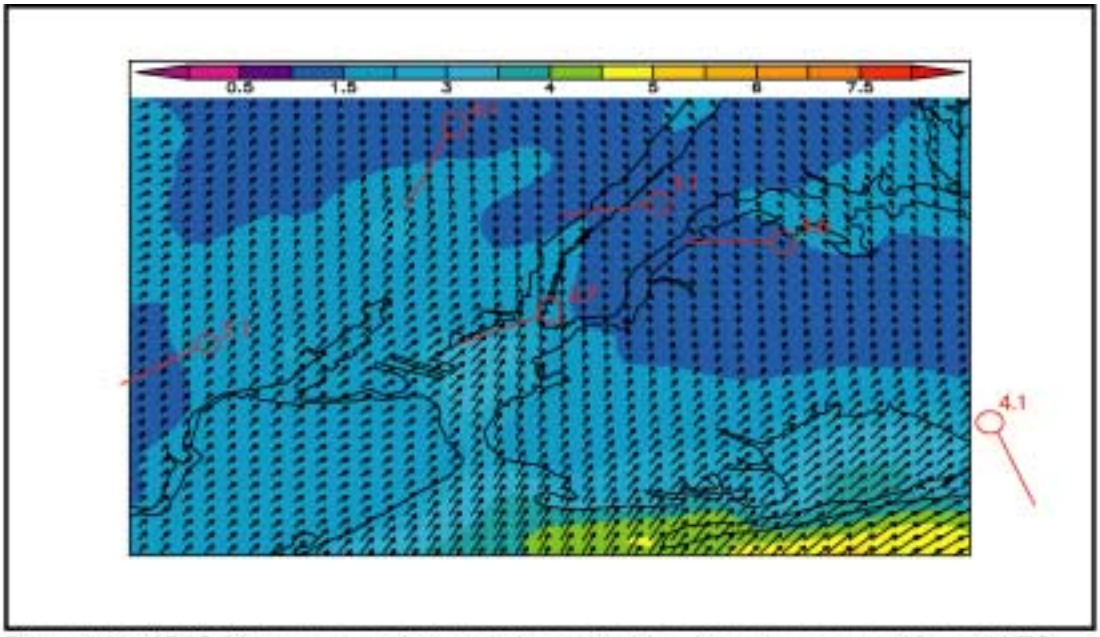

Figure 5.12a ARPS 24-hour averaged 10 m wind speed (m/s) and direction computed from 12 UTC (07 LT) 13 November through 12 UTC (07 LT) 14 November. Averaged 24-hour 10-meter wind observations shown in Red with barb indicating direction from and number indicating speed (m/s).

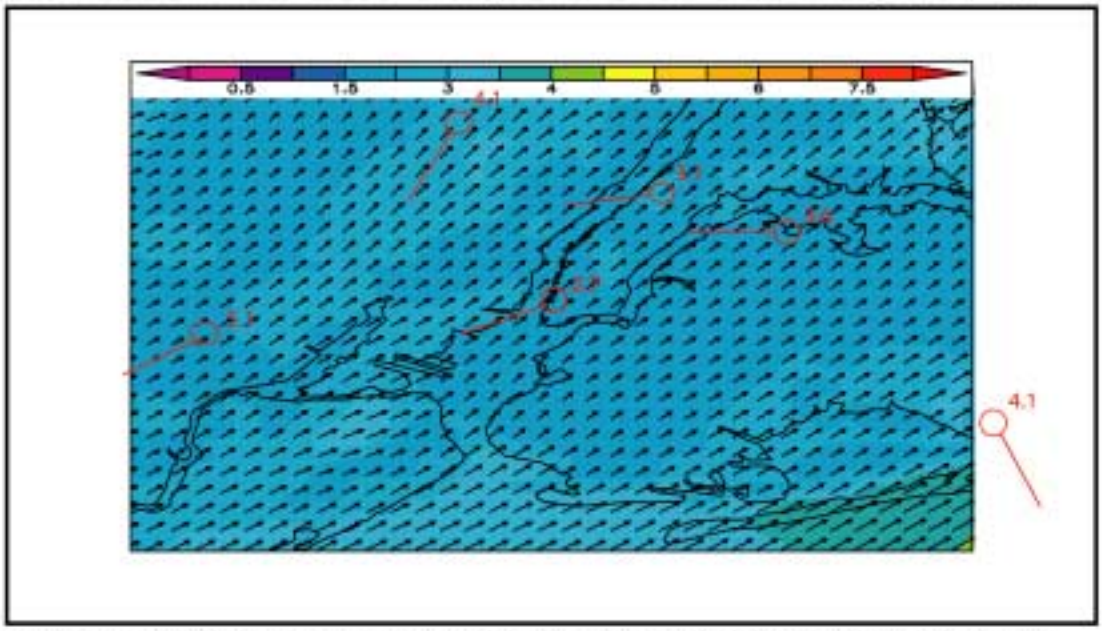

Figure 5.12b MM5 24-hour averaged 10 m wind speed (m/s) and direction computed from 12 UTC (07 LT) 13 November through 12 UTC (07 LT) 14 November. Averaged 24-hour 10-meter wind observations shown in Red with barb indicating direction from and number indicating speed (m/s).

The Teterboro ASOS site showed 24-h averaged southwesterly winds at 4.1 m/s. Furthermore, the MM5 simulation showed a 24-h averaged wind velocity of 3 m/s out of the southwest over the same region. Another important difference between the two simulations was found over the New York Harbor. The ARPS simulation showed a south-southwesterly wind over the region, with a speed of 2.5 m/s, while the MM5 simulation showed an averaged southwesterly wind at 2 m/s over the harbor. The independent tower over Lower Manhattan is directly adjacent to the New York Harbor, and is located on a pier that runs out over the water. The independent tower observed a 24-h averaged southwesterly wind at 2.6 m/s.

While the 24-h averaged wind velocity over the region is an important indicator of model performance, 12-h averaged wind velocities may be a better evaluative tool. The *first* 12-h period averages wind velocity from 12 UTC (07 LT) 13 November through 23 UTC (18 LT) 14 November and covers the "daytime" period. The *second* 12-h period averages wind velocity from 00 UTC (07 LT) 14 November through 11 UTC (06 LT) 14 November, inclusive, and covers the "nighttime" period. The "daytime" model simulated 12-h average surface wind velocities (m/s) are shown in Figures 5.13a (ARPS) and 5.13b (MM5). 12-h averaged surface wind velocity observations are shown in red, with the barb indicating direction from and the number indicating speed (m/s). When comparing both model simulations, there were several differences noted. For example, the ARPS simulation showed light (< .5 m/s) wind speeds and variable directions over much of Brooklyn, Queens and Manhattan. Conversely, the MM5 showed 12-h averaged wind velocities of 1.5 m/s out of the southwest over the same region.

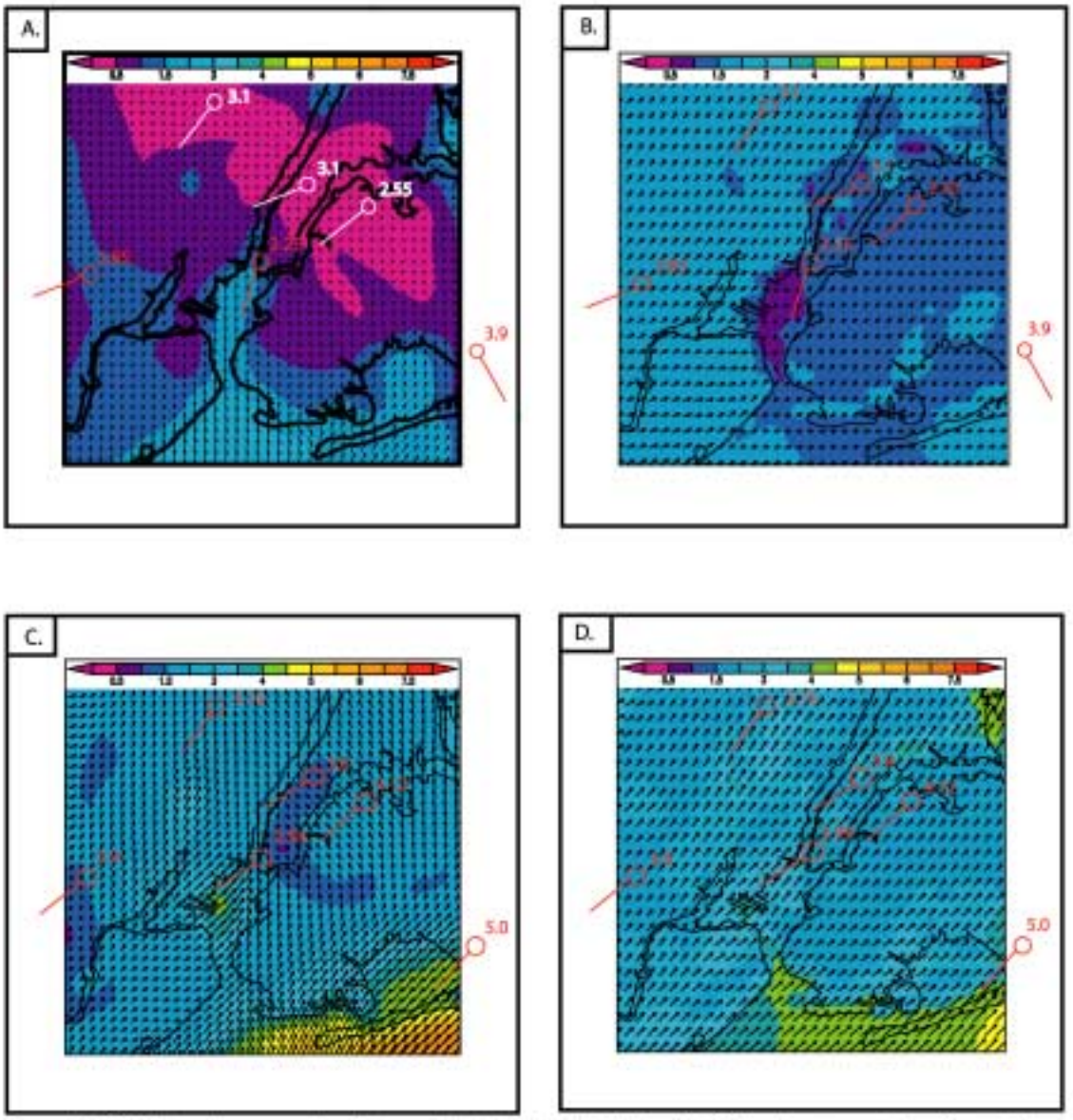

Figure 5.13 12-hourly averaged surface wind velocity (m/s) plots with 12-hourly averaged surface wind velocity observations shown in Red, with the barb indicating direction from and the number indicating speed (m/s). Figures A and B show the ARPS and MM5 12- hourly averaged surface wind velocity from 12 UTC (07 LT) 13 November through 23 UTC (18 LT) 13 November, respectively. Figures C and D show the ARPS and MM5 12-hourly averaged surface wind velocities from 00 UTC (19LT) 14 November through 11 UTC (06 LT)14 November with barb indicating direction from and number indicating speed (m/s).

The 12-h averaged observations from LaGuardia, Central Park and the independent tower showed a southwesterly wind flow with speeds between 2 and 3 m/s. Looking closely over New Jersey, subtle differences were observed between the two numerical simulations. For example, the ARPS simulated southwesterly winds over much of New Jersey with wind speeds less than 1 m/s. Conversely, the MM5 simulated southwesterly winds over much of New Jersey, with speeds greater than 1.5 m/s. The 12-h averaged observations from Teterboro and Newark showed wind velocities out of the southwest at 3.1 and 2.85 m/s, respectively. Another difference between the two simulations was found over the New York Harbor, where the ARPS simulation showed 12-h averaged wind velocities of 2 m/s out of the south. The MM5 simulation showed winds out of the south at less than 1 m/s over the harbor. As mentioned in the beginning of this section, the MM5 was initialized with 2 C cooler SST's over the New York Harbor than the ARPS simulation, likely leading to the development of a more stable boundary layer, and less turbulent momentum transfer to the surface.

The "nighttime" model simulated 12-h average surface wind velocities (m/s) are shown in Figures 5.13c (ARPS) and 5.13d (MM5). The 12-h averaged surface wind velocity observations are shown in red, with the barb indicating direction from and the number indicating speed (m/s). Looking closely over Brooklyn, Queens and Manhattan, several differences were observed between the ARPS and MM5 simulations. For example, the ARPS simulation showed southwesterly winds moving in off the Atlantic, decelerating and turning cyclonically as they move into Brooklyn and Queens. However, the MM5 simulation showed southwesterly winds over Brooklyn and Queens, with little indication of cyclonic turning. More specifically, the ARPS simulation showed 12-h

averaged winds out of the southeast over LaGuardia Airport and Central Park, while the MM5 simulation showed winds out of the southwest. Observations from the LaGuardia Airport and Central Park ASOS sites showed 12-h averaged winds out of the southwest, agreeing well with the MM5 simulation. Additionally, the ARPS simulation showed lower wind speeds over Manhattan than the MM5 simulation does. The ARPS simulation showed wind speeds less than 1.5 m/s over much of Central and Lower Manhattan, while the MM5 simulation showed wind speeds between 2 and 3 m/s over the same region. The 12-h averaged wind speed from Central Park is 3.1 m/s, while the ARPS simulation showed a wind speed of 1.5 m/s over Central Park. Conversely, the MM5 simulation showed a 12-h averaged wind speed of 3 m/s over the region, agreeing well with the surface observation. Despite the fact that roughness lengths we identical in both simulations, the ARPS simulation likely had lower average wind speeds because it was more influenced by the large roughness associated with Manhattan and Brooklyn. The 12-h averaged surface observations from New Jersey showed that a southwesterly flow pattern dominated the region during this 12-h period. The ARPS simulation indicated a cyclonic turning of the 10 m wind field over much of New Jersey, leading to forecasted southeasterly winds. The MM5 simulation did not show this effect, and indicated a southwesterly wind flow over all of New Jersey.

5.5 SUMMARY

Numerical simulations of wind velocity are complex over highly urbanized areas such as New York City. The development of the urban heat island and the heterogeneous roughness length characteristics are two important factors that influence the lower

troposphere atmospheric flow. In this study, the ARPS and MM5 simulated surface (10 m) wind fields were compared and contrasted with each other and with surface observations. Several differences were noted between the two simulations. For example, the ARPS simulation consistently forecasted a decelerating and cyclonically turning mesoscale wind flow over Brooklyn, Queens and Manhattan. Conversely, the MM5 simulation forecasted a southwesterly wind flow across the entire region, with very little deceleration and cyclonic turning. Research by Draxler (1986), Shreffler (1978, 1979) and Bornstein and Johnson (1977) found evidence for decelerating and cyclonically turning flows over highly urbanized areas. The MM5 simulation did show some cyclonic turning of the 10 m wind field over the lower Manhattan. This process is seen in Figure 5.7b where MM5 simulated west-southwesterly winds over the New York Harbor become more southwesterly as they encounter the urban core of lower Manhattan. Another notable difference between the simulations was the forecasted wind fields over the New York Harbor. The ARPS simulation consistently showed stronger winds than the MM5 model. With 2 C cooler SST's initialized in the MM5 simulation, a stable marine boundary layer developed over the New York Harbor, which likely limited the turbulent transfer of momentum. Additionally, there were notable differences between the two simulations over New Jersey. The ARPS simulation often showed some moderate cyclonic turning of the 10 m wind field over much of New Jersey, leading to forecasted southeasterly winds. The MM5 simulation did not show this effect, and indicated a southwesterly wind flow over all of New Jersey, matching surface observations from Newark and Teterboro ASOS throughout the study period.

The ARPS simulation showed a more defined sea breeze frontal formation and propagation than the MM5 simulation did. The 10 m independent instrumentation tower over lower Manhattan confirmed the timing and position of the frontal passage simulated by the ARPS model. While the MM5 model did not have a very well defined sea breeze frontal feature, the wind speed and direction did match up well with surface observations. Moreover, the ARPS simulated 10 m wind field was very responsive to the roughness length variations and urban heat island associated with New York City, as observed by tendency for cyclonic turning of the 10 m wind field over Brooklyn and Manhattan. The MM5 simulation was not as responsive to the roughness length variations and the urban heat island as the ARPS simulation. Both simulations had identical roughness length specifications and landuse data, so the differences are likely associated with the differences in the planetary boundary layer physics and SST data used in each simulation. The MM5 simulation used the Eta M-Y PBL model while the ARPS simulation used the Sun and Chang PBL model. Both models are 1.5 order TKE closure models. However, the Eta M-Y PBL parameterization uses a *local* closure approximation while the Sun and Chang PBL parameterization uses *non-local* closure. Additionally, in the dynamical turbulence layer, defined as the turbulent layer at the bottom of the surface layer, the ratio of height z and the Monin-Obukhov length scale (Stull, 1988) is small so that logarithmic wind profiles are used in the surface layer for both PBL models.

The differences in near-surface wind velocity between the ARPS and MM5 simulations over New York City may be the result of the sensitivity of each PBL model to roughness length variations in the dynamical turbulence layer. While both numerical models simulated the 10 m wind field well over the study period, the ARPS simulation

will be used for the following study of the urban heat island and sea breeze analysis over New York City. The ARPS model was selected because it more accurately and clearly represented the sea breeze front, and was more influenced by roughness length variations and nocturnal urban heat island affects than the MM5 simulation.

CHAPTER 6

EFFECTS OF THE URBAN HEAT ISLAND AND SEA-LAND BREEZE CIRCULATION

6.1 INTRODUCTION

An objective of this research is to study the evolution of the mesoscale boundary layer over the New York City Metropolitan area through numerical simulations. More specifically, the urban heat island effect and sea breeze front will be examined in detail. Because of the highly urbanized landscape characteristics of this region, high-resolution numerical simulations are challenging. The ARPS model simulation will be compared and contrasted with surface weather observations taken during a high-pollutant concentration event over New York City in November 2001. Results from the simulation will be used to study the diurnal structure and evolution of the mesoscale boundary layer over the region.

As discussed in Chapter 5, the ARPS model was initialized at 00 UTC 13 November 2001 and integrated over a 60-hr time period until 12 UTC 15 November 2001. This period was chosen because of the formation and propagation of a sea breeze front through lower Manhattan, and also because the synoptic pattern favored the development of the urban heat island. Synoptic features for this period were presented in Chapter 5. The ARPS simulation had a horizontal grid spacing of 1 km with 37 vertical sigma levels. Details of the model setup, including domain size and model input data were discussed in Chapter 3. For a more complete review of the model setup, including domain size and model input data, please refer back to Chapter 3 in this thesis.

6.2 ANALYSIS OF A SEA BREEZE FRONT OVER MANHATTAN

Model estimated 10-m wind direction (vectors) and speed (contoured in m/s) at 15 UTC (10 LT) 13 November is shown in Figure 6.1a. Surface wind observations are shown in red, with the barb indicating direction from and the number indicating speed (m/s). The surface wind flow was out of the north over much of the region at speeds less than 2 m/s. Under more careful examination, though, southerly surface winds were observed just south of Brooklyn and Staten Island, creating a weak convergence boundary. This feature was likely associated with a weakening land breeze front over the Atlantic Ocean. Figure 6.1b shows 100-meter wind velocity vectors and vertical velocity (contoured in m/s) valid 15 UTC (10 LT) 13 November. The 100 m wind flow showed winds out of the north over much of the domain, becoming more westerly over and just to the east of Staten Island. Looking at the vertical velocity contours, an enhancement in upward vertical motion was simulated over and just east of Staten Island where upward vertical velocities were near 0.15 m/s. This region corresponded to the simulated surface convergence associated with the weakening land breeze noted in Figure 6.1a.

Model estimated 10-m wind direction (vectors) and speed (contoured in m/s) at 18 UTC (13 LT) 13 November are shown in Figure 6.2a. As noted in Figure 6.1a above, surface wind observations are shown in red. Looking closely at Figure 6.2a, several distinct features were observed. There was a large convergence boundary simulated over portions of New Jersey, lower Manhattan, Queens and Brooklyn.

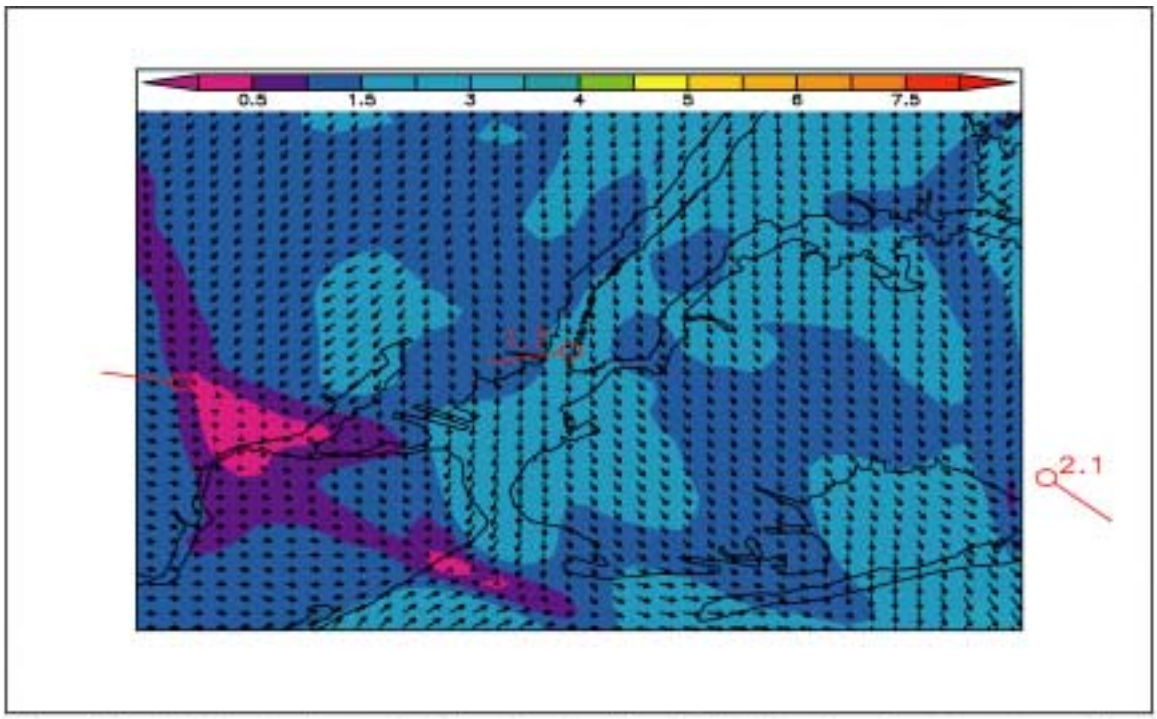

Figure 6.1a. ARPS simulated 10 m wind velocity (m/s) valid 15 UTC (10 LT) 13 November 2001. 10 m wind observations shown in Red with the barb showing wind direction from, and the number indicating speed (m/s).

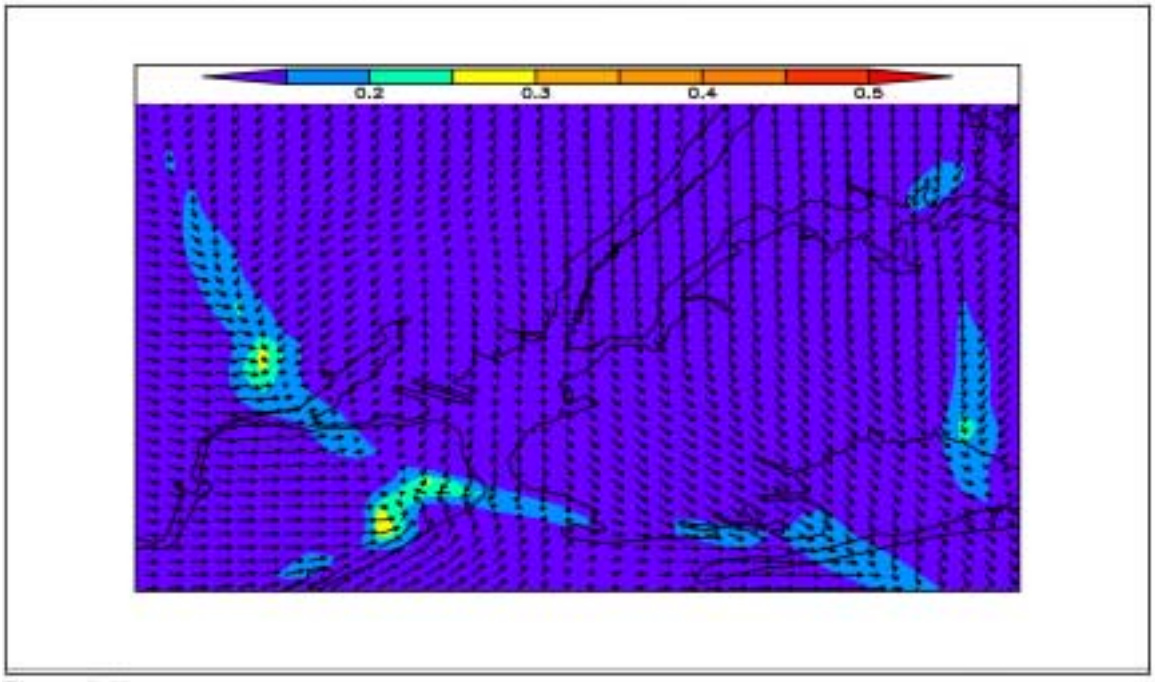

Figure 6.1b. ARPS simulated 100 m wind velocity vectors (m/s) and vertical velocity contours (m/s) valid 15 UTC (10 LT) 13 November 2001.

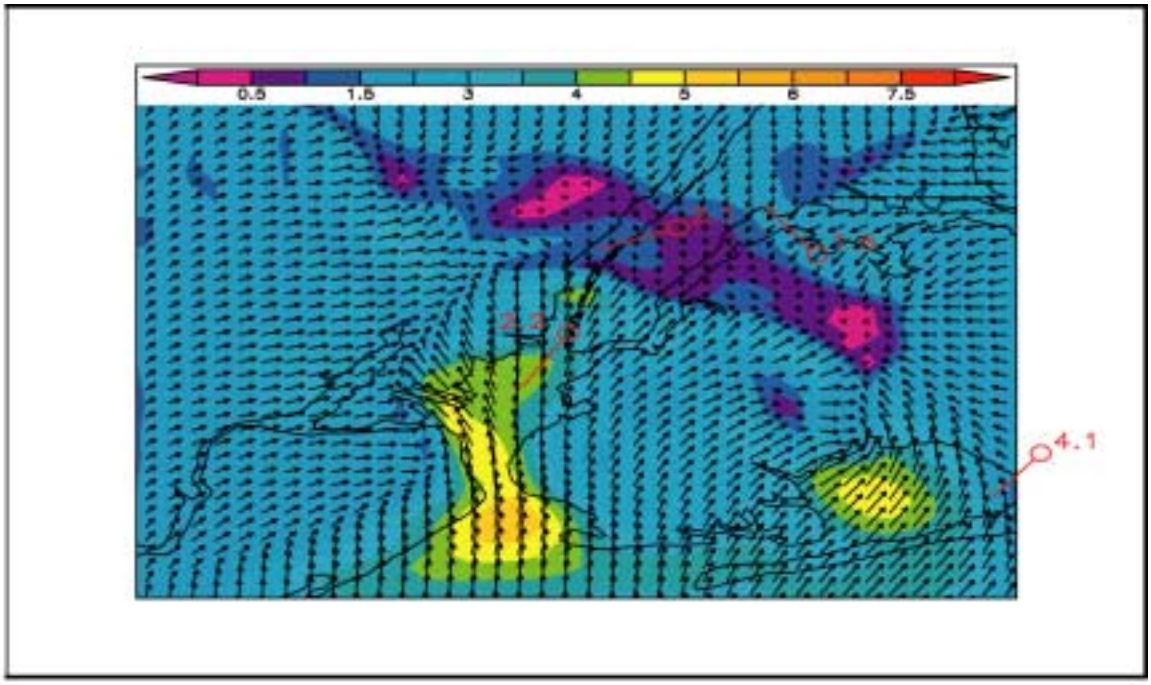

Figure 6.2a ARPS simulated 10 m wind velocity (m/s) valid 18 UTC (13 LT) 13 November 2001. 10 m wind observations shown in Red with the barb showing wind direction from, and the number showing speed (m/s).

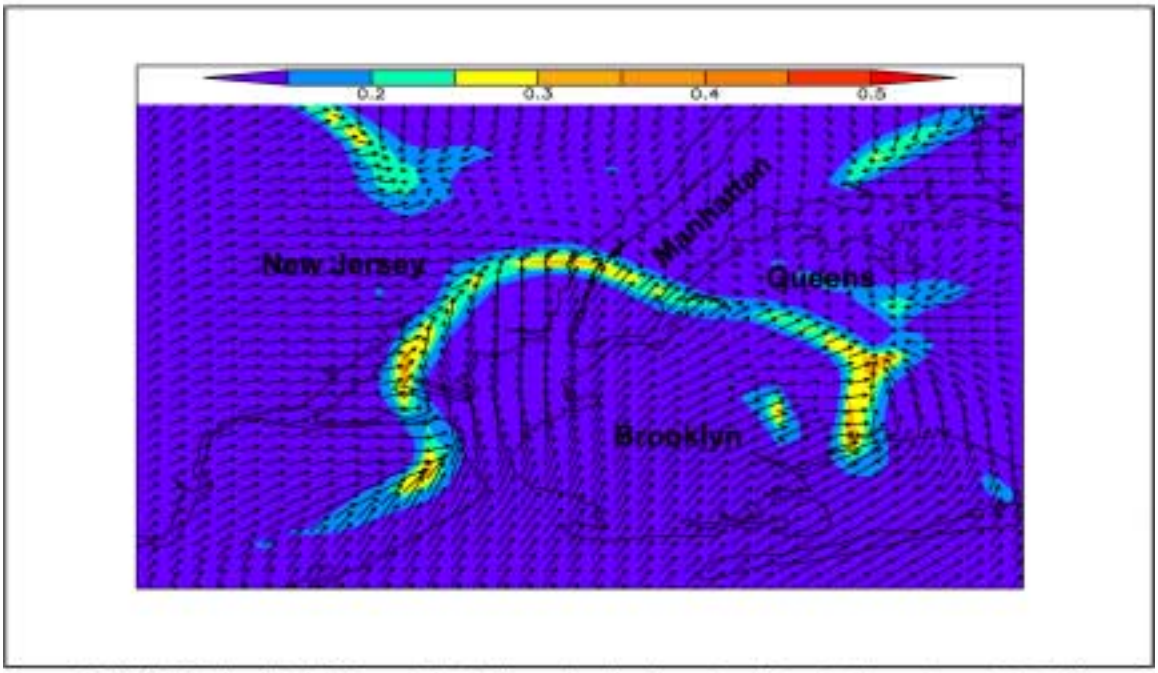

Figure 6.2b ARPS simulated 100 m wind velocity vectors (m/s) and vertical velocity contours (m/s) valid 18 UTC (13 LT) 13 November 2001.

To the north of this boundary, winds were moving from the north and northeast, while to the south of the boundary, winds were moving from the south and southwest. The independent 10 m tower over lower Manhattan, shown in plan view in Figure 2.1, added support to the model simulation, showing south-southwesterly winds associated with the passage of the sea breeze front. Observed surface temperatures over land were 12 C, while SST's were observed near 8 C. This thermal gradient was strong enough to develop a sea breeze front over the region. Another interesting feature was the area of enhanced wind speed simulated over the New York Harbor. The ARPS simulation was initialized with the Advanced Very High Resolution Radiometer (AVHRR) Sea Surface Temperature (SST) analyses archived at 1.44 km to allow for a more accurate simulation of boundary layer features along the land-water interface. Figure 6.2b showed 100 m wind velocity vectors and vertical velocity (contoured in m/s) valid 18 UTC (13 LT) 13 November. A very distinct convergence boundary was observed over the region in an omega-like pattern. The convergence boundary stretched from Staten Island northward into New Jersey, and then spread eastward across lower Manhattan into Queens and Brooklyn before turning southward into Jamaica Bay. Associated with this convergence zone were areas of enhanced upward vertical velocities. Model simulated vertical motion predicted upward vertical velocities between 0.2 and 0.35 m/s as seen in Figure 6.2b. Bornstein (1994) performed numerical simulations over the same area and observed a similar frontal alignment that extended through Staten Island, across lower Manhattan and eastward through Queens and Brooklyn. Figure 6.3a shows a high-resolution map of the New York City Metropolitan area.

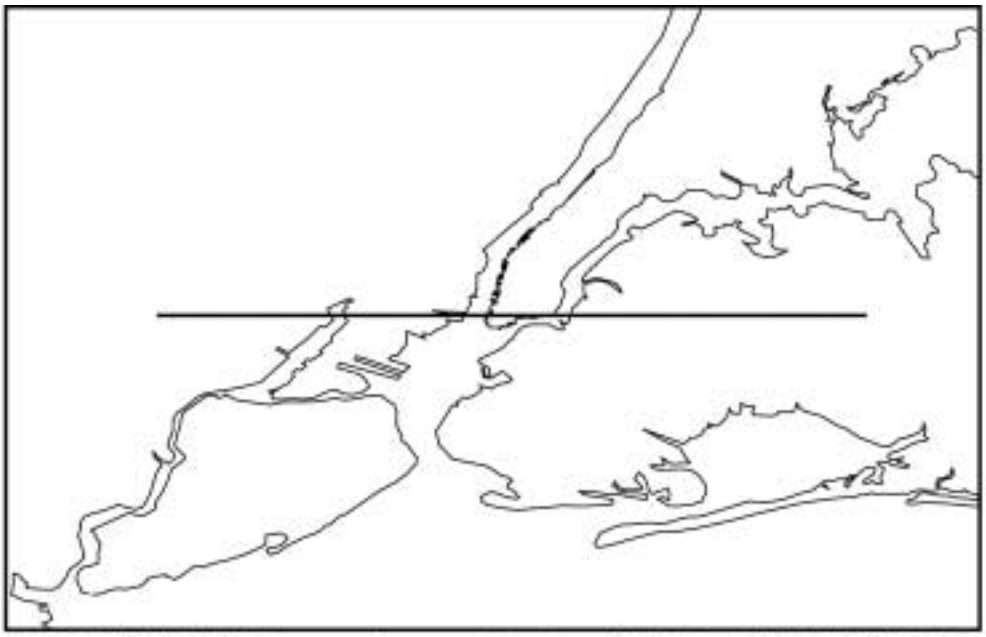

Figure 6.3a Vertical Velocity cross-section over extreme lower Manhattan valid 18 UTC (13 LT) 13 November 2001.

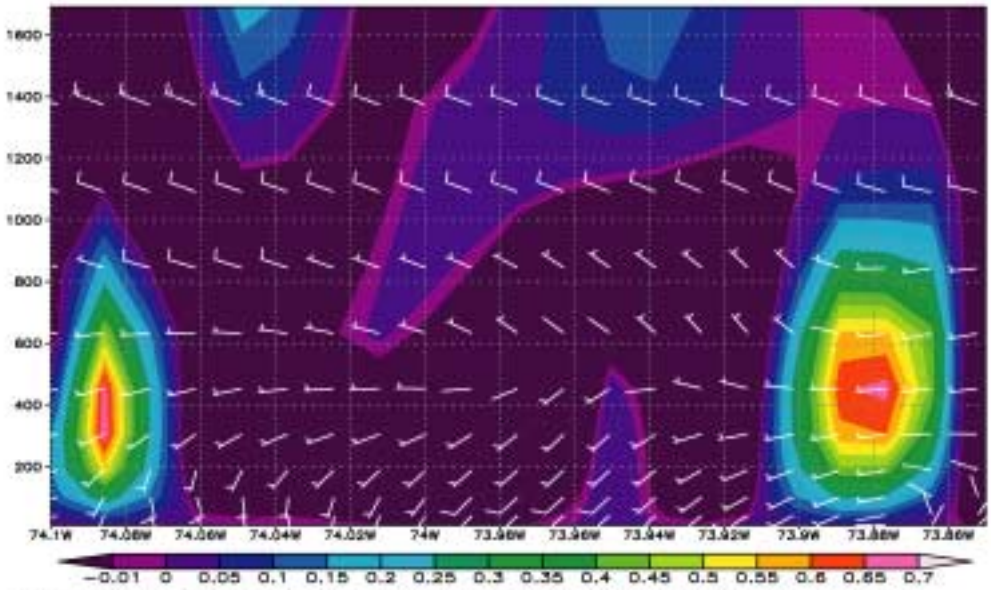

Figure 6.3b Vertical Velocity (m/s) cross-section (m) through a sea-breeze front over extreme southern Manhattan Island valid 18 UTC (13 LT) 13 November 2001.

The dark line indicates the location of a model simulated vertical cross-section, displayed from west to east, shown in Figure 6.3b. Shown in Figure 6.3b are wind barbs (m/s) and vertical velocity (m/s) shading. Two regions of enhanced upward vertical motion were simulated. The first region was over New Jersey, where a maximum upward vertical velocity of 0.7 m/s is simulated. This matched the area of enhanced 100 m level convergence simulated over the same region shown in Figure 6.2b. Another region of enhanced upward vertical motion was evident over Queens and Brooklyn. A well-defined maximum of upward vertical motion exceeding 0.6 m/s was simulated over this region, agreeing closely with the zone of enhanced 100 m convergence simulated in Figure 6.2b over the same area. With southerly winds simulated in the lowest 250 m of the vertical cross-section and westerly to northwesterly winds simulated above 300 m, it is concluded that this frontal feature was shallow in vertical extent. This simulated feature agreed well with previous research by Michael (1998) and Bornstein (1994), who showed similar results using WSR-88D imagery and numerical simulations, respectively.

Model estimated 10-m wind direction (vectors) and speed (contoured in m/s) at 21 UTC (16 LT) 13 November is shown in Figure 6.4a. With the exception of some easterly winds over extreme northern Manhattan Island, the entire model domain showed southerly winds. Looking more closely, there was a zone of maximum surface wind speed over the New York Harbor, where speeds of 5 m/s were simulated. Figure 6.4b shows 100 m wind velocity vectors and vertical velocity (contoured in m/s) valid 21 UTC (16 LT) 13 November. A region of enhanced convergence and vertical motion was simulated over northern Manhattan.

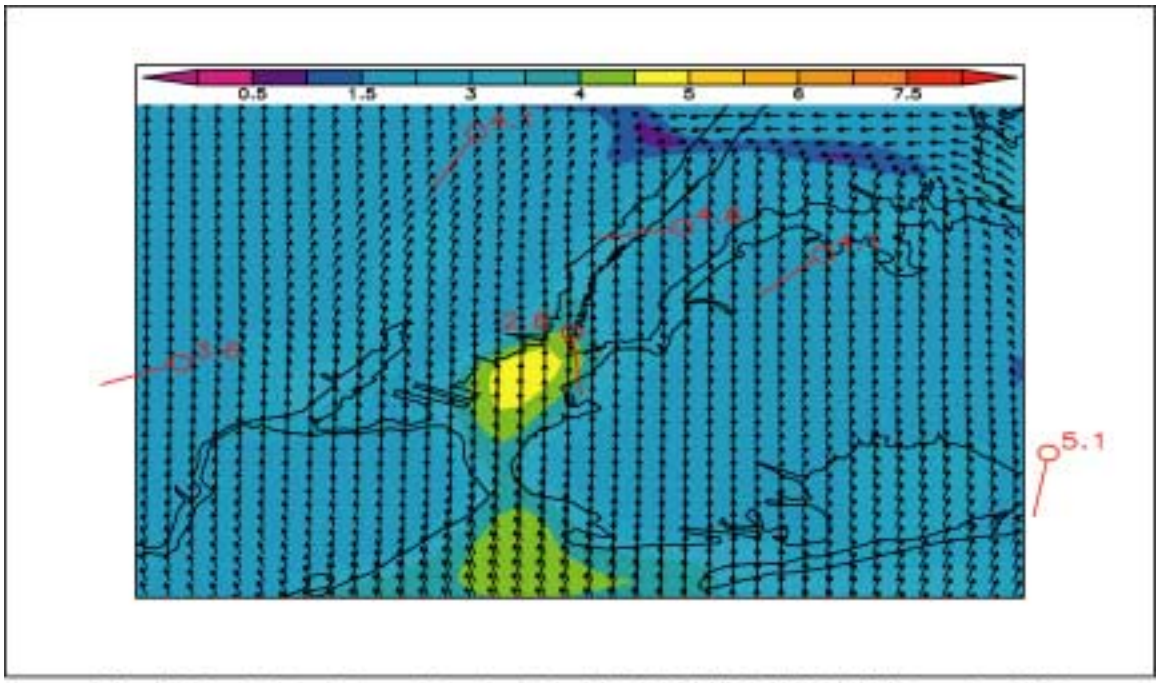

Figure 6.4a ARPS simulated 10 m wind velocity (m/s) valid 21 UTC (16 LT) 13 November 2001. 10 m wind observations shown in Red with the barb showing wind direction from, and the number indicating speed (m/s).

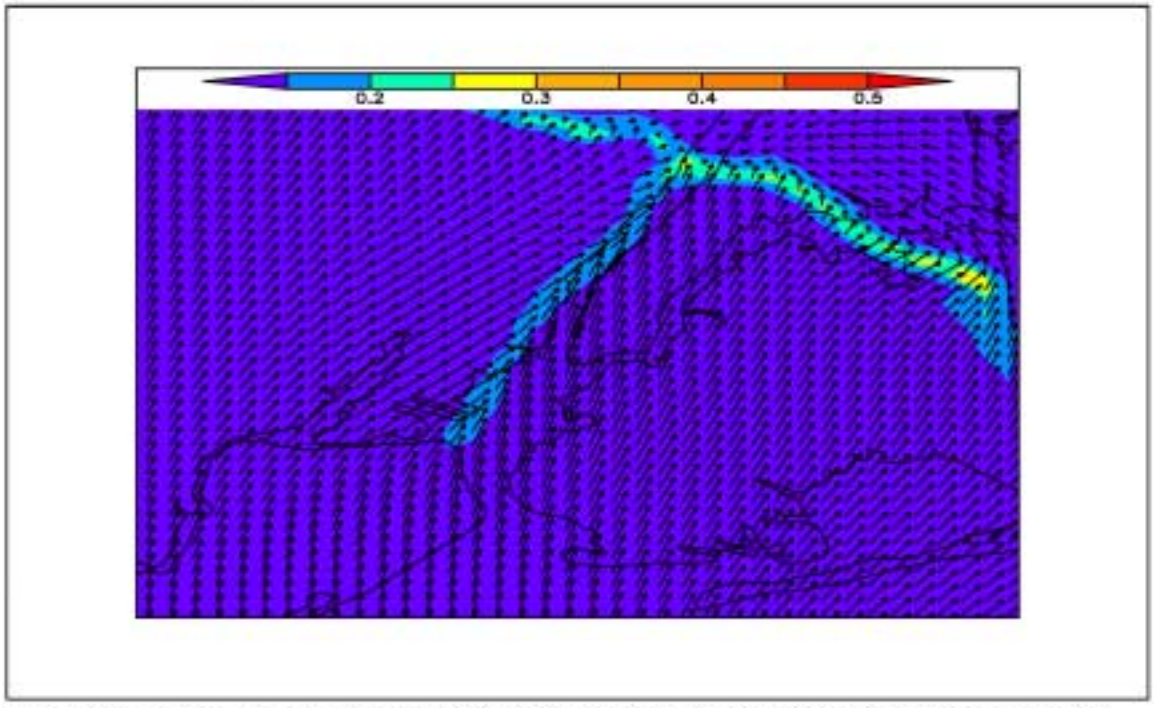

Figure 6.4b ARPS simulated 100 m wind velocity vectors (m/s) and vertical velocity contours (m/s) valid 21 UTC (16 LT) 13 November 2001.

This was likely associated with the northernmost extent of the sea breeze's inland propagation. Upward vertical velocity values exceeding 0.2 m/s were simulated as a result of the low-level convergent forcing.

Figure 6.5a shows a detailed surface map of the New York City metropolitan area. The dark line indicates the location of a model simulated vertical cross-section, displayed from west to east, shown in Figure 6.5b. The cross-section was centered over the World Trade Center disaster recovery site (~40.50 N –74 W). Shown in Figure 6.5b are wind barbs (m/s) and TKE (m^2 s^{-2}) valid at 17 UTC (12 LT) 13 November. This was immediately before the sea breeze front moved through lower Manhattan. Turbulence kinetic energy, (TKE), is a measure of the intensity and effectiveness of turbulence and is useful in determining mixing heights. The TKE budget equation is presented in equation (6.1).

$$\frac{\partial \bar{e}}{\partial t} = \frac{g}{\bar{\theta v}}(\overline{w'\theta v'}) - \overline{u'w'}\frac{\partial \bar{U}}{\partial z} - \partial\frac{(\overline{w'e})}{\partial z} - \frac{1}{p}\frac{\partial(\overline{w'p'})}{\partial z} - \in \qquad (6.1)$$

In equation (6.1) $\frac{\partial \bar{e}}{\partial t}$ is storage or tendency of TKE, $\frac{g}{\bar{\theta v}}(\overline{w'\theta v'})$ is the buoyant production or consumption term, $-\overline{u'w'}\frac{\partial \bar{U}}{\partial z}$ is the mechanical or shear production/loss term, $-\partial\frac{(\overline{w'e})}{\partial z}$ is the turbulent transport of TKE, $-\frac{1}{p}\frac{\partial(\overline{w'p'})}{\partial z}$ is the pressure correlation term and $-\in$ is the viscous dissipation of TKE (Stull, 1988). The ARPS model uses equation (6.1) to simulate TKE over the region. Additionally, equation (6.1) allows for quantitative insight into the importance of the individual turbulent production terms.

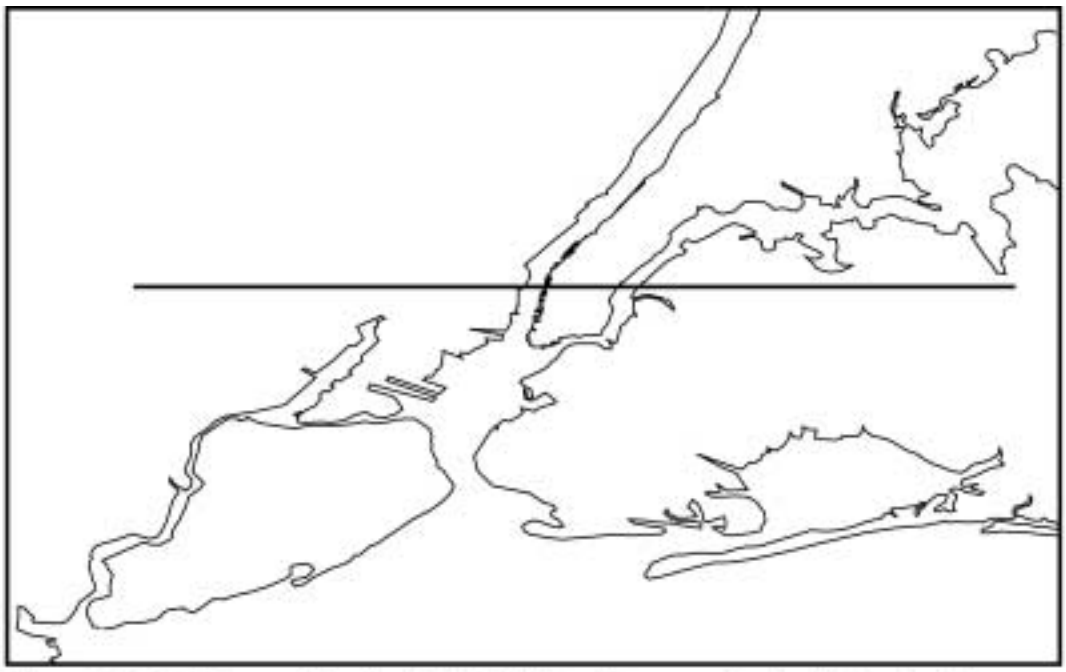

Figure 6.5a Detailed map of the New York City Metropolitan area showing the location of the vertical cross-section shown below.

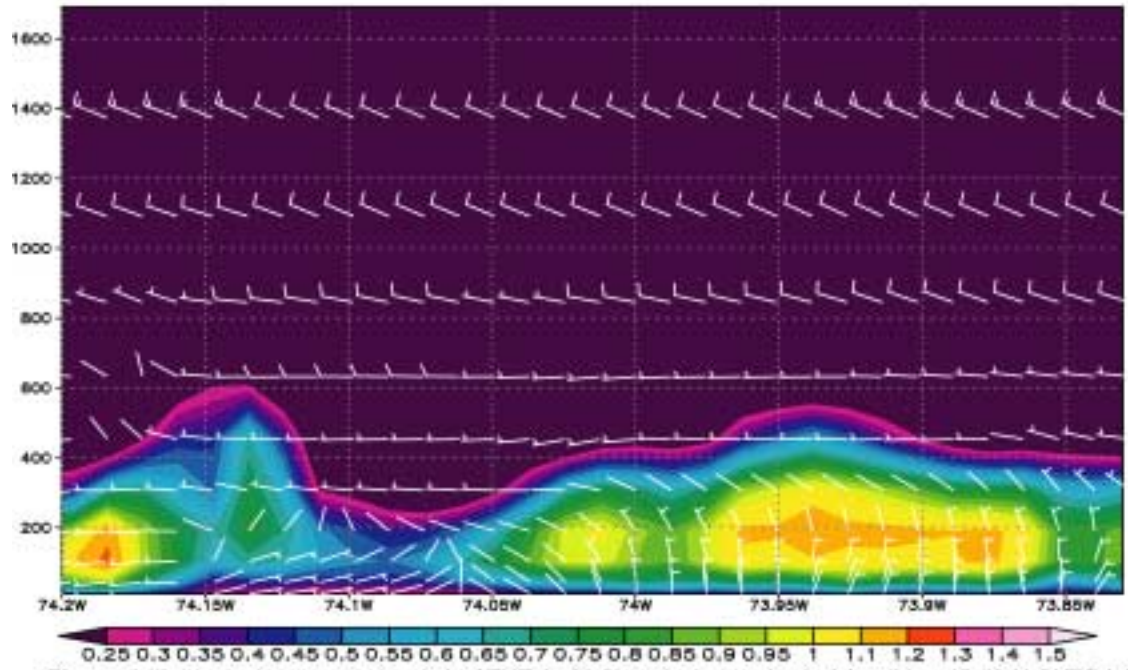

Figure 6.5b Vertical cross-section (m) of TKE (m2/s2) and wind barbs (m/s) valid at 40.50 N (WTC LAT) at 17 UTC (12 LT) 13 November 2001.

This analysis will be completed from west to east on Figure 6.5b. Several features stand out in this simulated cross-section. The first was the maximum in TKE, exceeding 1.2 m^2 s^{-2} at an altitude of 150 m over New Jersey which was directly associated with a boundary layer height approaching 600 m. This was the largest boundary layer height simulated over the entire cross-section at this time. Another notable feature was the localized minimum in TKE, less than 0.45 m^2 s^{-2}, and a boundary layer height of 275 m observed just to the east of New Jersey. This feature corresponded to the location of the Hudson River, and is the result of a more statically stable maritime airmass, thus limiting the growth of the boundary layer. Just to the east of this region, around –74 W was another region of high TKE exceeding 1 m^2 s^{-2}. The boundary layer height grew from 275 m over the Hudson River to greater than 400 m over this region. This TKE enhancement was likely associated with urban heating over lower Manhattan. Just to the east of this localized TKE maximum was a region of slightly less energetic turbulence. TKE values went from greater than 1.1 m^2 s^{-2} to less than 0.8 m^2 s^{-2}, and the boundary layer height remained 400 m. This region of less energetic turbulence was located over the East River, and was a result of a slightly more stable maritime airmass. Just to the east of the East River was a large region of TKE greater than 1.1 m^2 s^{-2}, and simulated boundary layer heights between 450 and 500 m. This region was associated with Long Island. The wind field in Figure 6.5b showed westerly winds above 600 m (the maximum height of the boundary layer based on TKE) over the entire cross-section, while a more complex wind pattern was simulated below this level. Located between –74.15 ˚W and –74 ˚W, near surface wind directions were from the east and east-northeast. Figure 6.6 shows a model simulated vertical cross-section, valid 18 UTC (13 LT) 13 November 2001.

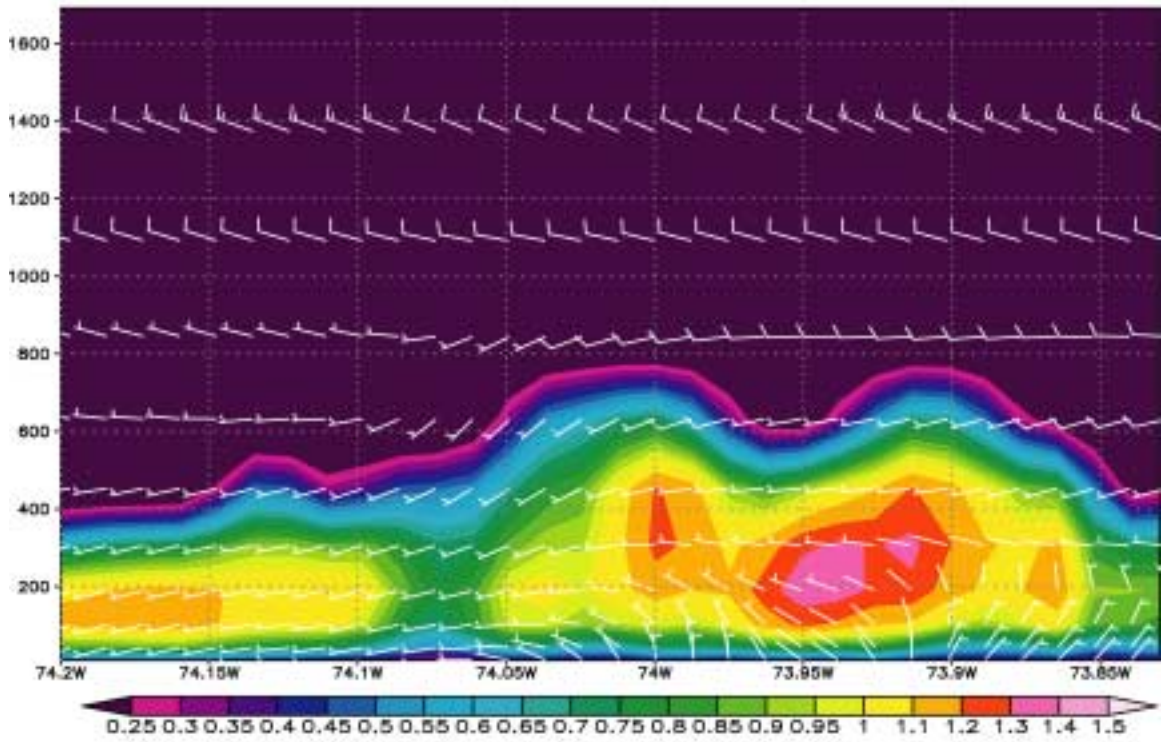

Figure 6.6 Vertical cross-section (m) of TKE (m2/s2) and wind barbs (m/s) valid at 40.50 N at 18 UTC (13 LT) 13 November 2001.

Just as in Figure 6.5b, the cross-section was centered over the World Trade Center disaster recovery site (~40.50 ˚N –74 ˚W). Shown in Figure 6.6 are wind barbs (m/s) and TKE (m^2 s^{-2}) valid 18 UTC (13 LT) 13 November, just as the sea breeze front was moving into lower Manhattan. The vertical distribution of TKE was very similar to the pattern shown in Figure 6.5b, with a few exceptions. While a localized TKE maximum exceeding 1.1 m^2 s^{-2} was simulated over New Jersey, the boundary layer height decreased from 600 m at 17 UTC (12 LT) 13 November, as shown in Figure 6.5b, to less than 550 m at 18 UTC (13 LT). Similarly to Figure 6.5b, there was a relative minimum of turbulent energy between New Jersey and Manhattan over water. This air column, directly over the Hudson River, showed TKE readings near 0.7 m^2 s^{-2}, and was likely associated with a more stable maritime airmass. A maximum in TKE, exceeding 1.2 m^2 s^{-2}, was evident directly over lower Manhattan. The boundary layer height was also maximized in this region, approaching 800 m, experiencing a growth of nearly 400 m between 17 UTC and 18 UTC (12 and 13 LT). This rapid growth was likely associated with greater amounts of surface layer heating which was a direct result of the largely urbanized landuse. To the east of this feature was a localized minimum in boundary layer height, around 600 m, associated with the more statically stable East River. Boundary layer heights quickly rebounded to the east of this region, over Long Island, and again approached 800 m. TKE is also maximized over Long Island, with values exceeding 1.3 m^2 s^{-2}. The TKE maximum was located at a depth of 200 to 300 m, or approximately one-third the height of the boundary layer, which agreed theoretically with the expected region of maximum turbulent energy (Stull 1988). The vertical wind field remained very similar to Figure 6.5b.

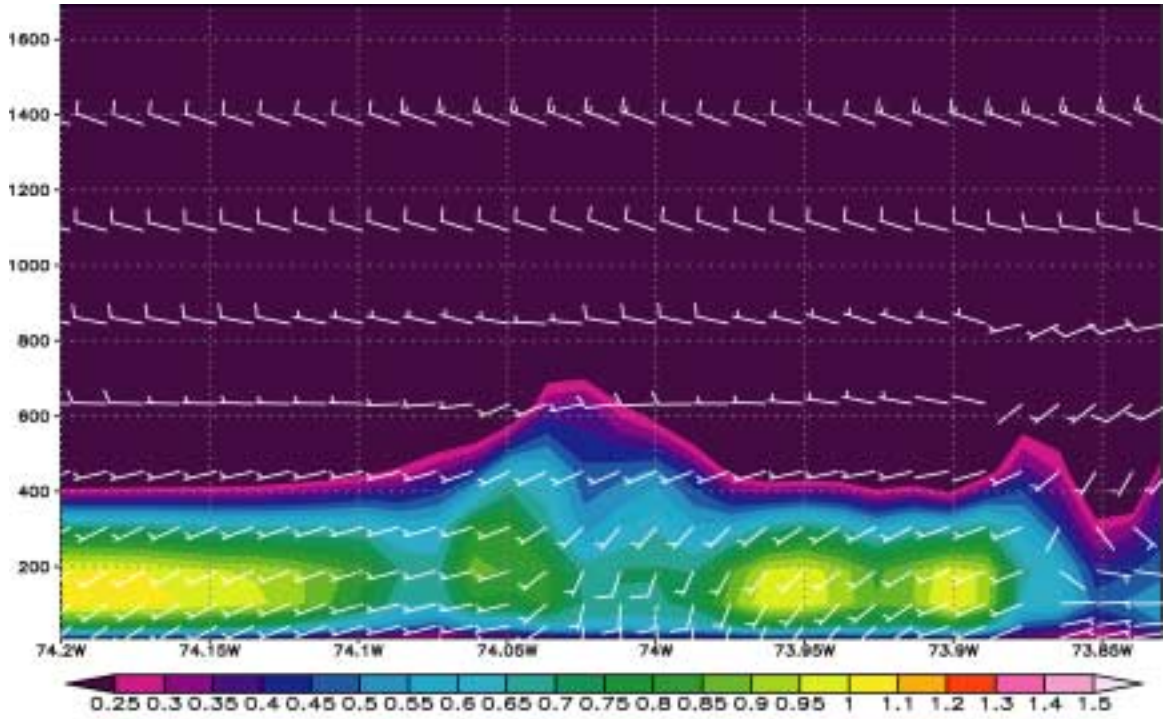

Figure 6.7 Vertical cross-section (m) of TKE (m2/s2) and wind barbs (m/s) valid at 40.50 N at 19 UTC (14 LT) 13 November 2001.

The wind flow was generally from the north over the lowest 100 m of the simulated cross-section, with the exception of a more westerly component developing over New Jersey. This component was a result of the developing convergence zone associated with the strengthening sea breeze front south of lower Manhattan. Above 100 m, 5 m/s westerly winds were simulated over New Jersey and Manhattan, while a northwesterly wind associated with enhanced turbulent energy was simulated above 100 m over western Long Island. Over eastern Long Island, the wind field above 100 m was out of the north and northeast at 5 m/s. A comparison of model simulated 100 m winds and SODAR data is discussed in a later section. Figure 6.7 shows a model simulated vertical cross-section identical in spatial coverage to Figure 6.5b. Just as in Figure 6.5b, the cross-section was centered over the World Trade Center disaster recovery site (~40.50 ˚N –74 ˚W). Shown in Figure 6.7 are wind barbs (m/s) and TKE (m^2 s^{-2}) valid 19 UTC (14 LT) 13 November, just after the sea breeze front moved through lower Manhattan. There were some pronounced differences between the model simulated cross-sections at 18 UTC and 19 UTC (13 and 14 LT) 13 November. For example, the surface layer wind field had veered from a more northeasterly direction to a southerly direction over the Hudson River, lower Manhattan and most of Long Island. This wind shift was in association with the sea breeze passage through the region between 18 and 19 UTC (13 and 14 LT). The maximum TKE values decreased from greater than 1.3 m^2 s^{-2}at 18 UTC to 1 m^2 s^{-2}at 19 UTC. The maximum boundary layer height fell from 800 m to 650 m over Lower Manhattan. This decrease in boundary layer height may be attributed to a more stable maritime airmass, thermal internal boundary layer, ushered in by the passage of the sea breeze front.

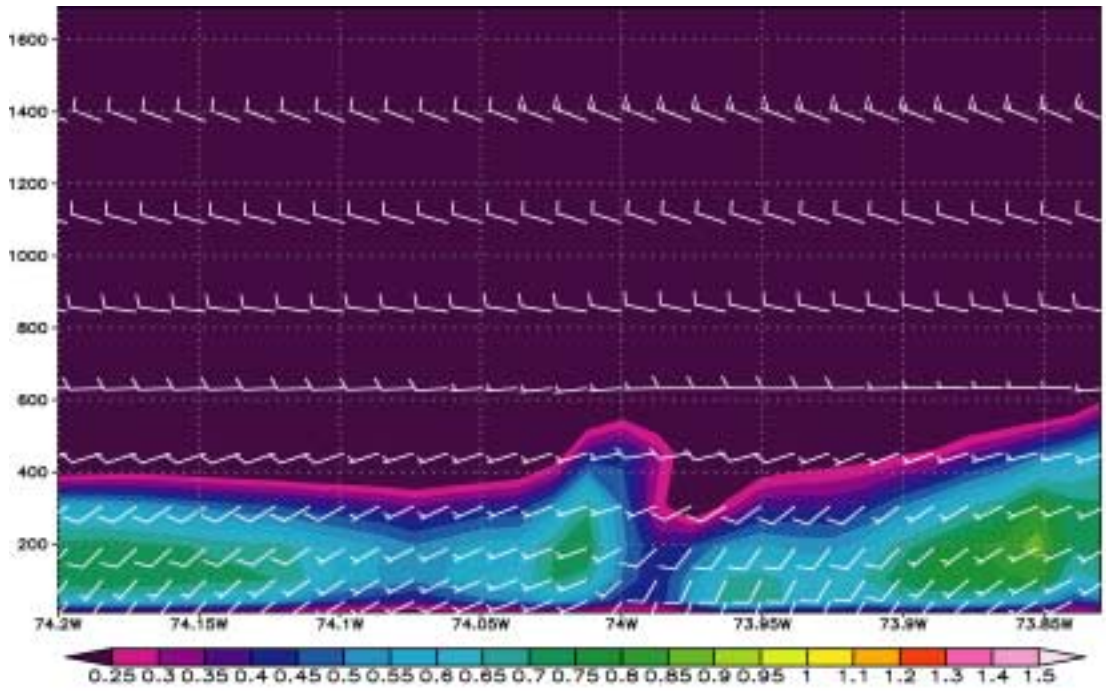

Figure 6.8 Vertical cross-section (m) of TKE (m2/s2) and wind barbs (m/s) valid at 40.50 N at 20 UTC (15 LT) 13 November 2001.

Looking closely at the 10 m wind velocity valid 19 UTC (14 LT) over the region, wind speeds were greater than 4 m/s out of the south over the Hudson River, while they were less than 2 m/s over most of New Jersey, Manhattan and Long Island. The winds over water were much stronger than over land because much less friction is experienced over water.

Figure 6.8 shows a model simulated vertical cross-section identical in spatial coverage to Figure 6.5b. Just as in Figure 6.5b, the cross-section was centered over the World Trade Center disaster recovery site (~40.50 ˚N –74 ˚W). Shown in Figure 6.8 are wind barbs (m/s) and TKE (m^2 s^{-2}) valid 20 UTC (15 LT) 13 November. The low-level wind field had continued to evolve in time, as southwesterly winds were now evident over the entire region covered in the cross-section. The wind field was southwesterly below 400 m and westerly above 500 m, with a transition zone in between. Wind speeds were generally less than 10 m/s throughout the cross-section, with some 15 m/s winds observed above 1400 m. With maximum heights less than 550 m over lower Manhattan, the boundary layer continued to have relatively less turbulence as compared to 17 UTC (12 LT) simulations. Three regions were simulated where TKE values exceed 0.75 m^2 s^{-2}; including New Jersey, lower Manhattan and Long Island. Additionally, there were two regions of weaker turbulent energy observed; they were located over the Hudson River and the East River. This was consistent with a more statically stable boundary layer associated with the modified airmass present over both these rivers.

The surface wind field was less than 3 m/s through 18 UTC (13 LT) 13 November over much of the New York City area. This mesoscale wind regime favored the development and inland propagation of a sea breeze front by allowing differential heating to be

maximized between the land and water. There appears to be a critical offshore wind speed of approximately 4.0 m/s (Bornstein and Johnson, 1977) to the development of the sea breeze. Through 18 UTC (13 LT) on 13 November, the surface wind speed was less than the critical wind speed defined by Bornstein and Johnson (1977). This allowed for the development and inland penetration of the sea breeze front. This was shown in Figure 6.6, where the maximum boundary layer height at 18 UTC (13 LT) over the region was simulated over lower Manhattan. More specifically, the boundary layer height over lower Manhattan was nearly 800 m, while the boundary layer height was less than 600 m over New Jersey. After 18 UTC (13 LT) 13 November, however, the surface wind velocity increased from less than 3 m/s out of the west to greater than 4 m/s out of the south-southwest. An analysis of the effects of the urban heat island over New York City during the nighttime hours of 13 and 14 November 2001 is presented in the next section.

6.3 SIMULATED STRUCTURE OF THE NOCTURNAL BOUNDARY LAYER

Model estimated 10-m wind direction (vectors) and speed (contoured in m/s) at 00 UTC (19 LT) 14 November are shown in Figure 6.9a. Surface wind observations (m/s) are shown in red. Strong southerly wind speeds (>5 m/s) are simulated over the New York Harbor and Atlantic Ocean. As these winds moved over Brooklyn, Queens and lower Manhattan, they slowed down and began to back toward the west. Model estimated 100 m wind direction (vectors) and speed (contoured in m/s) at 00 UTC (19 LT) are shown in Figure 6.9b. South-southwesterly winds were simulated over the entire region, at speeds between 6 and 9 m/s.

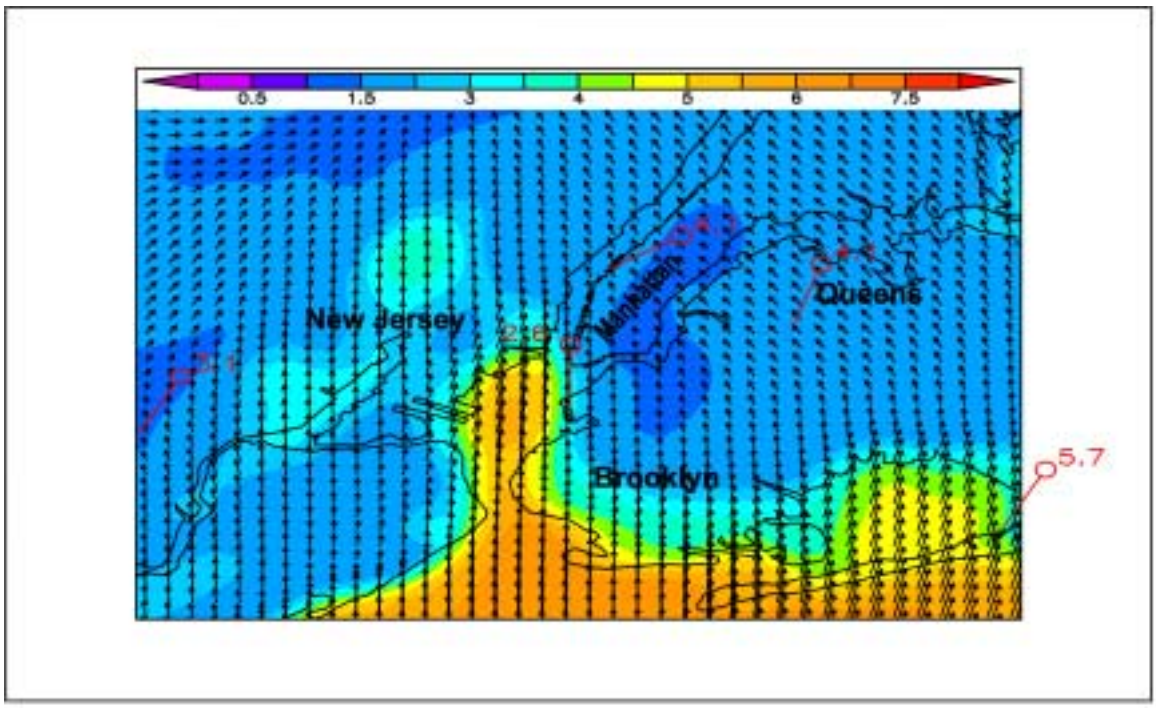

Figure 6.9a ARPS simulated 10 m wind velocity (m/s) valid 00 UTC (19 LT) 14 November 2001. 10 m wind observations shown in Red with the barb showing wind direction from, and number indicating speed (m/s).

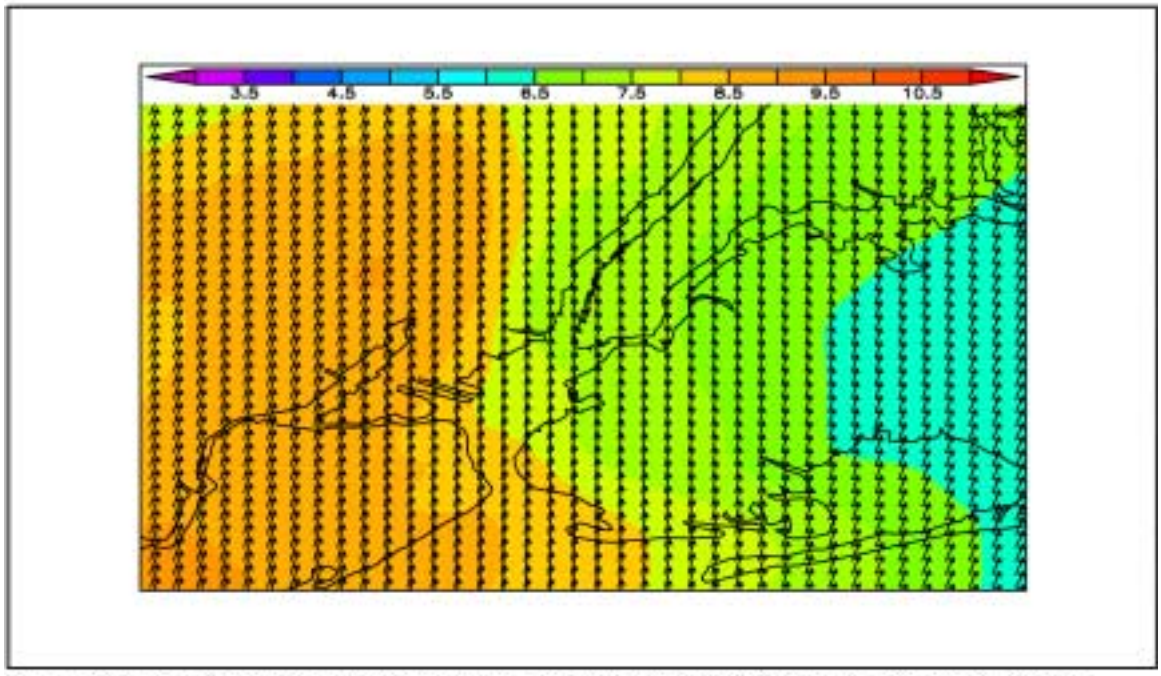

Figure 6.9b ARPS simulated 100 m wind velocity (m/s) valid 00 UTC (19 LT) 14 November 2001.

Similar to Figure 6.9a, there was a slowing of wind speeds as the underlying landscape became more urbanized over Brooklyn, Queens and Manhattan, but the 100 m winds did not back toward the west as they encountered the increased roughness length associated with New York City. Because the 100 m winds did not turn cyclonically like the 10 m winds, it is suggested that this cyclonic turning was a direct result of microscale urban influences on the mean 10 m wind flow. This simulated feature was in agreement with observational findings by Bornstein and Johnson (1977) that showed nighttime events during stronger flow regimes (>4 m/s) were associated with distinctive roughness induced cyclonic turning in the winds over the main core of Manhattan and Brooklyn.

Model estimated 10 m wind direction (vectors) and speed (contoured in m/s) at 03 UTC (22 LT) 14 November is shown in Figure 6.10a. Surface wind observations (m/s) are shown in red. A very complex wind flow pattern is shown in Figure 6.10a. Southwesterly winds in excess of 4 m/s were simulated over the New York Harbor. As the winds entered the urban core of lower Manhattan, they began to slow to less than 2 m/s and back cyclonically, becoming more southerly over central Manhattan Island. A region of calm winds with speeds less than 0.5 m/s was simulated over Brooklyn and extreme eastern lower Manhattan. This calm wind was likely a result of the frictional drag caused by the high roughness length associated with lower Manhattan and Brooklyn. Model estimated 100 m wind direction (vectors) and speed (contoured in m/s) at 03 UTC (22 LT) are shown in Figure 6.10b. Similar to the 10 m winds, the 100 m winds slowed, from 10 m/s to 6 m/s, as they moved over the more urbanized landscape associated with Manhattan and Brooklyn. However, unlike the 10 m winds, the 100 m winds did not turn cyclonically, remaining southwesterly throughout the entire region.

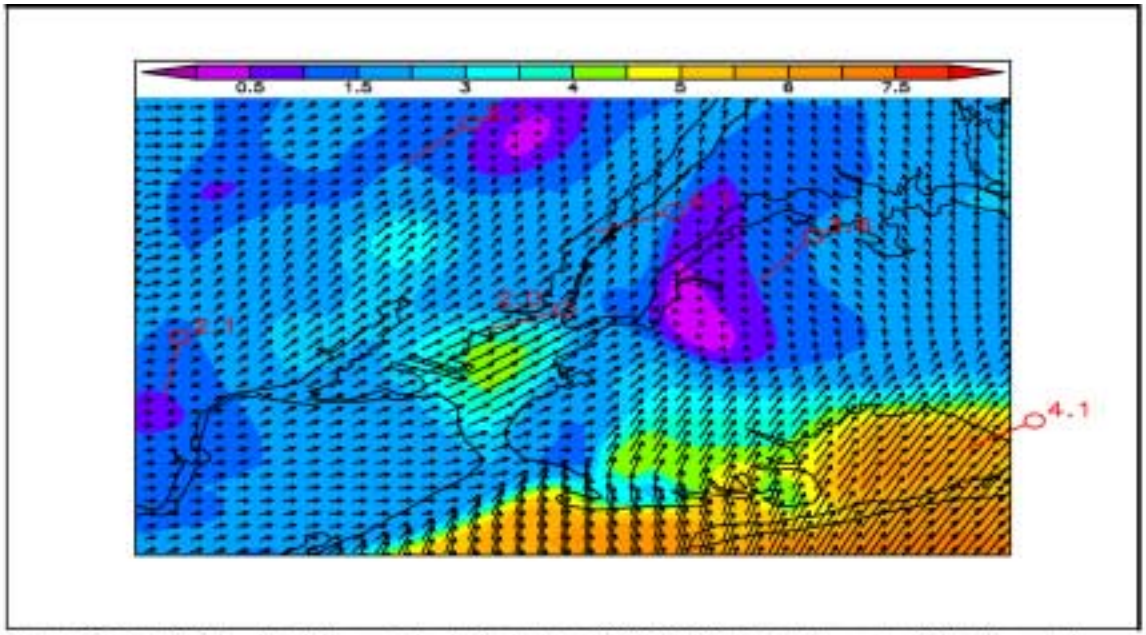

Figure 6.10a ARPS simulated 10 m wind velocity (m/s) valid 03 UTC (22 LT) 14 November 2001. 10 m wind observations shown in Red with the barb showing wind direction from, and number indicating speed (m/s).

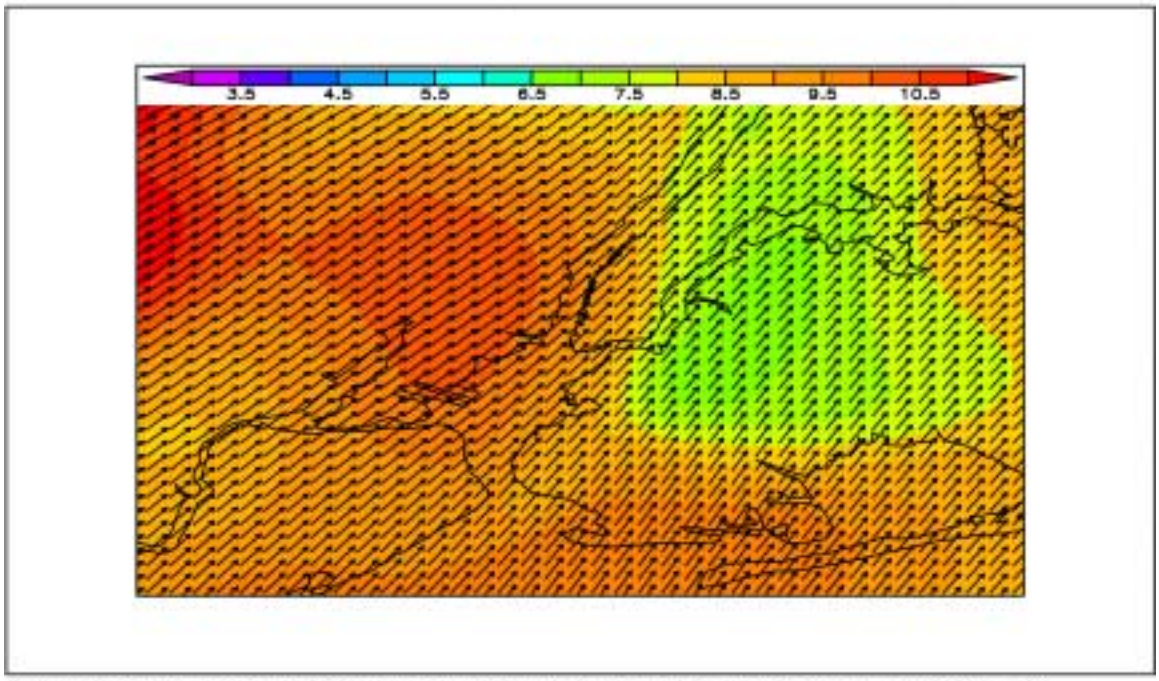

Figure 6.10b MM5 simulated 100 m wind velocity (m/s) valid 03 UTC (22 LT) 14 November 2001.

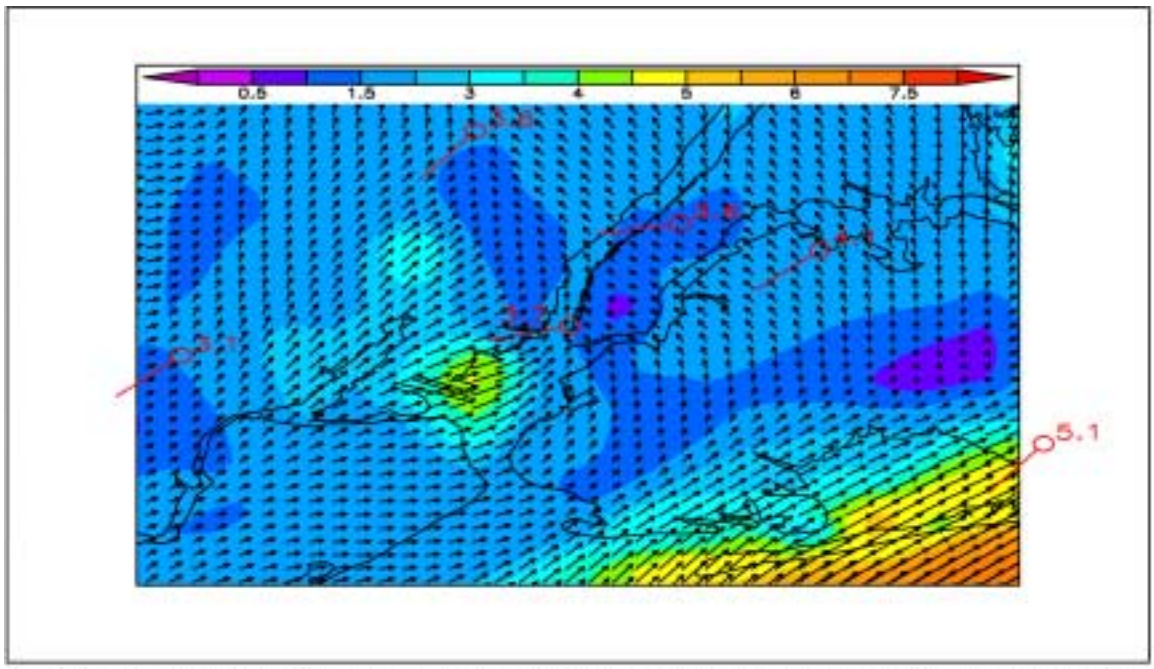

Figure 6.11a ARPS simulated 10 m wind velocity (m/s) valid 06 UTC (01 LT) 14 November 2001. 10 m wind observations shown in Red with the barb showing wind direction from, and the number speed (m/s).

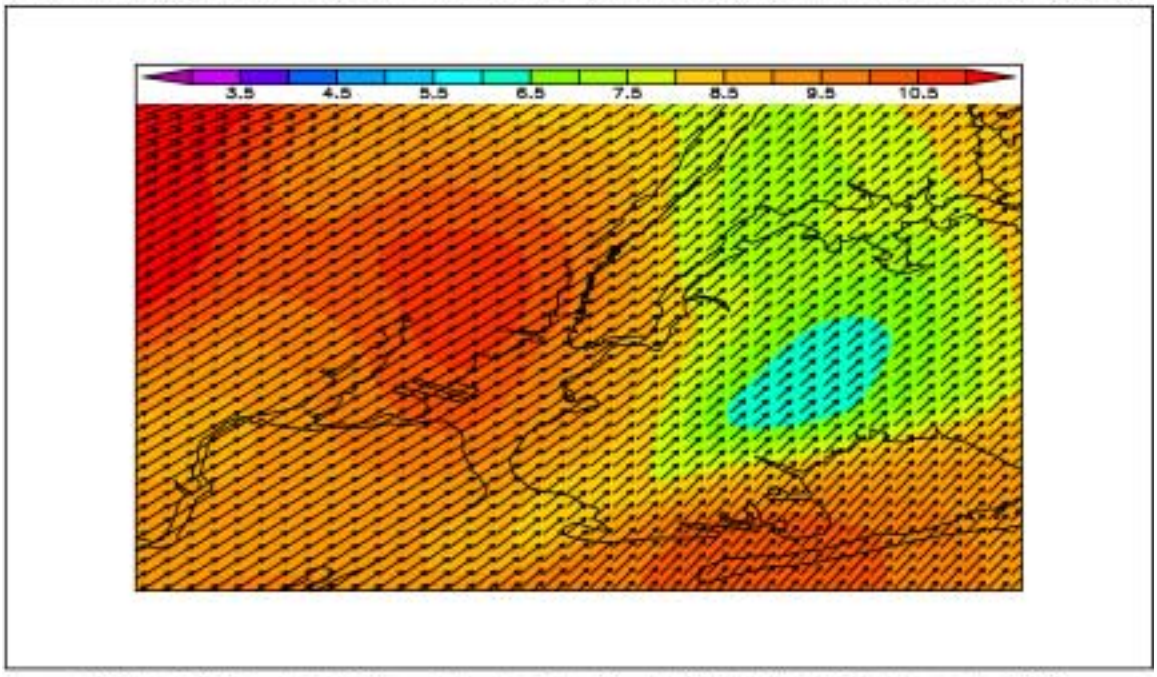

Figure 6.11b ARPS simulated 100 m wind velocity (m/s) valid 06 UTC (01 LT) 14 November 2001.

This feature was similar to Figures 5.9a and 5.9b and was in agreement with observational findings by Bornstein and Johnson (1977) that showed nighttime events during stronger flow regimes (>4 m/s) were associated with distinctive roughness induced cyclonic turning in the winds over the main core of Manhattan and Brooklyn.

Model estimated 10 m wind direction (vectors) and speed (contoured in m/s) at 06 UTC (01 LT) 14 November is shown in Figure 6.11a. Surface wind observations (m/s) are shown in red. Southwest winds between 3 and 4 m/s were simulated over the New York Harbor as shown in Figure 6.11a. As these winds approached lower Manhattan, they began to slow to less than 1.5 m/s and became more southerly and southeasterly. The same effect was observed over Brooklyn and Queens. A region of light and variable winds was simulated just to the east of lower Manhattan. This region was likely associated with a developing urban heat island convergence zone (SethuRaman and Cermak 1974). Additionally, there was a region of enhanced near surface wind speed over southern portions of Brooklyn, possibly related to the unstable boundary layer associated with the urban heat island. Southwesterly winds in excess of 4 m/s were simulated over the Atlantic Ocean. As these winds moved over Brooklyn and Queens, they slowed to less than 2 m/s, and became southeasterly as they moved deeper into the urban core. Model estimated 100 m wind direction (vectors) and speed (contoured in m/s) at 06 UTC (01 LT) is shown in Figure 6.11b. Similar to Figure 6.11a, strong southwesterly winds in excess of 9 m/s slowed to less than 6 m/s over Brooklyn, Queens and Manhattan as a result of the increased roughness over the region. However, no discernable turning of the wind field was simulated over the entire region.

This was similar to features simulated in Figures 6.9b and 6.10b, and is in agreement with observational findings by Bornstein and Johnson (1977) that showed nighttime events during stronger flow regimes (>4 m/s) were associated with distinctive roughness induced cyclonic turning in the winds over the main core of Manhattan and Brooklyn.

Figure 6.12a shows a detailed map of the New York City Metropolitan area. Labeled on Figure 6.12a are the letters B and C, which correspond to the location of surface energy budget time series, shown in Figures 6.12b and 6.12c. Figures 6.12b and 6.12c show the energy budget over lower Manhattan and eastern New Jersey between 12 UTC (7 LT) 13 November and 6 UTC (01 LT) 15 November, respectively. Surface latent heat flux is shown in green, surface sensible heat flux is shown in red, ground diffusive heat flux is shown in black and net radiation is shown in yellow. All fluxes are plotted in W m^{-2}. The surface energy budget equation is shown in equation 6.2 (Stull, 1988).

$$(-Q^*_s + Q_G) = Q_H + Q_E \qquad (6.2)$$

In equation (6.2), the net radiation is represented by $-Q^*_s$, while the ground fluxes are represented by Q_G. Surface sensible heat flux is represented by Q_H, while the latent heat flux is represented by Q_E. There are several interesting features observed on the two time series simulations. The simulated energy budget time series over lower Manhattan, shown in Figure 6.12b, will be discussed first. Of interest was the occurrence of negative surface sensible heat flux between 00 UTC and 03 UTC (19 and 22 LT) 14 November. Sensible heat flux values around –50 W m^{-2} were simulated during this period. After 03 UTC (22 LT), the surface sensible heat flux became 0 W m^{-2} by 04 UTC (23 LT). By 05 UTC (00 LT), the surface sensible heat flux became positive, and remained positive until 21 UTC (16 LT).

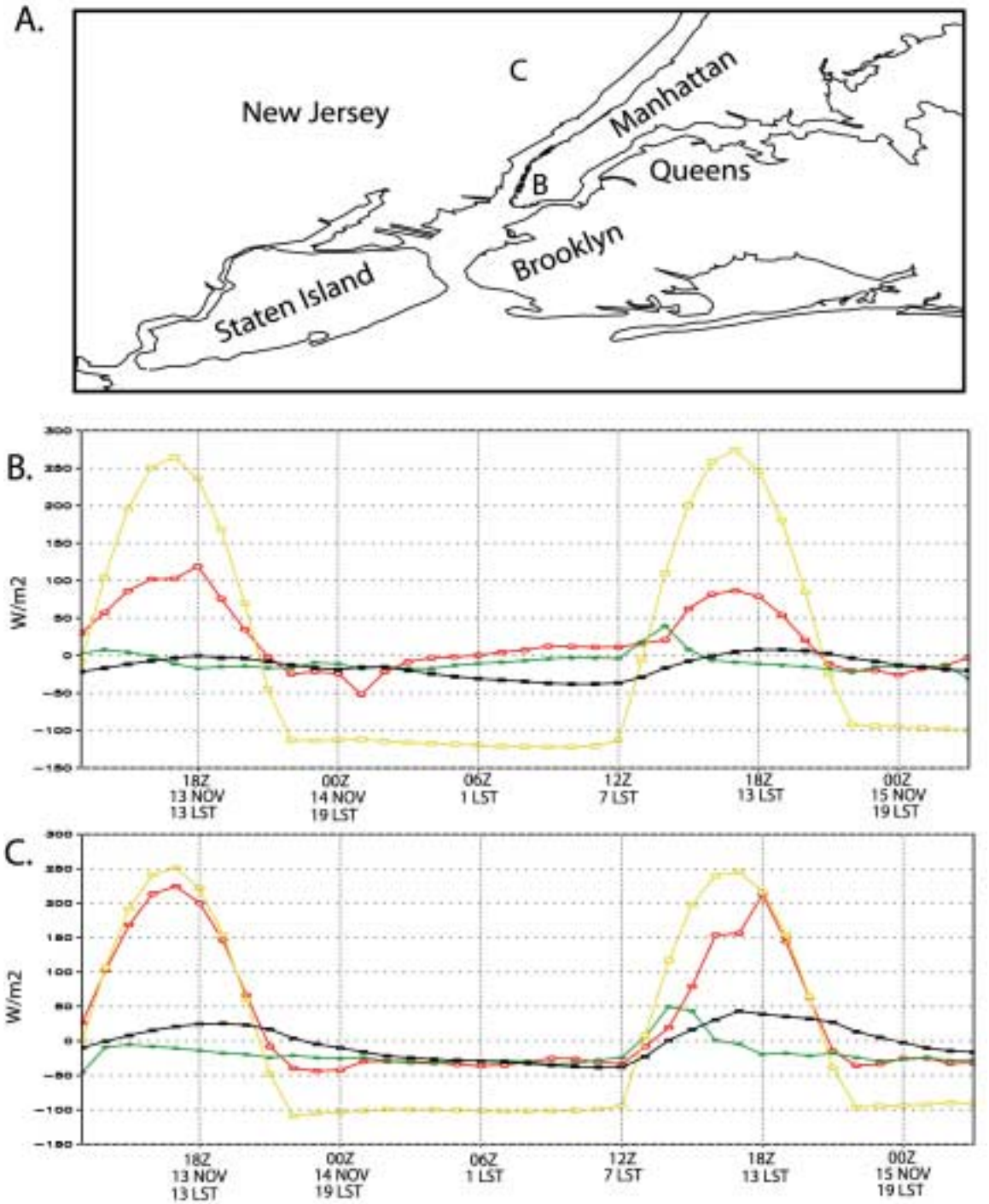

Figure 6.12a Detailed map of the New York City metropolitan area. **Figures 6.12b** and **6.12c** show the surface energy budget over lower Manhattan (labeled B on the map) and over New Jersey (labeled C on the map). Surface latent heat flux is shown in green, surface sensible heat flux is shown in red, ground diffusive heat flux is shown in black, and net radiation is shown in yellow, respectively. All fluxes are simulated in W/m2.

Positive surface sensible heat fluxes during the night over lower Manhattan were likely the result of the urban heat island (SethuRaman and Cermak, 1974). The simulated energy budget time series over New Jersey is shown in Figure 6.12c. The simulated surface sensible heat flux values showed a less complex diurnal variation than the simulated surface sensible heat flux values over lower Manhattan. Over New Jersey, the surface sensible heat flux values were positive during the daytime hours and became negative as nighttime approached (17 LT). Simulated surface sensible heat flux values remained negative throughout the night as the urban heat island did not seem to affect the near surface boundary layer structure over New Jersey. In addition to the differences in simulated surface sensible heat flux values during the night, the energy budget time series over lower Manhattan and New Jersey also showed differences between maximum surface sensible heat fluxes. Surface sensible heat flux values of 225 W m^{-2} were simulated over New Jersey at 17 UTC (12 LT) 13 November, while surface sensible heat flux values of 120 W m^{-2} were simulated over lower Manhattan at the same time. Additionally, surface sensible heat flux values of greater than 200 W m^{-2} were simulated over New Jersey at 18 UTC (13 LT) 14 November, while surface sensible heat flux values of less than 100 W m^{-2} were simulated over lower Manhattan at the same time. The simulated surface sensible heat flux values were smaller over lower Manhattan because of the southwest flow moving over the Hudson River and Atlantic Ocean causing boundary layer airmass modification over lower Manhattan. Near surface winds were southwesterly over New Jersey as well, however, these winds were associated with a continental airmass and did not experience any marine airmass modification. Surface latent heat flux simulations were very similar between New Jersey and lower Manhattan,

with very little amplitude above or below 0 W m^{-2}. This seems reasonable, as surface latent heat flux values over a highly urbanized area are expected to be near zero, and over a residential area, slightly positive.

Several features simulated in the above surface energy budget plots showed the signature of an urban heat island. More specifically, the surface sensible heat flux simulation time series over lower Manhattan was only briefly negative during the nighttime hours of 13 and 14 November, between 21 UTC (16 LT) 13 and 03 UTC (22 LT) 14 November. By 04 UTC (23 LT) 14 November, the surface sensible heat flux became positive and remained positive through 21 UTC (16 LT) 14 November. Positive surface sensible heat fluxes are often associated with daytime conditions when incoming shortwave insulation is maximized. However, it is suggested that the urbanized structures associated with lower Manhattan act as heat holding materials that have a tendency to keep surface temperatures significantly warmer at night (urban heat island). In turn, positive surface sensible heat fluxes are generated over lower Manhattan, and are directly associated with the effects of the urban heat island.

Figure 6.13a shows vertical TKE (m^2 s^{-2}) wind speed (kts) and potential temperature (K) time series over the World Trade Center (WTC) disaster recovery site valid 12 UTC (7 LT) November through 6 UTC (01 LT) 15 November (Time is shown in both local and UTC formats). Figure 6.13b is a SODAR profile taken from WTC Instrumentation Site in lower Manhattan on 13 November through 12 UTC (07 LT) 14 November (Time is shown in both local and UTC formats). Wind barbs are shown using the standard knots notation. (Please note that the lowest (15 m) observation is typically unreliable, so it should be ignored). From Figure 6.13a, several features are immediately apparent.

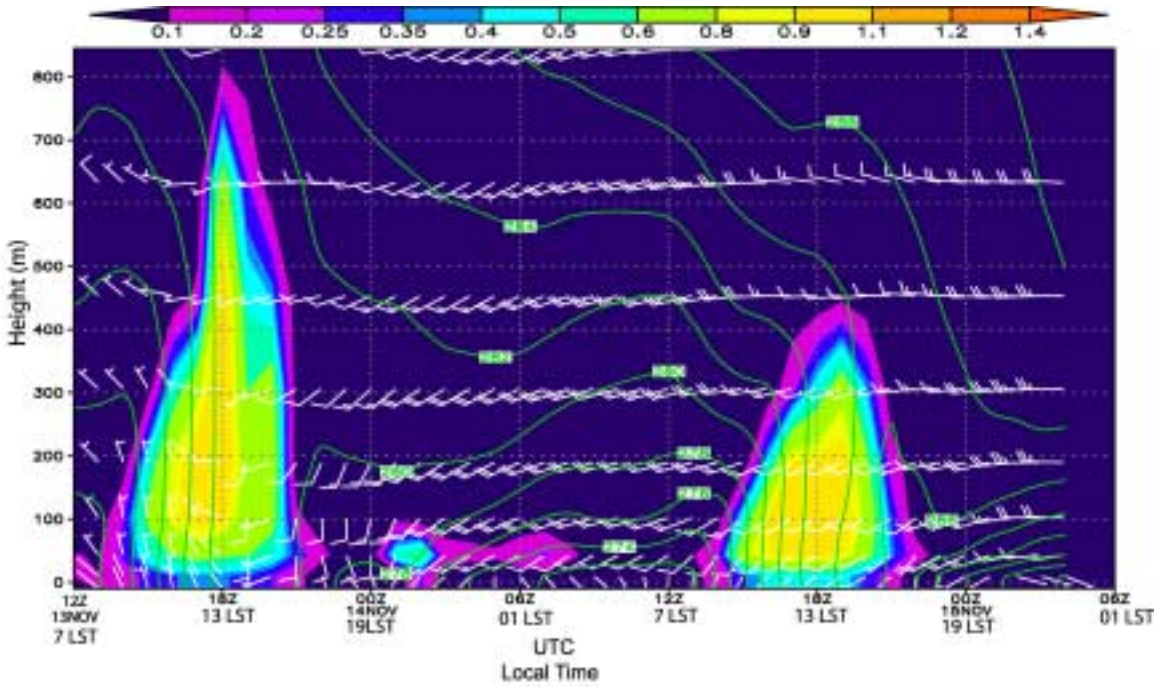

Figure 6.13a Time series vertical profile of turbulent kinetic energy (m2/s2), horizontal wind (kt) and potential temperature (K) simulated by ARPS at the WTC site. TKE is color shaded, potential temperature is contoured with green lines and wind is shown by standard barbs notation in knots.

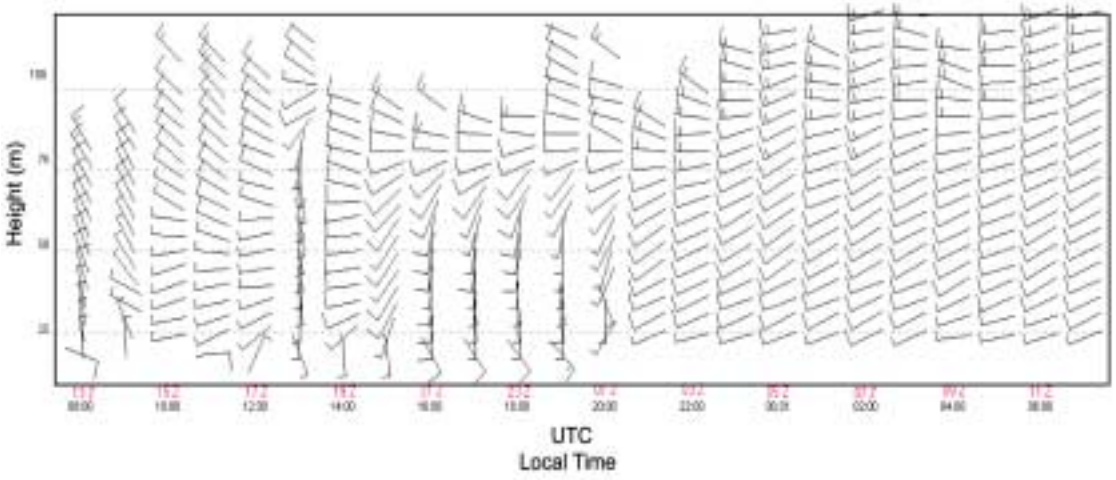

Figure 6.13b Model 4000 miniSODAR profile at the WTC Instrumentation site in lower Manhattan on November 13-14, 2001. Wind barbs use the standard knots notation. The lowest (15 m) observation is typically unreliable, so it should be ignored. Time is shown in both local and UTC time formats.

The first feature analyzed was the region of maximum TKE simulated between 16 UTC (11 LT) and 19 UTC (14 LT) 13 November. Boundary layer heights reached nearly 800 m at 18 UTC (13 LT), with TKE values greater than 1.2 m^2 s^{-2} between 300 and 450 m. Another feature was the boundary layer wind field between 16 UTC and 19 UTC (11 LT and 14 LT). Winds below 300 m were simulated from the north with a magnitude of 5 kts. Between 18 and 19 UTC (13 and 14 LT), the wind direction changed from northerly to southerly following the passage of the sea breeze front. Data from the SODAR, shown in Figure 6.13b, verifies the ARPS simulation, showing the wind shift from northerly to southerly around 18 UTC (13 LT). Additionally, there was a region of enhanced turbulence and wind speed simulated between 01 and 08 UTC (20 and 03 LT) 14 November with low-level winds simulated between 10 and 15 kts. Analysis from the SODAR data also showed a region of maximum low-level winds of 15 kts observed at 00 UTC (19 LT) 14 November. This feature may be a result of the urban heat island effect and will be discussed in more detail below. After 02 UTC (21 LT) 14 November, the low-level wind flow was simulated and was also observed out of the southwest at 10 kts. Another region of maximum TKE and boundary layer height was simulated between 16 UTC and 21 UTC (11 and 16 LT) 14 November. This region differed significantly from the boundary layer structure on 13 November. For example, the maximum boundary layer height was approximately 400 m lower on the 14 November than it was on 13 November, 800 m to 400 m. The maximum TKE simulated on 14 November was less than 0.95 m^2 s^{-2}, which was observed at 18 UTC (13 LT). This was significantly less than the 1.2 m^2 s^{-2} of TKE simulated on 13 November. It is apparent from examining the time series and SODAR data that the synoptic scale wind flow overwhelmed any mesoscale

and microscale meteorological processes directly related with the urban heat island after 08 UTC (03 LT) 14 November. Southwesterly winds of 10 kts (5 m/s) and greater were observed during this time period, which likely kept the boundary layer well mixed and homogenous over the entire study area.

Figure 6.14a shows a detailed map of the New York City Metropolitan Area showing the location of the vertical cross-section shown below in Figure 6.14b. Figure 6.14b shows a cross-sectional analysis of TKE (m^2 s^{-2}) that is color shaded, potential temperature (K) shown in green contours and wind barb (kts) valid 01 UTC (20 LT) 14 November. This period matched the period of maximum nocturnal TKE over the WTC site shown in Figure 6.13a. TKE values range between 0.2 and 0.5 m^2 s^{-2}, and were very localized around –74.01 ˚W, or *just* to the west of the WTC site over the Hudson River. TKE values less than 0.1 m^2 s^{-2} were simulated over the rest of the cross-section. Looking carefully at the potential temperature contours shown in green on Figure 6.14b, the vertical potential temperature structure showed a pronounced maximum at 20 m of 278 K relating well with the maximum in TKE. As shown in Figure 6.13a, there was a region of TKE greater than 0.15 m^2 s^{-2} simulated over the WTC site from 00 UTC (19 LT) 14 November through 08 UTC (03 LT) 14 November. There was a maximum in TKE of 0.5 m^2 s^{-2} simulated over the WTC site at 01 UTC (20 LT) 14 November as shown in a time series cross-section in Figure 6.13a and as shown in a spatial cross-section in Figure 6.14b. This maximum in TKE occurs over the Hudson River and lower Manhattan, as shown in Figure 6.14b, with TKE values less than 0.1 m^2 s^{-2} simulated over the rest of the region. It appears that this TKE maximum is directly related to the influence of the urban heat island.

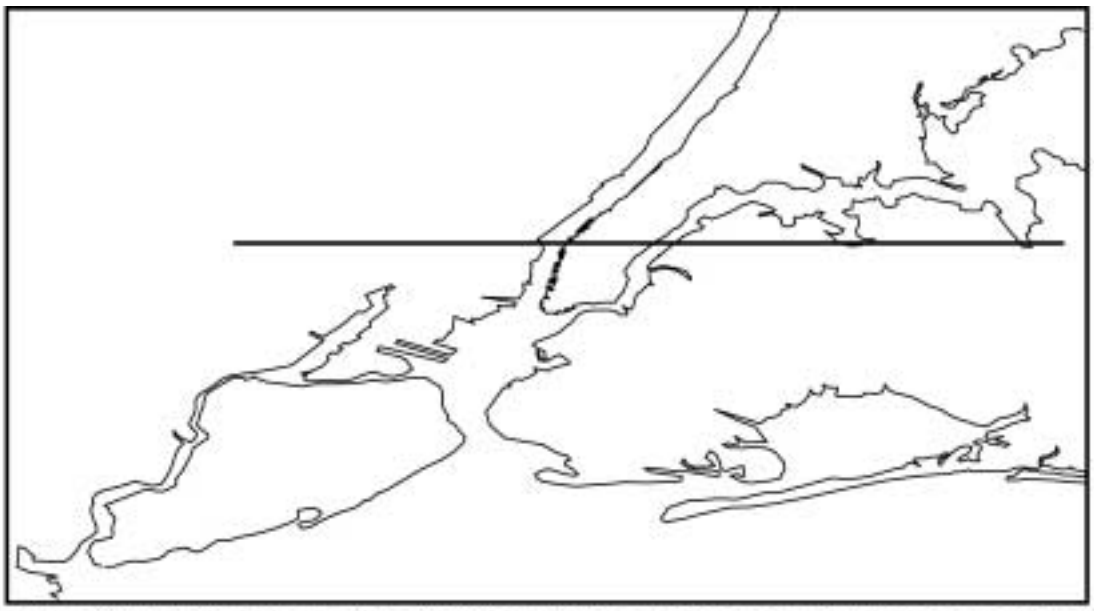

Figure 6.14a Detailed map of the New York City Metropolitan area showing the location of the vertical cross-section shown below.

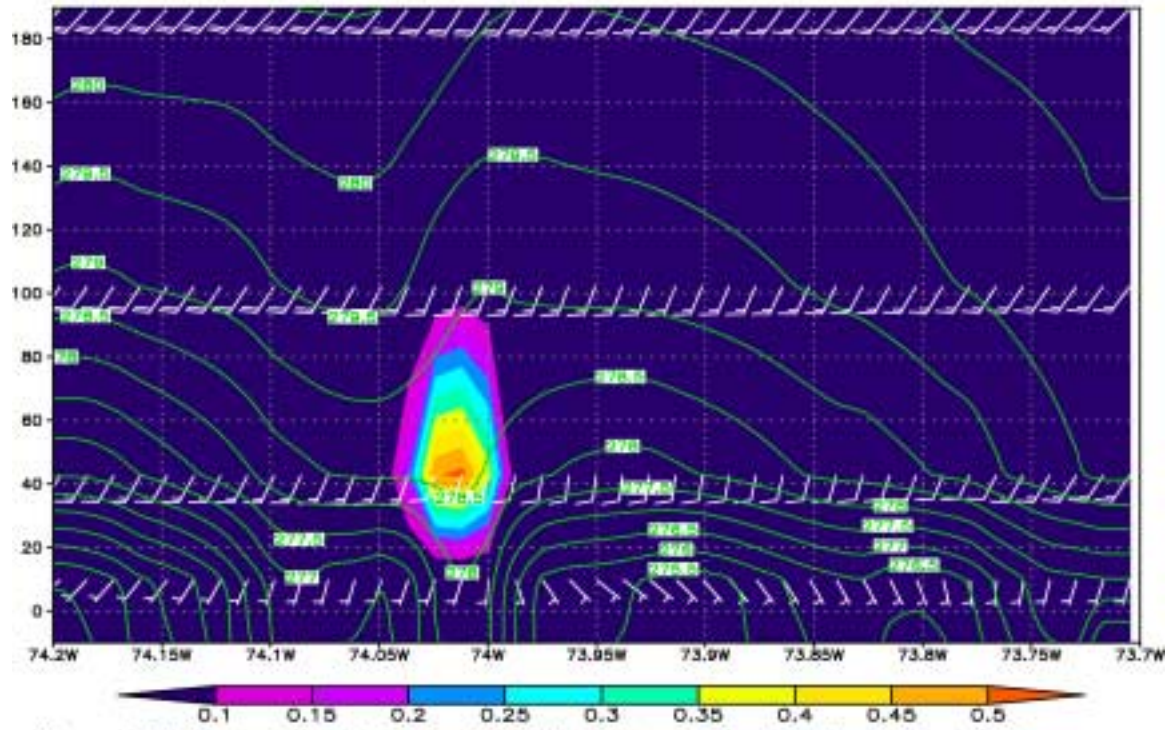

Figure 6.14b Cross-sectional analysis of TKE shaded in m2/s2, potential temperature (K) in green contours and wind barbs (kts) valid 01 UTC (20 LST) 14 November as shown in **Figure 6.14a**.

The location and structure of the nocturnal boundary layer over lower Manhattan is consistent with this result and agrees well with previous research studying the urban heat island by SethuRaman and Cermak (1974) through physical modeling and Bornstein and Johnson (1977) based on a field study over New York City.

6.4 BOUNDARY LAYER STRUCTURE DURING A STRONGER WIND REGIME

Figure 6.15 shows a model-simulated vertical cross-section identical in spatial coverage to Figure 6.5b. Just as in Figure 6.5b, the cross-section was centered over the World Trade Center disaster recovery site (~40.50 ˚N –74 ˚W). Shown in Figure 6.15 are wind barbs (kts) and TKE (m^2 s^{-2}) valid 18 UTC (13 LT) 14 November 2001. The cross-section was dominated by strong (10 kts and higher) southwesterly winds below 200 m. The boundary layer height was nearly uniform over the entire cross-section, with depths of approximately 250 m. Several regions of very energetic turbulence were also simulated, with values exceeding 1.1 m^2 s^{-2} over New Jersey, lower Manhattan and Long Island. However, these regions of turbulence were not as strong and well defined as they were on 13 November, as shown in Figures 6.5b through 6.8. It is reasoned that with such a strong low-level synoptic scale flow, the boundary layer became well mixed and any microscale effects on the 10 m wind from the urbanized landscape were greatly reduced.

Figure 6.16 shows a model-simulated vertical cross-section identical in spatial coverage to Figure 6.5b. Just as in Figure 6.5b, the cross-section was centered over the World Trade Center disaster recovery site (~40.50 ˚N –74 ˚W). Shown in Figure 6.16 are wind barbs (kts) and TKE (m^2 s^{-2}) valid 19 UTC (14 LT) 14 November 2001.

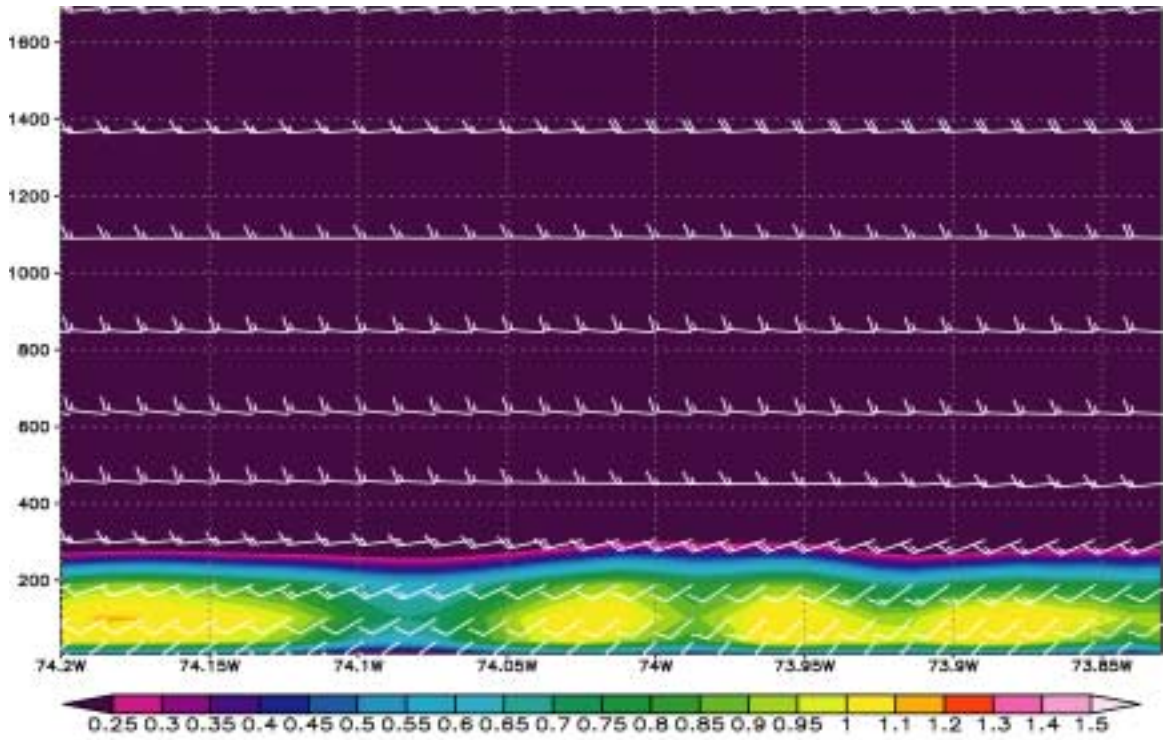

Figure 6.15 Vertical cross-section (m) of TKE (m2/s2) and wind barbs (kts) valid at 40.50 N at 18 UTC (13 LT) 14 November 2001.

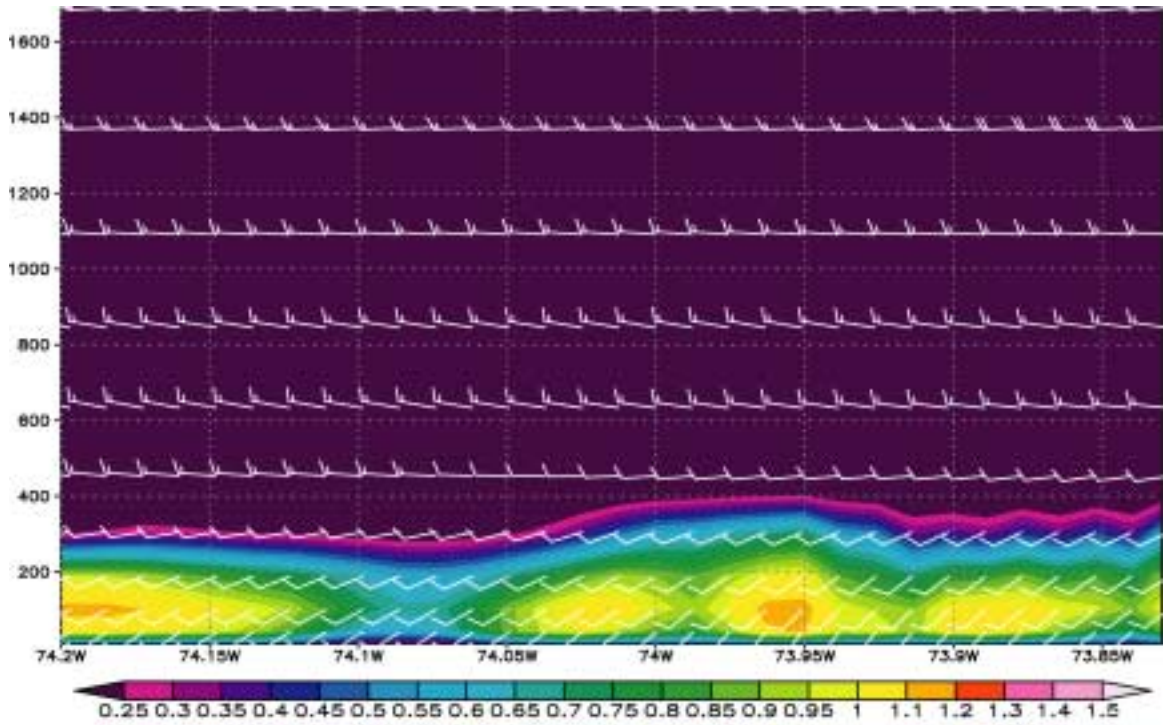

Figure 6.16 Vertical cross-section (m) of TKE (m2/s2) and wind barbs (kts) valid at 40.50 N at 19 UTC (14 LT) 14 November 2001.

The low-level wind flow in Figure 6.16 is consistent with the low–level wind flow in Figure 6.15, 10 kt southwesterly winds below 400 m. Above 400 m, the wind flow is westerly between 10 and 15 kts. Similar to Figure 6.15, there are several distinct regions of high TKE simulated over New Jersey, lower Manhattan and Long Island. The boundary layer over lower Manhattan and Long Island grew to nearly 400 m in depth, with a TKE maximum between 1.1 and 1.2 m^2 s^{-2} over far western Long Island. It is interesting to note that this cross-section did not simulate a lower boundary layer height over the Hudson River, where a simulated boundary layer height of 380 m was nearly identical to the simulated boundary layer height over lower Manhattan. There may be several reasons for this. One explanation was the strong low-level wind flow simulated and observed over the region. As mentioned above, there is a critical wind speed of approximately 4.0 m/s (Bornstein and Johnson, 1977) at which the urban roughness influences the low-level flow and structure. In Figure 6.16, the low-level winds were much stronger than this critical wind speed, thereby reducing the effects of the urban heat island on the low-level wind flow and the boundary layer structure.

Figure 6.17 shows a model simulated vertical cross-section identical in spatial coverage to Figure 6.5b. Just as in Figure 6.5b, the cross-section was centered over the World Trade Center disaster recovery site (~40.50 ˚N –74 ˚W). Shown in Figure 6.17 are wind barbs (kts) and TKE (m^2 s^{-2}) valid 20 UTC (15 LT) 14 November 2001. In Figure 6.17 the wind flow below 400 m was out of the southwest at 10 kts over the entire cross-section. Above 400 m, the wind flow was westerly between 10 and 15 kts. Similar to Figure 6.17, there were several localized regions of maximum TKE.

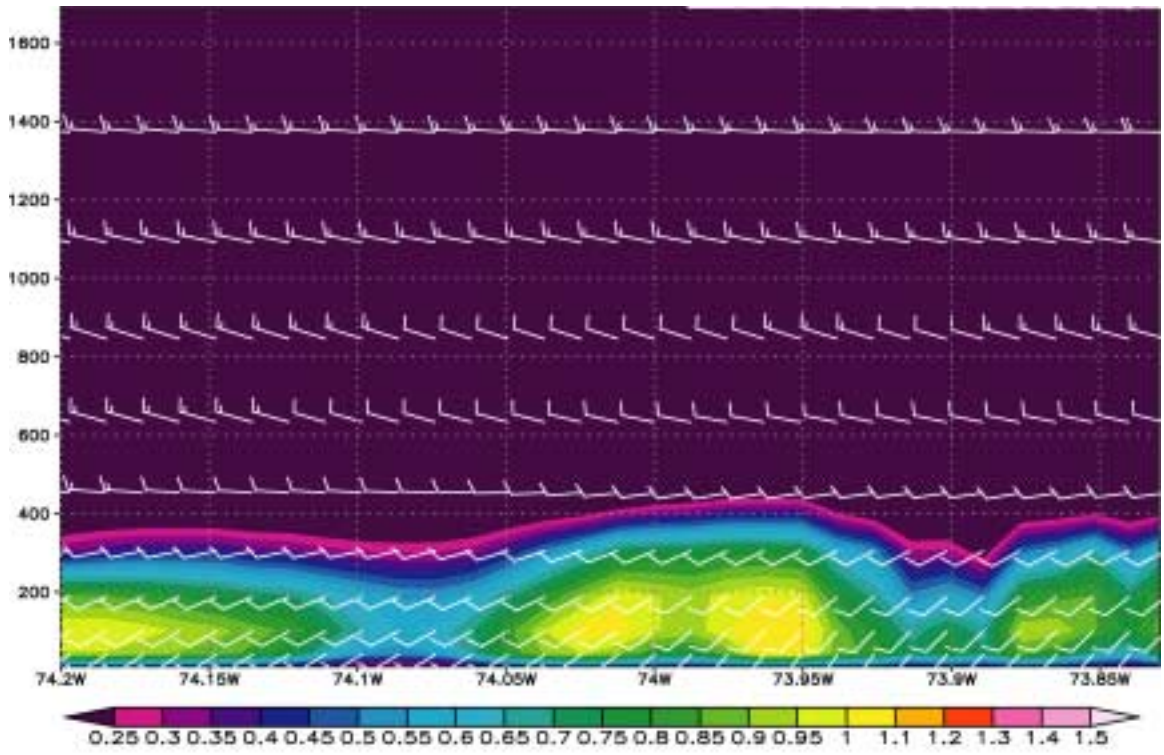

Figure 6.17 Vertical cross-section (m) of TKE (m2/s2) and wind barbs (kts) valid at 40.50 N at 20 UTC (15 LT)14 November 2001.

Between far eastern New Jersey and western Long Island, there was an elongated region of maximum TKE, centered roughly over lower Manhattan. In this region, simulated TKE values ranged between 1 and 1.1 $m^2 s^{-2}$. Boundary layer heights were over 400 m in this region. It remained difficult to find any discernable impacts of the urbanized landscape on the low-level wind flow or the boundary layer structure. However, it is noted that we are not able to simulate the effects of individual buildings, which greatly influence low-level wind flow.

The 10 m wind field was greater than 4 m/s from 00 UTC (19 LT) 13 November through 12 UTC (07 LT) 14 November. This mesoscale wind regime did not favor the development of a sea breeze front, as the boundary layer was uniformly mixed over the entire region. Another interesting feature during this time period was the homogenous low-level wind flow over the area. Southwesterly winds of 10 kts (5 m/s) and greater were observed during this time period. Such strong and uniform low-level winds are very important processes to study when numerically simulating mesoscale and microscale meteorological variables over a highly urbanized area such as New York City. For example, previous research on the urban blocking phenomenon over New York City has concluded that there is a critical wind speed of approximately 8 kts (4.0 m/s) at which the urban roughness influence the low-level wind flow and boundary layer structure during daytime conditions (Bornstein and Johnson, 1977). It is evident from examining the cross-sections simulated in Figures 6.15 through 6.17 that the synoptic scale wind flow overwhelmed any mesoscale and microscale meteorological processes directly related to the urban heat island and urban blocking effects.

6.5 CONCLUSIONS

The main goal of this chapter is to present the simulations of mesoscale and microscale meteorological processes over the New York City Metropolitan area by the ARPS model. The numerical study focused on the structure and evolution of the boundary layer from 12 UTC (07 LT) 13 November 2001, through 12 UTC (07 LT) 15 November 2001. This period was chosen because high ground level pollutant concentrations were measured over Manhattan and portions of surrounding boroughs.

Several important components of the boundary layer structure were analyzed in this study, including low-level wind flow, TKE and boundary layer height variations, vertical motion and the surface energy budget. The ARPS model simulated the development and inland penetration of sea breeze front over the region between 15 UTC (07 LT) 13 November and 21 UTC (16 LT) 13 November. The sea breeze front formed because of strong differential heating between the landmasses of the region and the Atlantic Ocean, which developed due to the presence of a light and variable synoptic scale flow. The ARPS simulation showed the sea breeze front moving through lower Manhattan between 18 and 19 UTC (13 and 14 LT) 13 November, which agreed well with both SODAR and 10 m tower observations from an independent instrumentation cluster maintained by the EPA and State Climate Office of North Carolina in lower Manhattan (shown in plan view in Figure 2.1). The position and structure of the sea breeze front over the region also agreed well with previous studies by Bornstein (1994) who performed numerical simulations over the same area and observed a similar frontal alignment that extended through Staten Island, across lower Manhattan and eastward through Queens and Brooklyn.

The nocturnal boundary layer was also studied using surface and 100 m wind simulations, as well as surface energy budget figures and TKE cross-sections. Several conclusions are now presented using data from the 10 m and 100 m wind velocity simulation presented in Figures 6.9 through 6.11. All 10 m wind figures showed a slowing and cyclonic backing of the 10 m wind flow as the wind moved over Brooklyn, Queens and Manhattan. All 100 m wind figures showed a slowing of the wind flow, but no discernable alteration of flow direction. This simulated feature was in agreement with observational findings by Bornstein and Johnson (1977) that showed nighttime events during stronger flow regimes (>4 m/s) were associated with distinctive roughness induced cyclonic turning in the winds over the main core of Manhattan and Brooklyn.

Additionally, several features simulated in the surface energy budget plots shown in Figures 6.12b and 6.12c show the signature of an urban heat island. More specifically, the surface sensible heat flux simulation time series over lower Manhattan was only briefly negative during the nighttime hours of 13 and 14 November, between 21 UTC (16 LT) 13 and 03 UTC (22 LT) 14 November. By 04 UTC (23 LT) 14 November, the surface sensible heat flux became positive and remained positive through 21 UTC (16 LT) 14 November. Positive surface sensible heat fluxes are often associated with daytime conditions when incoming shortwave insulation is maximized. However, it is suggested that the urbanized structures associated with lower Manhattan act as heat holding materials that have a tendency to keep surface temperatures significantly warmer at night. In turn, positive surface sensible heat fluxes are generated over lower Manhattan, and are directly associated with the urban heat island.

Figure 6.13a shows a region of TKE greater than 0.15 m^2 s^{-2} simulated over the WTC site from 00 UTC (19 LT) 14 November through 08 UTC (03 LT) 14 November. There was a maximum in TKE of .5 m^2 s^{-2} simulated over the WTC site at 01 UTC (20 LT) 14 spatial cross-section in Figure 6.14b. This maximum in TKE occurred over the Hudson River and lower Manhattan, as shown in Figure 6.14b, with TKE values less than 0.1 m^2 s^{-2} simulated over the rest of the region. It is suggested that this TKE maximum was directly related to the influences of the urban heat island. Supporting this statement were the location and structure of the nocturnal boundary layer over lower Manhattan, which agreed well with previous research studying the urban heat island by SethuRaman and Cermak (1974) and Bornstein and Johnson (1977).

The daytime boundary layer structure over Manhattan was also analyzed during a synoptically driven high wind flow regime (>4 m/s). The surface layer wind field was greater than 4 m/s from 00 UTC (19 LT) 13 November through 12 UTC (07 LT) 14 November. Conclusions are now presented about the boundary layer structure between 12 UTC (07 LT) 14 November and 20 UTC (15 LT) 14 November. The mesoscale wind regime present during this period did not favor the development of a sea breeze front as the boundary layer was uniformly mixed over the entire region. This period was characterized by a homogenous low-level wind flow over the area. Southwesterly winds of 10 kts (5 m/s) and greater were observed during this period. Previous research by Bornstein and Johnson (1977) concluded that there is a critical wind speed of approximately 8 kts (4.0 m/s) at which the urban roughness influences the low-level wind flow and boundary layer structure during daytime conditions (Bornstein and Johnson, 1977). It is evident from examining the cross-sections simulated in Figures 6.15 through

6.17 that the synoptic scale wind flow overwhelmed any mesoscale and microscale meteorological processes directly related with the urban blocking phenomena.

CHAPTER 7 SUMMARY AND CONCLUSIONS

The main objectives of this investigation were to observationally analyze and numerically simulate the mesoscale and microscale boundary layer structure over New York City. Observations from two SOund Detection And Ranging (SODAR) units, a 10 m micrometeorological tower and five Automated Surface Observing Stations (ASOS) were examined during several synoptic scale flow regimes. Numerical simulations were conducted to explore the complex mesoscale boundary layer structure over New York City. The first numerical investigation examined the ability of two high-resolution mesoscale prediction models, the Advanced Regional Prediction System (ARPS) and the Mesoscale Model 5 (MM5); to simulate the complex near surface flow over the New York City area. The second numerical investigation examined the urban heat island, urban roughness effect and sea breeze structure over the New York City region. In support of these numerical studies, high-resolution, simulations were performed on a 1 km grid.

The boundary layer investigation described in this thesis used a variety of tools to assist in an improved understanding of the complex variations that occur in the lower troposphere as a result of surface heterogeneities. A combination of observations from a surface observation network and SODAR cluster and high-resolution numerical modeling were used to better understand mesoscale boundary layer structure over New York City.

An observational analysis of mesoscale boundary layer structure over New York City was presented in Chapter 3. The “climatological” flow regimes observed over New York City region were presented in this section. The categories are southerly, westerly and

northerly with these further divided by the estimated flow strength (light or strong). The light and strong flow classification was determined by the critical wind speed of 4.0 m s^{-1} that has been linked to the urban heat island (Bornstein and Johnson, 1977) and sea breeze development (Arritt, 1993). Four flow regimes dominated: light southerly (18%), strong southerly (18%), strong westerly flow (17%), and light and variable flow (16%). These regimes occurred on 70 % of the days. The remaining periods were light westerly (9%), light northerly (6%), strong northerly (7%) and other (9%), respectively.

Additionally, the effects of wind directions on the roughness lengths observed over lower Manhattan were also analyzed. The roughness lengths could not be determined for the for the 0-89 and 90-179 degree flow directions. For the 180-269 degree flow directions, the averaged aerodynamic roughness length was 0.7 m. Lastly, for the 270-359 degree flow directions, the averaged aerodynamic roughness length was 0.9 m. Both these values seemed reasonable, as the flow pattern between 180 and 359 degrees moved over the Hudson River before being measured by the instrumentation cluster. The SODAR was used for in the roughness length calculation above 10 m. Friction velocities were also estimated for the wind profiles. The averaged friction velocity for the 180-269 degree flow directions is .30 m/s while the averaged friction velocity for the 270-359 degree flow directions was .478 m/s.

Two case studies were made to study the effects of the near surface wind flow on the development of the urban heat island over lower Manhattan. The first period was selected to study the effects of near surface winds moving from off the water on the development of the urban heat island over lower Manhattan. The mean temperature over the study period at Central Park, LaGuardia and the 10 m tower was between 1 and 2 C higher that

surrounding locations. Wind speed observations from JFK and the 10 m micrometeorological tower in lower Manhattan were greater than wind speeds observed from the other locations during much of the study period. With the exception of Teterboro, 2.30 m/s, Central Park had the lowest mean wind speed during the study period, 2.80 m/s. This was likely a result of near surface winds decelerating as they encountered higher roughness lengths associated with Manhattan Island. Observations from a miniSODAR over lower Manhattan were also studied. A nighttime mixed layer was observed over lower Manhattan This apparent mixed layer may be the result of urban heat island induced static instability, originating over Staten Island, allowing greater turbulent mixing in the nocturnal boundary layer. An additional case study was made and showed similar results to first study period.

A comparison of two high-resolution numerical model simulations, MM5 and ARPS, of near surface wind fields over New York City was presented in Chapter 5. In this study, the ARPS and MM5 simulated surface (10 m) wind fields were compared and contrasted with each other and surface observations. Several differences were observed between the two simulations. For example, the ARPS simulation consistently forecasted a decelerating and cyclonically turning mesoscale wind flow over Brooklyn, Queens and Manhattan. Conversely, the MM5 simulation forecasted a southwesterly wind flow across the entire region, with very little deceleration and cyclonic turning. The MM5 simulation did show some cyclonic turning of the 10 m wind field over the lower Manhattan. The ARPS simulation showed a more defined sea breeze frontal formation and propagation than the MM5 simulation did. The 10 m independent instrumentation tower over lower Manhattan confirmed the timing and position of the frontal passage simulated by the

ARPS model. Moreover, the ARPS simulated 10 m wind field was very responsive to the roughness length variations and urban heat island associated with New York City, as observed by tendency for cyclonic turning of the 10 m wind field over Brooklyn and Manhattan. The MM5 simulation was not as responsive to the roughness length variations and the urban heat island as the ARPS simulation. Both simulations had identical roughness length specifications and landuse data, so the differences were likely associated with the planetary boundary layer scheme used in each numerical model.

A high-resolution simulation of a sea breeze front, roughness length heterogeneities, and the urban heat island over New York City was presented in Chapter 6. Several important components of the boundary layer structure were analyzed in this chapter, including low-level wind flow, TKE and boundary layer height variations, vertical motion and the surface energy budget. The ARPS model simulated the development and inland penetration of the sea breeze front over the region. The sea breeze front formed because of strong differential heating between the land of the region and the Atlantic Ocean, in the presence of a light and variable synoptic scale flow. The ARPS model simulated the sea breeze front moving through lower Manhattan during this period and agreed well with both SODAR and 10 m tower observations from an independent instrumentation cluster maintained by the EPA and State Climate Office of North Carolina in lower Manhattan. The general structure of the sea breeze front over the region also agreed with previous studies by Bornstein (1994) who performed numerical simulations over the same area and observed a similar frontal alignment that extended through Staten Island, across lower Manhattan and eastward through Queens and Brooklyn.

The nocturnal boundary layer was also studied using surface and 100 m wind simulations, as well as surface energy budget figures and TKE cross-sections. 10 m wind simulations showed a slowing and cyclonic turning of the 10 m wind flow as the wind moved over Brooklyn, Queens and Manhattan, while 100 m wind simulations showed a slowing of the wind flow, but no discernable alteration of flow directions. This simulated feature was in agreement with observational findings by Bornstein and Johnson (1977) that showed nighttime events during stronger flow regimes (>4 m/s) were associated with distinctive roughness induced cyclonic turning in the winds over the main core of Manhattan and Brooklyn.

Additionally, simulated surface energy budget shows the presence of an urban heat island. More specifically, the surface sensible heat flux simulation time series over lower Manhattan was only briefly negative during the nighttime hours of 13 and 14 November, and quickly became positive for the rest of the nighttime hours. It appears that the urbanized structures associated with lower Manhattan act as heat holding materials that have a tendency to keep surface temperatures significantly warmer at night (urban heat island). In turn, positive surface sensible heat fluxes are generated over lower Manhattan, and are directly associated with the urban heat island.

Vertical profiles of TKE and wind velocity were also examined. Several simulated profiles showed a maximum in TKE over lower Manhattan during nighttime conditions. It appears that this TKE maximum is directly related to the influences of the urban heat island. The simulated location and structure of the nocturnal boundary layer over lower Manhattan are consistent with the results and agreed well with previous research

on urban heat islands by SethuRaman and Cermak (1974) and Bornstein and Johnson (1977).

The daytime boundary layer structure over Manhattan was also analyzed during a synoptically driven high wind flow regime (>4 m/s). The mesoscale wind regime present during this period did not favor the development of a sea breeze front with southwesterly winds of 5 m/s and greater observed during this period. This period was characterized by a homogenous low-level wind flow over the area. Southwesterly winds of 10 kts (5 m/s) and greater were observed during this period. Simulated results show that the synoptic scale wind flow overwhelmed any mesoscale and microscale meteorological processes directly related with the urban blocking phenomena.

Additional near surface wind and temperature data are needed to further evaluate the numerical model's ability to accurately simulate the mesoscale boundary layer over New York City and for data assimilation into numerical models. Accurate and reliable boundary layer wind data over New York City has proven difficult to obtain. The high noise levels and tall structures in lower Manhattan do not allow for very accurate and consistent boundary layer wind data from SODAR's, as discovered during this study.

LIST OF REFERENCES

Albers, S.C., 1995: The LAPS wind analysis. *Weather and Forecasting*, **10**, 342-352.

Angell, J. K., D. H. Pack, C. R. Dickson and W. H. Hoecker, 1971: 'Urban influence on nighttime airflow estimated from tetroon flights', *J. Appl. Meteor.*, **10**, 194-205.

Arritt, R. W.: 1993, 'Effects of large scale flow on characteristic features of the seabreeze', *J. Appl. Meteor.* **32**, 116-125.

Arya, S. P., 1999. Air Pollution and Dispersion Meteorology. Oxford University Press, New York.

Arya, S. P., 1988: Introduction to Micrometeorology. Academic Press, San Diego.

Atkins, N. T., and Wakimoto: 1997, 'Influences of the synoptic-scale flow on sea breezes observed during CAPE', *Mon. Wea. Rev.* **125**, 2112-2130.

Bornstein, R. D., 1968: 'Observations of the urban heat island effect in New York City', *J. Appl. Meteor.*, **7**, 575-582.

Bornstein et. al., 1994, Observation and simulation of urban-topography barrier effects on boundary layer structure using the three-dimensional TVM/URBMET model. "Air Pollution and its Application X", Plenum Press, New York, 1994.

Bornstein, R. D. and D. S. Johnson, 1977: 'Urban-rural wind velocity differences', *Atmos. Environ.*, **11**, 597-604.

Bratseth, A.M., 1986: Statistical interpolation by means of successive corrections. *Tellus*, **38A**, 439-447.

Brown, R. M. and S. SethuRaman, 1981: Temporal variation of particle scattering coefficients at Brookhaven National Laboratory, New York. Atmospheric Environment, 15, 1733-1737.

Businger, J.A., J.C. Wyngaard, Y. Izumi and E.F. Bradley, 1971: Flux profile relationships in the atmospheric surface layer. J. Atmos. Sci., **28**, 181-189.

Case, J.L., Manobianco, J., Oram, T.D., Garner, T., Blottman, P.F. and Spratt, S.M., 2002: Local Data Integration over east-central Florida using the ARPS Data Analysis System. *Weather and Forecasting*, **17**, 3-26.

Crescenti, G. H., 1998 'The degradation of Doppler SODAR performance due to noise: A review', *Atmos. Environ.*, **32**, 1499-1509.

Crescenti, G. H., 1999: A study to characterize performance of various ground-based remote sensors. NOAA Technical Memorandum ERL ARL-229, 286p

Deardorff, J.W., 1972: Numerical investigation of neutral and unstable planetary boundary layers. *J. Atmos. Sci*., **29**, 91-115.

Draxler, R. R., 1986: 'Simulated and observed influence of the nocturnal urban heat island on the local wind field', *J. Climate Appl. Meteor*. **25,** 1125.

Dupont, E., L. Menut, B. Carissimo, J. Pelon and P. Flamant, 1999: 'Comparision between the atmospheric boundary layer in Paris and its rural suburbs during the ECLAP experiment', *Atmos. Environ.*, **33**, 979-994.

Frizzola J. A. and E. L. Fisher, 1963: 'A series of sea breeze observations in the New York City area', *J. Appl. Meteor.*, **2**, 722-739.

Gilliam, R. G., Childs, P. P., H. Huber and S. Raman, 2003: Metropolitan Scale Transport and Dispersion from the New York World Trade Center Following September 11, 2001. Part I: An Evaluation of The CALMET Meteorological Model. NOAA Technical Document.

Gilliam, R. G., H. Huber and S. Raman, 2001: "Qualitative observational analysis of PBL using remote SODAR and tower measurements", 11th Symposium on Meteorological Observations and Instrumentation; 14-18 Jan 2001; Albuquerque, NM.

Gilliam, R. G., 2001: "Influence of surface heterogeneities on the boundary layer structure and diffusion of pollutants" M.S. Thesis, Department of Marine, Earth and Atmospheric Sciences. N.C. State University, Raleigh, NC.

Grell, G., J. Dudhia, and D. Stauffer, 1995: A Description of the Fifth-Generation Penn State/NCAR Mesoscale Model (MM5). Mesoscale and Microscale Meteorology Division, NCAR/TN-398+STR, 117 pp.

Hogrefe, C., S.T. Rao, P. Kasibhatla, G. Kallos, C.J. Tremback, W. Hao, D. Olerud, A. Xiu, J. McHenry and K. Alapaty, 2001: 'Evaluating the performance of regional-scale photochemical modeling systems: Part I-meteorological predictions', *Atmospheric Environment*. **35**, 4159-4174.

Janjic, Z., 1994: The step-mountain Eta coordinate: Further developments of the convective, viscous sublayer, and turbulence closure schemes. *Mon. Wea. Rev*., **122**, 927-945.

Lee, D. O., 1979: 'The influence of atmospheric stability and the urban heat island on urban-rural wind speed differences', *Atmos. Environ.*, **13**, 1175-1180.

Lin Y-L, Farley RD, Orville, HD, 1983: Bulk Parameterization of the snow field in a cloud model. *J Climate Appl Meteor***. 22**; 1065-1092.

Noilhan, J. and S. Planton, 1989: 'A simple parameterization of land surface processes for meteorological models', *Mon. Wea. Rev.* **117**, 537-549.

Micheal P., M. Miller, J.S. Tongue, 1998: Sea breeze regimes in New York City region--Modeling and Radar Observations. Transactions of Second Conference on Coastal Atmospheric and Oceanic Prediction and Processes, 78th AMS Annual Meeting, 11-16 January 1998 Phoenix, Arizona

Oke, T. R., 1987: *Boundary Layer Climates.* Halsted Press New York.

O'Brien, J.J., 1970: A note on the vertical structure of the eddy exchange coefficient in the planetary boundary layer. *J. Atmos. Sci.*, **27**, 1213-1215.

Raynor, G. S., S. Raman and R. M. Brown, 1979: 'Formation and characteristics of coastal internal boundary layers during onshore flows', BNL Report 21668. *Boundary Layer Meteorology*, 16, 487-514.

Reiss, N.M., J. Kwiatkowski, K. Gurer, J.R. Cermak and R. Avissar, 1996: "The New Jersey Sea Breeze Experiment (NESBEX): Movement and Structure of the New Jersey Sea Breeze as Diagnosed from Doppler Radar and Other Measurements". First NARSTO-Northeast Data Analysis Symposium and Workshop, Norfolk, VA, 10-12 December 1996.

Simpson, J.E., Mansfield, D.A., and Milford, J.R.: 1977: 'Inland penetration of sea-breeze fronts', *Quart. J. Roy. Meteor. Soc.*, **103**, 47-76.

Scire, J.S., D.G. Strimaitis and R.J. Yamartino, 2000: 'A User's Guide for the CALPUFF Dispersion Model, Version 5', Earth Tech, Inc. Concord.

Scire, J.S., F. R. Robe, M.E. Fernau and R.J. Yamartino, 2000: 'A User's Guide for the CALMET Meteorological Model, Version 5', Earth Tech, Inc. Concord.

SethuRaman, S. and J. E. Cermak, 1974: Physical modeling of flow and diffusion over an urban heat island. Adv. in Geophys. 18B, 223-240.

Stull, Roland B. An Introduction to Boundary Layer Meteorology.

Kluwer Academic Publishers, Norwell, MA 1988

Sun, W.Y., and C.Z. Chang, 1986: 'Diffusion model for a convective layer. Part I: Numerical simulation of convective boundary layer', *J. Climate Appl. Meteor*. **25**, 1445-1453.

United States Geological Survey, Land Use Land Cover Data (LULC), Web address: http://edc.usgs.gov/products/landcover/lulc.html

Wong, K. K. and R. A. Dirks, 1978: 'Mesoscale perturbations on airflow in the urban mixed layer. *J. Appl. Meteor.*, **17**, 677-688.

Xue, M., 1995: Advanced Regional Prediction System (ARPS) Users Guide, Version 4.0. Center for Analysis and Prediction of Storms, pp. 380.

Xue, M., K.K. Droegemeier and V. Wong, 2000: 'The advanced regional prediction system (ARPS)- A multi-scale nonhydrostatic atmospheric simulation and prediction tool. Part I: Model dynamics and verification', *Meteorology and Atmospheric Physics*. **75**, 161-193.

Xue, M., K.K. Droegemeier, V. Wong, A. Shapiro, K. Brewster, F. Carr, D. Weber, Y. Liu and D. Wang, 2001: 'The advanced regional prediction system (ARPS) - A multi-scale nonhydrostatic atmospheric simulation and prediction tool. Part II: Model physics and applications', *Meteorology and Atmospheric Physics*. **76**, 143-165.

Zhang, J., F.H. Carr and K. Brewster, 1998: ADAS cloud analysis. *Preprints, 12th Conf. On Numerical Weather Prediction*, Phoenix, AZ, Amer. Meteor. Soc., 185-188.